Cape Peninsula
University of Technology

ANALYSIS OF GREENHOUSE GAS EMISSION FROM REACTIVE MATERIALS AND ITS THERMODYNAMICS

By

RAMOSHWEU SOLOMON LEBELO

(Student Number 210277165)

BSc(Ed) (NWU), MTech (TUT)

Thesis submitted in fulfillment of the requirements for the degree

Doctor of Technology: Mechanical Engineering

Cape Peninsula University of Technology

Supervisor: Professor O. D. Makinde

Senior Professor & Director, Institute for Advanced Research in

Mathematical Modelling & Computations,

Cape Peninsula University of Technology, South Africa.

YEAR: 2013

DECLARATION

I, Ramoshweu Solomon LEBELO, declare that the contents of this thesis represent my own work, and that the thesis has not previously been submitted for academic examination towards any qualification. Furthermore, it represents my own opinions and not necessarily those of the Cape Peninsula University of Technology.

_____ _____

Signed Date

Acknowledgements

I would like to express my sincere appreciation to my supervisor, Prof O. D. Makinde for giving me this project, assistance, patience and organizing financial assistance. I also want to thank Vaal University of Technology for financial assistance and Cape Peninsula University of Technology for giving me the opportunity to study for this degree. I also appreciate contributions done by my colleagues from Mathematics department, Dr Kenneth Zimba, Dr Kazeem Okosun, Lazarus Rundora and Isaac Takaidza. My family also for allowing me time and giving me courage to study. Above all I give glory and honour to God the Almighty who gave me the ability and strength to complete the studies.

Dedication

To the Lord God Almighty and all people who played a major role to encourage me to persuade my studies. To my children, Rearabilwe, Rorisang and Bontle, be motivated.

Abstract

The environment is polluted by many gases of which carbon dioxide is one of them and unfortunately during the emission of carbon dioxide, oxygen, which is very important for keeping all species alive, is depleted. Increased industrial activities led to more emission of carbon dioxide and ultimately global warming arose as a result of the greenhouse effect. Global warming has resulted with high temperatures and carbon dioxide production in the atmosphere and it was necessary to come up with mathematical modelling to investigate processes that may try to reduce temperature rise, carbon dioxide emission and oxygen depletion in a stockpile of combustible material.

The work done in this thesis considered three differential equations, first for temperature behaviour, second for oxygen depletion and third for carbon dioxide emission. The three equations were solved simultaneously for a reactive slab of combustible material. An exothermic reaction in a stockpile of combustible material results due to the reaction of oxygen with reactive hydrocarbon material and the products are usually heat and carbon dioxide. A detailed discussion on this part is given in chapter 1, and also some definitions of terms applied in this work, together with literature review, statement of problem, aim of the study, objectives of the study and methodology are part of the chapter.

In chapter 2, the nonlinear partial differential equations governing the process are derived. The derivation of these formulae follows the Eulerian description of fluid flow which considers how properties of fluid flow change at a fluid element confined within a fixed space and time (x, y, z, t), in other words, a control volume is applied. The temperature behavior within a reactive slab is described by energy equation and the oxygen depletion and carbon dioxide emission equations are described by conservation of species equations. Derivation of boundary conditions following Newton's law of cooling are discussed, together with initial conditions.

The equations derived in chapter 2 are used in chapter 3 to numerically investigate thermal decomposition, oxygen depletion and carbon dioxide emission in a reactive slab of combustible material. The governing partial differential equations were first made dimensionless and solved numerically using Semi-Implicit Finite-Difference scheme.

Chapter 4 considers the effects of thermal radiation on carbon dioxide emission and oxygen depletion. Radiation is assumed to take place only on the upper surface of the rectangular slab of

combustible material and symmetric boundary conditions of the first kind were considered. In this case a steady state situation was considered and ordinary differential equations were used for the investigation.

The effects of both convective and radiative heat loss on carbon dioxide emission, oxygen depletion and thermal stability are investigated in chapter 5. Asymmetric boundary conditions for convective heat loss were assumed on the lower and upper surfaces, whereas symmetric boundary conditions for radiative heat loss were considered as in chapter 4. In both chapters 4 and 5, the governing ordinary differential equations were solved using the Runge-Kutta-Felberg method coupled with Shooting method technique. It should be noted that in this study we assumed the slab to be undergoing an n^{th} order oxidation chemical reaction.

Conclusions and Recommendations including further work are covered in chapter 6.

Nomenclature

a	Slab half width
$\boldsymbol{A}$	Pre-exponential factor
Bi_1	Thermal Biot number at slab's lower surface
Bi_2	Oxygen Biot number at slab's upper surface
$\mathbf{Bi_1}$	Biot number at slab's lower surface
$\mathbf{Bi_2}$	Biot number at slab's upper surface
Bi_3	Carbon dioxide Biot number
c_p	Specific heat at constant pressure
C	Oxygen concentration ($kgmol^{-1}$)
C_A	Species A mass concentration
$\boldsymbol{C}$	CO_2 concentration (Arrhenius' greenhouse law)
$\mathbf{C_o}$	Baseline CO_2 concentration (Arrhenius' greenhouse law)
C_w	Oxygen concentration at the slab surface ($kgmol^{-1}$)
D	Oxygen diffusivity in the slab
e	Internal energy
E	Activation energy ($Jmol^{-1}$)
E	Error estimate in RKF45
ΔF	Radiative forcing (Arrhenius' greenhouse law)
h, h_1	Heat exchange/transfer coefficient
h_2	Coefficient of oxygen transfer between the slab and the surrounding air
h_3	Coefficient of carbon dioxide transfer between the slab and the surrounding air
g_1	Heat transfer coefficient (slab lower surface)
g_2	Heat transfer coefficient (slab upper surface)
k	Rate constant (s^{-1})

k Thermal conductivity (diffusivity) of the reacting slab ($Js^{-1}m^{-1}K^{-1}$)

K Boltzmann constant (JK^{-1})

l Planck number (Js)

m Numerical exponent

n Order of reaction

N Avagadro's number

Nu Nusselt number

P Carbon dioxide concentration ($kgmol^{-1}$)

P_w Carbon dioxide concentration at the slab surface ($kgmol^{-1}$)

q_i Heat flux

Q Heat of reaction (Jkg^{-1})

Q_A Reaction rate source

Q_E Heat source

R Universal gas constant ($JK^{-1}mol^{-1}$

Ra Radiation parameter

s Scalar

sh Optimal step size

Sh_1 Dimensionless oxygen transfer rate at slab's surface

Sh_2 Dimensionless carbon dioxide transfer rate at slab's surface

$\bar{t}$ Time (s)

T Absolute temperature of the slab (K)

T_0, T_∞ Cold surrounding absolute temperature (ambient temperature) (K)

T_a Activation temperature

T_w Surface temperature of the slab (K)

$\frac{u^2}{2}$ Kinetic energy in *x* direction

$\frac{V^2}{2}$ Kinetic energy in *y* direction

V Magnitude of the velocity vector in the *x*, *y* and *z* directions

$\frac{w^2}{2}$ Kinetic energy in *z* direction

$\bar{y}$ Slab rectangular distance (m)

Greek letters

α Oxygen diffusivity parameter

β_1 Oxygen consumption rate parameter

β_2 Carbon dioxide emission rate parameter

σ Carbon dioxide diffusivity parameter

ϵ Error control tolerance

ε Emissivity of the slab

$\mathcal{E}$ Total energy in control volume

γ Carbon dioxide diffusivity in the slab

γ_p Polanyi parameter

λ Modified Frank-Kamenetskii parameter

μ Dimensionless activation energy parameter

ϕ Stefan-Boltzmann constant (W/m^2K^4)

ψ Diffusivity coefficient

θ Dimensionless temperature

ϱ Constant (Arrhenius' greenhouse law)

Φ Dimensionless oxygen concentration

Ψ Dimensionless carbon dioxide concentration

ρ Density

ρ_A Species *A* mass flux

ρu Momentum flux through $\Delta y \Delta z$ face in the *x* direction

ρv Momentum flux through $\Delta x \Delta z$ face in the *x* direction

ρw Momentum flux through $\Delta x \Delta y$ face in the *x* direction

δ Average diameter of molecule

$\delta_{A^*B^*}$ Collision radius between species A^* and B^*

$\varphi_{A^*B^*}$ Species reduced mass

v Vibration frequency (s^{-1})

$\bar{v}$ Characteristic speed of colliding species

ω Heat conduction coefficient

Contents

Papers Published or Submitted for Publication.

Articles already published or submitted for publication.

(1) Makinde, O. D., Chinyoka, T. & Lebelo, R. S. 2011. Numerical investigation into CO_2 emission, O_2 depletion and thermal decomposition in a reacting slab. *Mathematical Problems in Engineering*. 208426: 1-19. (2011) (PUBLISHED)

(2) Lebelo, R. S & Makinde, O. D. Modelling the impact of radiative heat loss on CO_2 emission, O_2 depletion and thermal stability in a reactive slab. *Applied Mathematics and Information Science Journal.* SUBMITTED – 2012. The paper was also presented at the 55^{th} Annual Congress of South African Mathematical Society at Stellenbosch University, South Africa. 31-10-2012 to 02-11-2012.

(3) Lebelo, R. S & Makinde, O. D. Analysis of CO_2 emission, O_2 depletion and thermal stability in a convecting and radiating reactive slab. *Thermal Science Journal.* SUBMITTED – 2012.

List of Figures

List of Tables

Chapter 1
Introduction

In this study the greenhouse gas carbon dioxide's (CO_2) contribution to greenhouse effect is investigated in a stockpile of combustible material. Spontaneous exothermic reaction in a stockpile of a combustible material can only occur in the presence of oxygen. This invariably leads to the emission of greenhouse gases, depletion of oxygen in the environment and thermal instability of the material. Mathematically, this scenario is governed by a system of nonlinear differential equations which may be tackled both numerically and analytically in order to gain an insight into the inherent complex dynamics in the system. Greenhouse effect is responsible for global warming and in this study we shall extend understanding and knowledge about the effect of exothermic reactions on global warming, due to greenhouse effect. Kyoto Protocol (an agreement negotiated by many countries to cut emissions of not only carbon dioxide, but of also other greenhouse gases) has not succeeded to stop emission of the greenhouse gases which encourages climate change and global warming. The study intends also to produce results that will bring understanding of measures that can be taken to lessen both emission of CO_2 and depletion of O_2, and to identify control measures of temperature rise in spontaneous combustion processes to avoid explosions. Greenhouse gases and the greenhouse effect are discussed. Again a discussion on combustion of hydrocarbons and their chemical kinetics are outlined.

1.1 Definition of Terms

Some of the terms that are relevant to this study are defined as follows:

1.1.1 Greenhouse Gases

Greenhouse gases are gases in the atmosphere that trap heat energy from the sun. The presence of greenhouse gases makes it difficult for all heat from the sun to escape back into space. It is suggested by most scientists like Wallington et al [73] that the temperature of the Earth would be about 30 ^{0}C colder if greenhouse gases were unavailable. The coldness could be unfavourable to sustain our ecosystem. As a result greenhouse gases help to regulate the climate by trapping heat.

The heat trapped is held in a form of warm-air blanket surrounding the Earth [55]. This process is the main cause of the greenhouse effect as according to Moll [57]. The common greenhouse gases found in the atmosphere are water vapour (H_2O), carbon dioxide (CO_2), methane (CH_4), ozone (O_3), nitrous oxide (N_2O), hydro fluorocarbons (HFCs), perfluorocarbons (PFCs) and sulphur hexafluoride (SF_6). Greenhouse gases are also accelerated by human activities, as outlined by Fierro *et al* [24] in the following ways.

- **Burning natural gas, coal and oil** -including gasoline for automobile engines-raises the level of carbon dioxide in the atmosphere.
- **Some farming practices and land-use changes** increase the levels of methane and nitrous oxide.
- **Many factories produce long-lasting industrial gases** that do not occur naturally, yet contribute significantly to the enhanced greenhouse effect and "global warming" that is currently under way.
- **Deforestation** also contributes to global warming. Trees use carbon dioxide and give off oxygen in its place, which helps to create the optimal balance of gases in the atmosphere. As more forests are logged for timber or cut down to make way for farming, fewer trees are left to perform this critical function.
- **Population growth** is another factor in global warming, because as more people use fossil fuels for heat, transportation and manufacturing the level of greenhouse gases continues to increase. As more farming occurs to feed millions of new people, more greenhouse gases enter the atmosphere.

1.1.2 Greenhouse Effect

Greenhouse effect is the rise in temperature that the Earth experiences due to trapping of heat energy from the sun by greenhouse gases. The trapped heat energy is the one reflected by the Earth's surface. Following Moll [57], research has shown that about 30% of the heat energy or sunlight toward Earth is deflected by the outer atmosphere and scattered back into space. About 70% of the remaining heat energy reaches the Earth's surface and is reflected upward again as infrared radiation (slow moving energy). The infrared radiation is absorbed by greenhouse gases which slow its escape from the atmosphere. Greenhouse gases transfer the absorbed energy to

other components of the atmosphere. The absorbed energy is re-radiated in all directions and this transfers energy to the surface and lower atmosphere, as a result the temperature there becomes higher than it would be if direct heating by solar radiation were the only warming mechanism [73]. This mechanism is fundamentally different from that of an actual greenhouse. The actual greenhouse works by isolating warm air inside the structure so that heat is not lost by convection. The basic mechanism of the greenhouse effect, according to Betz [8] is as follows: The Earth receives energy from the Sun in the form of visible light. This light is absorbed by the Earth's surface and re-radiated as thermal radiation. Some of this thermal radiation is absorbed by the atmosphere and re-radiated both upwards and downwards; that radiated downwards is absorbed by the Earth's surface. Thus the presence of the atmosphere results in the surface receiving more radiation than it would were the atmosphere absent; and it is thus warmer than it would otherwise be. The greenhouse effect mechanism, as described by the United States Environmental Protection Agency (EPA), is illustrated by the diagram below.

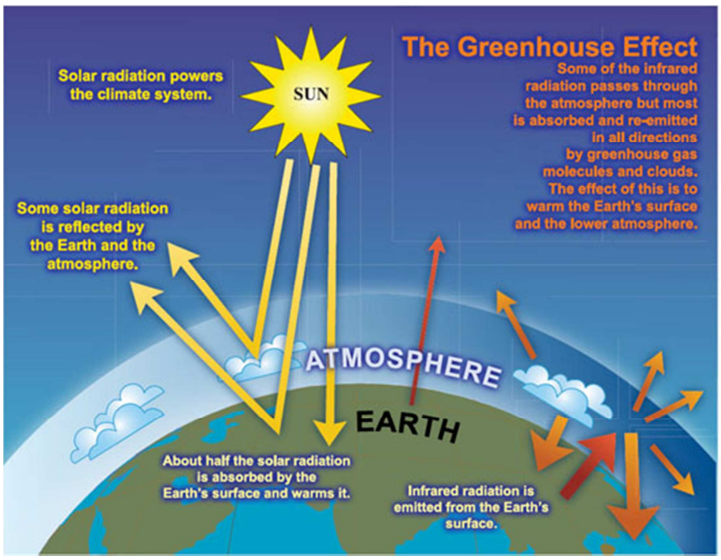

Figure 1.7: Simple diagram of greenhouse effect

Some of common greenhouse gases and their contribution to greenhouse effect are: water vapour (36-70%), carbon dioxide (9-26%), methane (4-9%) and ozone (3-7%) [8]. A contribution to the greenhouse effect by a gas is affected by its characteristics and its abundance. For example, Houghton [31] points out that on a molecule-for-molecule basis methane is about eighty times stronger greenhouse gas than carbon dioxide, but it is present in much smaller concentrations so

that its total contribution is smaller. It is not possible to state the exact percentage of the greenhouse effect caused by a certain gas, because some of the gases absorb and emit radiation at the same frequencies as others. As a result the total greenhouse effect is not just simply the sum of the influence of each gas, therefore the higher ends of the ranges quoted are for each gas alone and the lower ends account for overlaps with the other gases. Clouds also absorb and emit infrared radiation and therefore have an effect on radiative properties of the greenhouse gases. They are thus the major non-gas contributors to the Earth's greenhouse effect.

1.1.3 Global Warming and Climate Change

This refers to the increase in the average temperature of global surface air and oceans. The increase in temperature affects the Earth's surface including land, water and near-surface air [73]. Human contribution to greenhouse effect increases the quantity of CO_2 in the atmosphere and therefore more greenhouse gases. The more greenhouse gases imply more infrared radiation trapped and held. This process gradually increases the temperature of the Earth's surface and the air in the lower atmosphere, and the result is global warming. According to the Union of Concerned Scientists, in an average year, a typical coal plant (500 megawatts) generates about 3.7 million tons of CO_2 which plays a major part in air pollution [32]. The CO_2 pollution is the principal human cause of global warming and climate change [74, 75]. The following diagram indicates the production of CO_2 over the past 200 years since industrialization started.

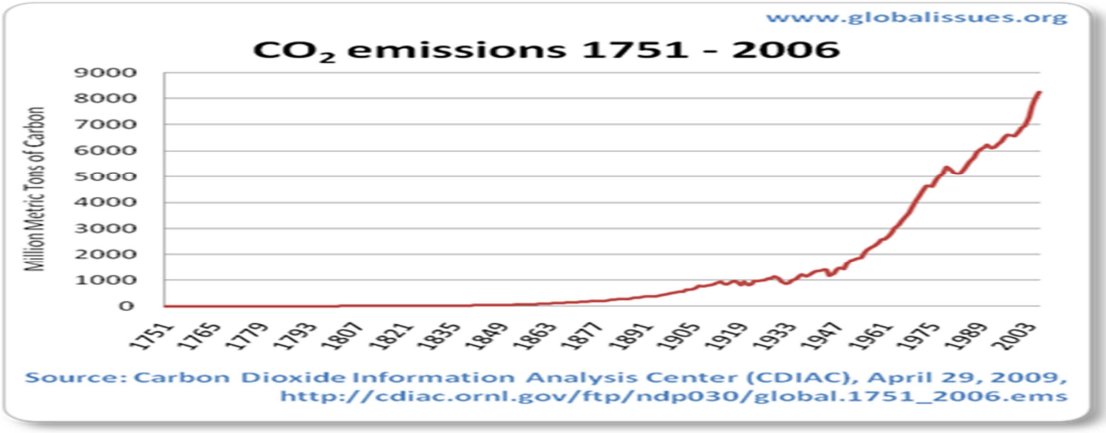

Figure 1.8: CO_2 emission 1751 – 2006

According to the 2007 Fourth Assessment Report by the Intergovernmental Panel on Climate Change (IPCC), global surface temperature has increased by 0.74 ± 0.18 ℃ during the 20th century [33, 37]. Scientists claim that during the entire 20th century, the average global temperature increased by about 0.6 ℃ (slightly more than 1 °F). The National Geographic Society gave evidence of global warming by the fact that the Earth's average temperatures have climbed 1.4 degrees Fahrenheit (0.8 ℃) around the world since 1880. The United Nations' Intergovernmental Panel on climate change (IPCC) also reported that Arctic ice is rapidly disappearing, and the region may have its first completely ice-free summer by 2040 or earlier. The ice loss already causes a suffering on polar bears and indigenous cultures. More evidence is that glaciers and mountain snows are rapidly melting. An example is Montana's Glacier National Park which is currently left with about 27 glaciers compared to the 150 in 1910 [25]. The following pictures show that global warming happens more quickly than predicted.

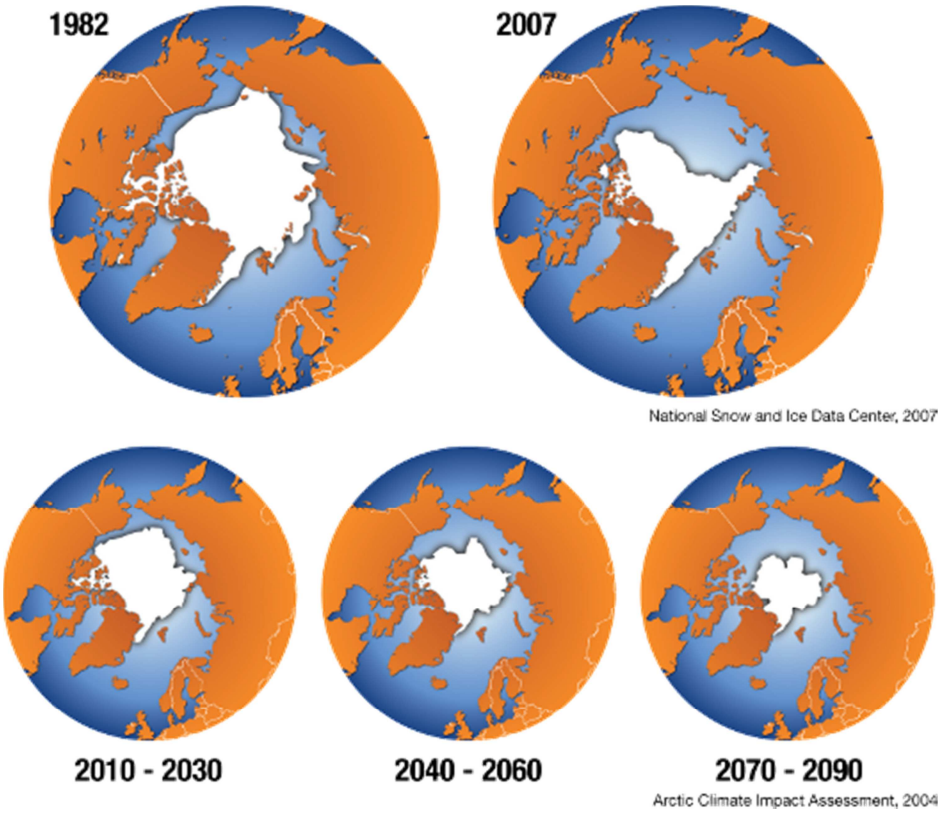

Figure 1.9: The decrease of Arctic sea ice, minimum extent in 1982 and 2007, the climate projections. UNEP/GRID-Arendal, 2007

The pictures are satellite observations that indicate that the arctic sea ice is decreasing. The projections, represented by the last three smaller pictures, for the rest of the century predict the continuous decrease of the sea ice. Climate scientists believe that the Arctic plays an unbelievable important role in the balance of the earth's climate as mentioned by Quadrelli *et al* [65]. It follows that the changes taking place in the arctic sea ice, may affect the whole planet tremendously.

Many scientists also agree that even a small increase in the global temperature would lead to significant climate and weather changes, affecting cloud cover, precipitation, wind patterns, the frequency and severity of storms, and the duration of seasons [10]. The rise in temperature would have the following effects:

- Raise the sea levels, reduce supplies of fresh water as flooding occurs along coastlines worldwide and salt water reaches inland.
- Extinction of many world's endangered species due to habitat change.
- Millions of people's lives would be affected, especially the poor who live in precarious locations or depend on the land for subsistence living.
- Increase in the spreading of diseases carried by animals or insects, for example, malaria.

Many scientists estimated that by the end of the 21st C the average global temperature will increase by approximately 1.4 to 5.8 ℃ . But other scientists argue that global warming is not a serious issue.

1.1.4 Spontaneous Combustion/Heating Materials

Spontaneous combustion is a process whereby a substance unexpectedly bursts into flame without ignition from an external source. The combustion is caused by the oxidation (combination of a substance with oxygen) of the substance within a material [61]. The following figure illustrates spontaneous combustion scenario.

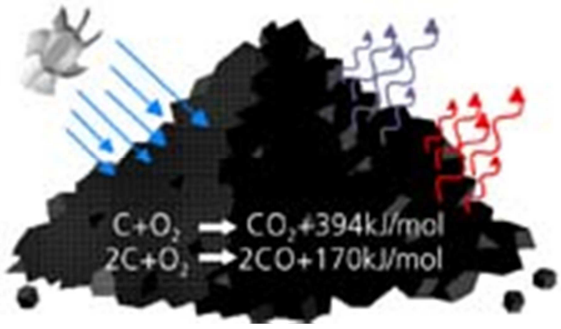

Figure 1.4: Reaction in stockpile

In the figure above, oxygen from the air reacts with the carbon of the coal and carbon-dioxide is released. This is an example of exothermic reaction, where heat will be released. Again, what happens in the process is that a substance undergoes a slow oxidation and the heat released cannot escape the substance. As a result the temperature of the substance rises until ignition takes place. Spontaneous combustion, as illustrated by figure 1.4, often occurs in piles of oily rags, green hay, leaves, or coal; it can constitute a serious fire hazard as according to Ozdeniz [61] and Corbett [18]. Judkins & Fulkerson [36] suggested that some common materials that can combust spontaneously include:

- Haystacks, compost piles and unprocessed cotton may self-ignite because of heat produced by bacterial fermentation.
- Grain dust in a hot metal silo can explode violently, destroying the structure.
- Linseed oil in a partially confined space (such as a pile of oil-soaked rags left out in an uncovered container) can oxidize leading to a buildup of heat and thus ignition.
- Coal can spontaneously ignite when exposed to oxygen which causes it to react and heat up when there is insufficient ventilation for cooling.

Spontaneous combustion contributes much to greenhouse gas emissions, hence its great influence on the greenhouse effect. The combustion process for all hydrocarbon materials is illustrated by equation (1.4) provided under subsection 1.1.5.1.2.

Carbon dioxide, the principal greenhouse gas, plays a major part in atmospheric temperature regulation. This concept was investigated by Swedish physical chemist Svante Arrhenius in the 1800’s. Arrhenius developed a theory to explain the ice ages, and in 1896 he was the first

scientist to speculate that changes in the levels of carbon dioxide in the atmosphere could substantially alter the surface temperature through the greenhouse effect, as mentioned by Clark [16]. He also predicted that emissions of carbon dioxide from the burning of fossil fuels and other combustion processes would cause global warming. Arrhenius was able to estimate that reducing CO_2 to its half would decrease temperatures by 4 - 5 ℃ and a doubling of CO_2 would cause a temperature rise by 5 - 6 ℃. He later adjusted the value downwards to 1.6 ℃ in his 1906 publication. His adjustment agrees with the recent 2007 estimates from IPCC that this value is likely to be between 2 and 4.5 °C as according to Karl & Trenberth [37]. During his time, his expectation for the rate of CO_2 levels to rise depended entirely on emissions. He expected CO_2 doubling to take about 3000 years. Today, due to high rate of CO_2 emissions, the doubling of the gas is estimated to take about a century. His greenhouse law states that: *if the quantity of carbonic acid* (*H_2CO_3*) *increases in geometric progression, the augmentation of the temperature will increase nearly in arithmetic progression.* This is expressed as follows: $\Delta F = \varrho \ln \mathbf{C}/\mathbf{C_o}$, where ΔF is radiative forcing measured in watts per square metre, ϱ is a constant assigned the value between 5 and 7, $\mathbf{C}$ represents CO_2 concentration measured in part per million by volume and $\mathbf{C_o}$ denotes a baseline or unperturbed CO_2 concentration. Arrhenius reaction is thus a description of a chemical reaction that gives the chemical formulae of both the reactants and products of the reaction. Balakrishnan *et al* [5] and Zaturska *et al* [78] agree that this applies to both exothermic (explosive) and non-exothermic (non-explosive) reactions, which are the main mathematical challenge of the theory of thermal explosion.

1.1.5 Combustion Chemistry

According to Dean *et al* [20] combustion chemistry is the part of chemistry that is concerned with combustion. This part of chemistry relates chemical potential energy to heat resulting from chemical reactions. Combustion chemistry considers also the study of mechanisms of hydrocarbons combustion including the thermodynamic and kinetic information thereof [74]. It is therefore necessary to start by looking at combustion in order to learn more about combustion chemistry.

1.1.5.1 Combustion

Combustion is described as a form of exothermic chemical reaction which involves two reacting species to produce carbon dioxide, water and heat [20, 28]. The reacting species in this study are fuel (hydrocarbon compound) and oxygen. Combustion involves also simultaneous collision of the reactants. The heat releases from the combustion process results with light that may be in the form of either glowing or a flame. The fuel can be in the gas, liquid or solid phase. In this study the solid phase fuel in the form of material stockpile is considered. Combustion of a fuel may be complete or incomplete.

1.1.5.1.1 Incomplete combustion

In an incomplete combustion the reaction takes place where oxygen is insufficient. The reaction therefore does not allow the fuel to react completely to produce carbon dioxide and water. Partially oxidised fuels produce toxic carbon monoxide (CO). The chemical equation for stoichiometric (chemically correct) burning of fuel in insufficient oxygen is as follows given by Frank-Kamenetskii [26]:

$$l\mathrm{C}_i\mathrm{H}_j + \left(l\left(\frac{i}{2}+\frac{j}{4}\right)\right)\mathrm{O}_2 \rightarrow li\mathrm{CO} + \left(\frac{lj}{2}\right)\mathrm{H}_2\mathrm{O} \tag{1.1}$$

An example that involved incomplete combustion of propane is as follows:

$$2\mathrm{C}_3\mathrm{H}_8 + 7\mathrm{O}_2 \rightarrow 2\mathrm{C} + 2\mathrm{CO} + 8\mathrm{H}_2\mathrm{O} + 2\mathrm{CO}_2 \tag{1.2}$$

1.1.5.1.2 Complete combustion

In complete combustion the products are always carbon dioxide, water and heat for exothermic reactions. The chemical expression for hydrocarbons burning in oxygen is:

$$\text{Fuel + oxygen} \rightarrow \text{carbon dioxide + water + heat.} \tag{1.3}$$

The general chemical equation for stoichiometric burning of fuel in oxygen is:

$$C_iH_j + \left(i + \frac{j}{4}\right) O_2 \rightarrow iCO_2 + \left(\frac{j}{2}\right) H_2O + \text{heat.} \quad (1.4)$$

An example of chemical reaction involving propane burning in oxygen is as follows:

$$C_3H_8 + 5O_2 \rightarrow 3CO_2 + 4H_2O + \text{heat.} \quad (1.5)$$

For the combustion of fuel taking place in air (a mixture of oxygen, 21%, and nitrogen, 79%) where oxygen is the source for combustion, nitrogen is added in the general equation [20]. The word equation is simply:

$$\text{Fuel + air} \rightarrow \text{carbon dioxide + water + nitrogen + heat} \quad (1.6)$$

The general chemical equation for stoichiometric burning of fuel in air is:

$$C_iH_j + \left(i + \frac{j}{4}\right) O_2 + 3.76\left(i + \frac{j}{4}\right) N_2 \rightarrow iCO_2 + \left(\frac{j}{2}\right) H_2O + 3.76\left(i + \frac{j}{4}\right) N_2 + \text{heat} \quad (1.7)$$

An example of chemical reaction as also shown by Naik & Dean [59], involving propane burning in air is as follows:

$$C_3H_8 + 5O_2 + 18.8N_2 \rightarrow 3CO_2 + 4H_2O + 18.8N_2 + \text{heat} \quad (1.8)$$

1.1.6 Chemical Kinetics

Chemical kinetics deals with how fast chemical reactions occur [26]. Kinetics therefore involves the dynamic study of interaction between molecules in a chemical reaction. Chemical kinetics also provides a way to describe dynamic events that affect changes which components of molecules undergo in a chemical reaction [77]. Elemental reactions are reaction equations that describe actual molecular activity occurring on the microscopical level. A generalised elemental reaction model for the reaction:

$$A + B \rightarrow C + D,$$

where A and B are reacting molecules that result with products C and D, is illustrated by the following diagram:

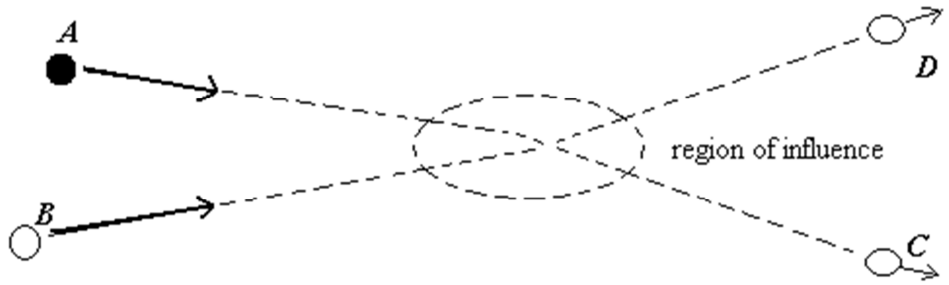

Figure 1.5: Kinetic model for molecular rearrangement via elemental reaction collisions

Following Chigier [28] the combustion of a hydrocarbon does not follow an elemental reaction model given by figure 1.5, because the interaction of hydrocarbon with oxygen is not the actual kinetic mechanism for carbon dioxide and water formation. The kinetic mechanism involves many steps which cannot be described by a simple model. The combustion of hydrocarbons is discussed below.

1.1.6.1 Reaction Mechanism

Combustion of hydrocarbons in oxygen involves a radical chain reaction where many distinct radical intermediates take part. A radical chain reaction involves radicals (atoms, molecules or ions with unpaired electrons) [26]. Free radicals may have a negative, positive or zero charge. The participation of radicals (chain carriers) makes it possible for reactants to be converted to products. As noted already, fuel combustion involves a number and variety of different chemical reactions that (i) start the chemical kinetic process, (ii) produce the short-lived reactive intermediate species(radicals), which generate all mechanisms and (iii) terminate the kinetic process resulting with products of combustion which are stable. During the fuel combustion process, a fuel molecule is broken down resulting with many different hydrocarbon portions, which are intermediate species. A generalised combustion reaction of fuel in oxygen given below is possible in low temperatures of less than 1000K (366 ℃). The key steps, although not all since many are missing, in the reaction as described by Carstensen *et al* [13] are as follows:

$$R^{\circ} + O_2 \rightleftharpoons RO_2^{\circ} \quad (1)$$

$$RO_2^{\circ} + RH \rightleftharpoons ROOH + R^{\circ} \quad (2)$$

$$ROOH \rightleftharpoons RO^{\circ} + OH \quad (3)$$

$$RO_2^{\circ} \rightleftharpoons R^{\circ}OOH \quad (4)$$

$$R^{\circ}OOH \rightleftharpoons cyRO + OH \quad (5)$$

$$R^{\circ}OOH + O_2 \longrightarrow \text{chain branching} \quad (6)$$

The combustion of hydrocarbons is assumed to be initiated by abstraction on hydrogen atom from the hydrocarbon to oxygen. The abstraction results with the hydroperoxide (HO_2°) radicals. The HO_2° radicals react further to give more hydroperoxides which decompose to give hydroxyl radicals (OH°). The hydroxyl radicals react with RH (volatile fuel) to form H_2O and the alkyl radical (R°). The R°radical then reacts with O_2 to give RO_2° (peroxy radical). A variety of these processes produce radicals of fuel and oxidising radicals. As mentioned, these intermediates are short-lived and therefore cannot be isolated.

The oxidation of hydrocarbons, according to the recent consensus due to Katimura [39] is that the two important reaction processes are:

$$H + O_2 \rightarrow O + OH$$

$$CO + OH \rightarrow CO_2 + H$$

The first reaction is responsible for the consumption of O_2 by H radicals, whereas the second reaction is responsible for converting CO to CO_2 and it also generates H radicals needed for the first reaction. To have an understandable trace of combustion mechanism of larger hydrocarbons, the lowest hydrocarbon, methane, is considered. The combustion example that is considered is for the reaction:

$$CH_4 + 2O_2 \rightarrow CO_2 + H_2O + \text{heat} \quad (1.9)$$

The reaction steps are outlined in the table that follows:

STEP	ACTION
$CH_3 + O \leftrightarrows CH_2O + H$	methyl radical consumed by oxygen atom
$CH_2O + H \rightarrow HCO + H_2$	H abstraction of CH_2O by H radical, the HCO decomposes rapidly to CO and H
$CH_3 + OH \rightleftharpoons CH_2 + H_2O$	Some CH_3 radicals will react with OH to give CH_2 radicals
$CH_2 + M \rightarrow CH_2 + M$	Some CH_2 radicals collide with some molecules to form stable CH_2
$CH_2 + O_2 \rightleftharpoons CO + H + OH$	Some CH_2 can react with O_2 to produce secondary branching, producing highly active H and OH
$CH_2 + O_2 \rightarrow HCO + OH$	CH_2 are still reactive, can react with O_2 to give HCO and OH
$CH_2 + H \rightleftharpoons CH + H_2$	Some CH_2 react with H radicals to form CH and H_2
$CH + H_2O \rightarrow CH_2O + H$ $CH + O_2 \rightarrow HCO + O$	CH radicals are quickly consumed by H_2O and O_2
$CH_3 + CH_2 \rightleftharpoons C_2H_4 + H$	Some CH_3 and CH_2 react to form C_2 species, which may undergo further oxidation or may form acetylene

Table 1.1: CH_4 combustion reaction steps

The diagram summarising the CH_4 combustion is represented as follows:

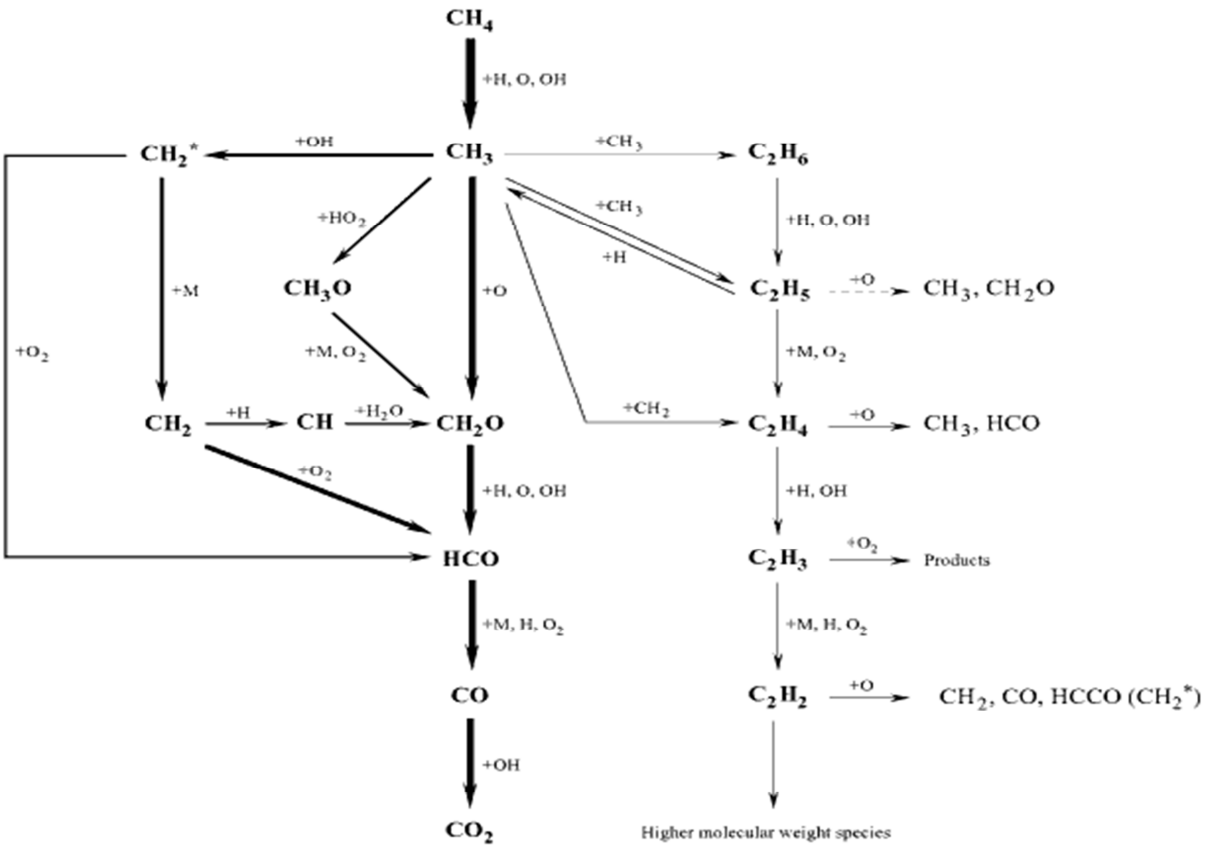

Figure 1.6: CH_4 combustion mechanism

The combustion reaction mechanism of a larger hydrocarbon is expected to be more complicated and includes many radicals.

1.1.6.2 Rate of Combustion

According to Clark [16] rate of combustion refers to the amount of mass of a material that goes through combustion over an amount of time, and it is expressed as g/s or kg/s. Increasing the temperature for any elementary reaction in a reaction mechanism has an influence on the reaction rate and little information on the pressure influence is known up to so far. Another factor that can be considered to have an influence on the reaction rate is due to the reacting species themselves. It is therefore necessary to consider the reacting species based on the law of mass action.

1.1.6.3 Mass Action Law

Following Moore [58] the law states that "at a constant temperature and pressure, the rate of chemical reaction is directly proportional to the concentration of the reacting substances raised to a particular exponent". For the generic elementary reaction

$$aA + bB \rightarrow P, \tag{1.10}$$

the law of mass action is expressed as follows

$$-\frac{d[A]}{adt} = -\frac{d[B]}{bdt} \propto [A]^{n_A}[B]^{n_B}, \quad \Rightarrow -\frac{d[A]}{adt} = -\frac{d[B]}{bdt} = \mathbf{k}[A]^{n_A}[B]^{n_B} \tag{1.11}$$

where $[A]$ and $[B]$ are the species A and B concentrations notation. **k** is the rate coefficient, n_A, n_B are the orders of reaction with respect to A and B respectively. The overall reaction order is $n_A + n_B$. An example to demonstrate this law is taken from the combustion of hydrogen in oxygen at some temperature and pressure to yield water. The equation is expressed as follows:

$$2\mathrm{H_2} + \mathrm{O_2} \rightarrow 2\mathrm{H_2O}. \tag{1.12}$$

The rate of combustion is found to be:

$$\frac{d[\mathrm{H_2O}]}{2dt} = -\frac{d[\mathrm{H_2}]}{2dt} = -\frac{d[\mathrm{O_2}]}{dt} = \mathbf{k}[\mathrm{H_2}]^{1.5}[\mathrm{O_2}]^{0.7} \tag{1.13}$$

The above equation is an example of a bimolecular or second order reaction.

For a general reaction mechanism given as follows,

$$\mathrm{Fuel} + a\mathrm{O_2} \rightarrow b\mathrm{CO_2} + c\mathrm{H_2O} + \mathrm{heat}. \tag{1.14}$$

The overall expression for the chemical reaction above is:

$$\frac{d[\mathrm{Fuel}]}{dt} = -[\mathrm{fuel}]^{n_{\mathrm{fuel}}}[\mathrm{O_2}]^{n_{\mathrm{O_2}}}\boldsymbol{A}e^{\left(\frac{-T_a}{T}\right)}, \tag{1.15}$$

where a, b and c are stoichiometric coefficients. n_{fuel}, $n_{\mathrm{O_2}}$, $\boldsymbol{A}$ and T_a are empirical (experimental) coefficients. T_a is the activation temperature which is consistently dependent on the temperature,

and it is helpful for modelling non-linearity in temperature. $\boldsymbol{A}$ is the pre-exponential factor as in Arrhenius law.

1.1.6.4 Arrhenius Law

In 1889 Svante Arrhenius, the Swedish Physical Chemist proposed the dependence of rate coefficient on temperature. He developed an important equation which shows that there is an exponential relationship between rate constant of a chemical reaction and temperature, as according to Clark [16]. He also proposed that the dependency of the rate constant on temperature could be expressed as follows:

$$\frac{d\ln\mathbf{k}(T)}{dT} = \frac{E}{RT^2}, \tag{1.16}$$

where E is called the activation energy with the unit $cal/mole$ or $joule/mole$. R is the gas constant. If E and R are taken as constants with respect to temperature, then integrating equation (1.16) gives:

$$\mathbf{k}(T) = \mathbf{k} = \boldsymbol{A}e^{-\frac{E}{RT}}, \tag{1.17}$$

where $\boldsymbol{A}$ is called the collision frequency (pre-exponential) factor. $\boldsymbol{A}$ can be calculated from collision theory which is discussed briefly in the section that follows:

1.1.7 Collision Theory

Figure 1.7 (*a*) gives a model of a collision that is not effective to result with a reaction whereas figure 1.7 (b) shows reactants with sufficiently vigorous collision that results in a reaction.

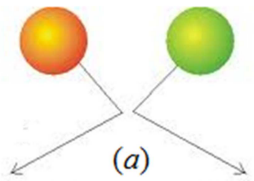

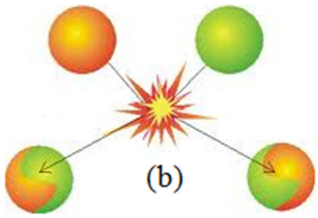

Figure 1.7(*a*): Non-vigorous collision **Figure 1.7(b):** Sufficiently vigorous collision

Collision theory gives a simple explanation to both mass action law and Arrhenius law, especially for bimolecular reactions like combustion of hydrocarbons [17]. Collision theory is applicable on condition that the reaction rate density should be proportional to the number of collisions per unit volume per unit time, multiplied by the probability that a collision produces new species. For a general reaction:

$$A^* + B^* \longrightarrow C^* + D^*, \tag{1.19}$$

the collision theory, for species B^* is thus:

$$\frac{number\ of\ collisions\ for\ one\ molecule}{unit\ volume \times unit\ time} = \frac{N_{B^*}}{v}\bar{v}\frac{\pi(2\delta)^2}{4}, \tag{1.20}$$

where $\frac{N_{B^*}}{v}$ is the number of B^*-molecules per unit volume (molar concentration of B^* time Avagadro's number) and δ is the average diameter of the B^*-molecules . Taking all reacting species into consideration, the following is obtained

$$\frac{number\ of\ total\ collisions}{unit\ volume \times unit\ time} = [A^*][B^*]\left(\frac{8KT}{\pi\varphi_{A^*B^*}}\right)^{1/2}\pi\delta^2{}_{A*B*}N. \tag{1.21}$$

The characteristic speed $\bar{v}$, which means that all collisions take place with the same relative velocity, was substituted according to Maxwell-Boltzman distribution to give equation (1.21). K is the Boltzmann's constant, $\delta_{A^*B^*}$ is the collision radius between species A^* and B^*, $\varphi_{A^*B^*} = \frac{m_{A^*}m_{B^*}}{m_{A^*}+m_{B^*}}$ is the reduced mass, N is the Avogadro's number, T is the temperature and $\left(\frac{8KT}{\pi\varphi_{A^*B^*}}\right)^{1/2}$ represents the average (mean) speed of molecules [58]. The probability for fertile (species

producing) collision to occur depends on the appropriate orientation $\left[e^{-\left(\frac{E}{RT}\right)}\right]$ of reacting species. $e^{-\left(\frac{E}{RT}\right)}$ is also the probability for a particular collision to form a reaction . Therefore:

$$(probabilty\ that\ a\ collision\ is\ fertile) \propto e^{-\left(\frac{E}{RT}\right)}.$$

Finally:

$$\frac{\chi}{V} = -\frac{d[A^*]}{dt} = -\frac{d[B^*]}{dt} = [A^*][B^*]\,\boldsymbol{A}\left(\frac{T}{\boldsymbol{K}}\right)^m e^{-\left(\frac{E}{RT}\right)}\ , \tag{1.22}$$

where $\boldsymbol{A}$ is the pre-exponential factor, $\boldsymbol{K}$ is the temperature unit (Kelvin). $\boldsymbol{K}$ is omitted in many literatures. Using equation (1.21), the pre-exponential factor $\boldsymbol{A}$, is described as follows, $\boldsymbol{A} = \left(\frac{8k_BT}{\pi\varphi_{A^*B^*}}\right)^{1/2}\pi\delta^2{}_{A^*B^*}N$ which represents the collision frequency of molecules in terms of relative speed. The parameters $\boldsymbol{A}, m$ and E from equation (1.22) are experimentally determined as mentioned earlier. The Polanyi equation

$$E = E_a^0 + \gamma_p \Delta H, \tag{1.23}$$

where ΔH is the heat of reaction and E_a^0 and γ_p are the Polanyi parameters, can be used to obtain an estimate of activation energy E. The advantage of using the Polanyi expression is that the parameters $\boldsymbol{A}$ and E can be used to approximate the rate law parameters without experimental work.

1.1.8 Activation Energy

This is the minimum energy the colliding molecules must possess for the chemical reaction to take place [58]. Consider the figure that follows:

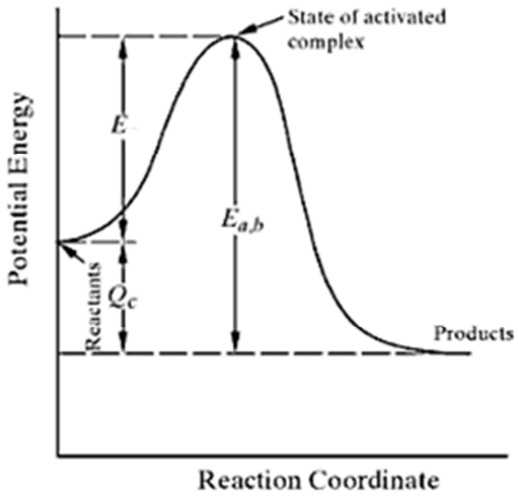

Figure 1.8: Potential Energy diagram

The figure above shows an exothermic reaction in which reactants must pass through the activated complex to form products. E is the energy difference between the activated complex and the reactants. That is:

$$E = E_{a,b} - Q_c \, , \tag{1.24}$$

where Q_c is the heat released (per mole) in the reaction. The factor $e^{-\left(\frac{E}{RT}\right)}$ represents the fraction of collisions having energy higher than E. The Arrhenius factor will decrease with increasing E for a given T. $E_{a,b}$ is the activation energy for the backward reaction. The backward reaction in the case of an exothermic reaction is slower, because of the largeness of the activation energy E. The larger the activation energy implies that the reaction is sensitive to temperature variations.

1.1.9 Convective Heat Loss

According to Çengel [14], convection is the transfer of heat from one place to another by the movement of fluids. The fluids include liquids, gases, plasmas, and some plastic solids, but in our case the fluids refer to gases movement to and fro a reactive slab of combustible material. Convection which involves cooling is also described by Newton's law of cooling, where the heat

transfer coefficient may be independent of the temperature difference between object and environment [12, 23]. Detailed description of Newton's law of cooling is given under section 2.5.1 in chapter 2.

1.1.10 Thermal Radiation

Thermal radiation in a reactive slab, due to exothermic reaction, is defined as an electromagnetic radiation in the wavelength range of 0.1 to 100 microns, and arises as a result of temperature difference between the slab's surface temperature and its surrounding temperature, following Katsoff [38]. Radiation energy per unit time from a hot body is proportional to the fourth power of the absolute temperature and it is expressed by Stefan-Boltzmann Law**.** According to Katsoff [38] and Richmond [67], a hot body radiating energy to its cooler surroundings has the net radiation heat loss rate expressed as

$$q = \varepsilon\phi(T^4 - T_0^4),$$

where q is heat transfer per unit time, ε is the body's emissivity, ϕ is Stefan-Boltzmann constant, T is hot body absolute temperature and T_0 is cold surrounding absolute temperature.

1.2 Literature Review

The study on greenhouse gas carbon dioxide emission in spontaneous ignition processes from stockpile of reactive combustible materials, such as heap of coal left for a long time at some electricity power stations, has received serious attention by many researchers. This is because the continual emission of carbon dioxide contributes a lot to the Greenhouse effect which has caused global warming and climate change in the world. Carbon dioxide is produced from chemical reactions, in which oxygen which is so needful for all live, reacts with carbon containing materials such as coal. Ozdeniz [61] studied spontaneous ignition in a stock pile of coal by considering external parameters such as air temperature, air humidity, atmospheric pressure, velocity and direction of wind. Fierro *et al* [24] also studied self-ignition in a coal stockpile. They explained in their research that various exothermic processes such as low temperature

oxidation, microbial metabolism, adsorption-desorption of water due to the differences between real and equilibrium moisture concentration of lignite and air and oxidation of pyrite may lead to self-heating of coal and spontaneous combustion. Both Ozdeniz [61] and Fierro *et al* [24] carried out experiments to find out which external parameters can reduce self-igniting of coal in a stockpile and they never considered embedded parameters such as Biot number, carbon dioxide diffusivity, oxygen diffusivity, activation energy of the reaction and others which are considered in our study.

The study of exothermic chemical reaction was explored by many researchers. Koriko & Amowaye [40] considered a steady state exothermic chemical reaction, where they took the diffusion of the reactant into account. They also assumed Arrhenius temperature dependence with variable pre-exponential factor. In their investigation they were able to come up with a nonlinear differential equation representing the temperature and Arrhenius expressions. Their study was based on mathematical description of thermal explosion which includes combined effects of Frank-Kamenetskii parameter, activation energy parameter and pre-exponential factor, on the temperature rise of the system. They succeeded to show the existence and uniqueness of the solution for the nonlinear differential equation. In our study we include these parameters and more. Makinde [52], in one of his investigations examined steady state solutions of strongly exothermic reaction of viscous combustible materials. The combustible materials were considered in a channel filled with saturated porous medium under Arrhenius kinetics. In his examination he did not consider reactant consumption. He applied Brinkman model in modeling his problem and he was able to construct solutions for the nonlinear boundary value differential equation problem using perturbation technique together with special type of Hermite-pade approximations. His examination provided important properties of temperature profiles including bifurcations and thermal criticality of the system were discussed. In our study we also consider thermal criticality and parameters which help to sustain thermal stability of the system.

The model in our study considers a rectangular slab which consists of combustible reactive material. The study of exothermic reaction within a reactive slab has also received attention from many researchers, because it has many applications in engineering such as heat transfer gauges, thermal insulations, metal casting, ice formation and thermal control of space vehicles. Aziz & Makinde [3] in their study investigated the inherent irreversibility in a rectangular slab with temperature-dependent internal heating. Their study provided the importance of knowledge on

the usefulness of the location of the maximum temperature within a rectangular slab as affected by various parameters. This knowledge provides a better understanding of heat treatment manufacturing processes in microtechnology and space vehicle equipment, for which precise control of the location of the maximum temperature is required. Further study involving a reactive slab of combustible material was done by Legodi & Makinde [44]. In their study they considered a steady state exothermic oxidation chemical reaction of order *n* in a slab with reactant consumption in the presence of convective heat and oxygen exchange with the surrounding ambient at the slab surface. Their investigation was able to show how various thermophysical parameters affect temperature and oxygen profiles in a reactive slab, but the product of the exothermic chemical reaction, carbon dioxide, was not considered. Again the radiative heat effect on thermal stability and oxygen depletion was not investigated.

In this research we extend the study done by Legodi & Makinde [44] by considering also the greenhouse gas carbon dioxide, in both convective and radiative heat exchange at the slab surfaces.

The transport equations for a reacting flow are the energy and species equations. The equations are accompanied by appropriate boundary conditions. Detailed derivation of the transport equations is discussed in chapter 2.

1.3 Statement of the Problem

As already discussed above, global warming is caused by the greenhouse effect due to greenhouse gases, where carbon dioxide is a major player. The carbon dioxide which contributes about 9-26% to the greenhouse gases is produced mainly by combustion of carbon containing materials in oxygen. The oxygen that is very important for life sustaining is used up during the carbon dioxide synthesis. The intention of this study is to investigate spontaneous combustion of carbon containing materials in exothermic reactions which results with emission of the greenhouse gas (CO_2). This study is therefore motivated by investigation of how the production of carbon dioxide can be reduced and so doing, preserving oxygen. The investigation extends to looking at processes that lessen oxygen depletion in the environment of materials that combust spontaneously, so as to reduce carbon dioxide emission, and ultimately alleviate global warming. Parameters which enhance thermal stability in a stockpile of combustible materials are also of

concern, and it is necessary to identify them so as to come up with measures that can control explosions due to exothermic reactions.

1.4 Aim of the Study

To investigate depletion of oxygen and emission of carbon dioxide in an environment of materials that combust spontaneously, and also to identify factors that can help avoid explosions in exothermic reactions.

1.5 Objectives of the Study

The objectives of the study are as follows:

(i) To investigate temperature profiles, oxygen profiles, carbon dioxide profiles and Nusselt number versus the rate of reaction profiles in an exothermic reaction of reactive slab.
(ii) To identify parameters that help to reduce oxygen depletion rate in an exothermic reactions within a reactive slab of combustible material.
(iii) To identify parameters that help to reduce carbon dioxide emission rate in an exothermic reactions within a reactive slab of combustible material.
(iv) To identify parameters that enable thermal stability in an exothermic reaction within a reactive slab of combustible material.

1.6 Methodology

This study considers a spontaneous exothermic reaction within a rectangular reactive slab of combustible material. This results into a system of differential equations that describe the temperature distribution, depletion and emission processes of oxygen and carbon dioxide respectively. The models are of the form of transport equations which include partial differential equations and ordinary differential equations, to describe the chemical species transport, the species being oxygen and carbon dioxide, and also the heat transfer within a rectangular reactive

slab. Appropriate numerical methods are employed to tackle the nonlinear differential equations problems. Maple Software will be utilised to implement the numerical algorithm on the computer.

1.7 Numerical Approach:

1.7.1 Semi-Implicit Finite Difference Scheme

This method is applied in chapter 3.

The scheme is built upon the concept of the implicit finite difference scheme outlined below.

The stencil below is used for the implicit finite difference scheme.

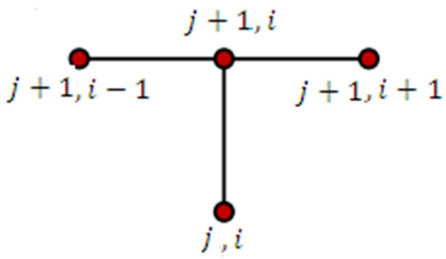

Figure 1.9: Implicit FDM stencil

Consideration of heat equation given by the following expression is used to demonstrate usage of the scheme.

$$\frac{\partial T}{\partial t} = k\frac{\partial^2 T}{\partial \bar{y}^2},$$

the left and right hand sides respectively become:

$$\frac{\partial T}{\partial t} \approx \frac{T_i^{j+1} - T_i^j}{\Delta t}, \tag{1.25}$$

$$\frac{\partial^2 T}{\partial \bar{y}^2} = \xi\left(\frac{T_{i+1}^{j+1} - 2T_i^{j+1} + T_{i-1}^{j+1}}{(\Delta\bar{y})^2}\right) + (1-\xi)\left(\frac{T_{i+1}^{j} - 2T_i^{j} + T_{i-1}^{j}}{(\Delta\bar{y})^2}\right), \tag{1.26}$$

where ξ is a chosen number such that $0 \leq \xi \leq 1$. Equation (1.26) is called semi-implicit difference scheme expression. If $\xi = 0.5$, then equation (1.26) takes the following form,

$$\frac{\partial^2 T}{\partial \bar{y}^2} = 0.5\left(\frac{T_{i+1}^{j+1}-2T_i^{j+1}+T_{i-1}^{n+1}}{(\Delta\bar{y})^2}\right) + 0.5\left(\frac{T_{i+1}^{j}-2T_i^{j}+T_{i-1}^{j}}{(\Delta\bar{y})^2}\right), \tag{1.27}$$

which gives the expression known as Crank-Nicolson.

Combining equations (1.25) and (1.26) gives the following

$$\frac{T_i^{j+1}-T_i^j}{\Delta t} = \xi\left(\frac{T_{i+1}^{j+1}-2T_i^{j+1}+T_{i-1}^{j+1}}{(\Delta\bar{y})^2}\right) + (1-\xi)\left(\frac{T_{i+1}^{j}-2T_i^{j}+T_{i-1}^{j}}{(\Delta\bar{y})^2}\right). \tag{1.28}$$

The rearrangement of equation (1.28) by multiplying with Δt, writing $r = \frac{\Delta t}{\Delta \bar{y}^2}$, and putting the largest time superscript on the left hand side, yields

$$-\xi r T_{i+1}^{j+1} + (1+2\xi r)T_i^{j+1} - \xi r T_{i-1}^{j+1} = r(1-\xi)T_{i+1}^{j} + [1-2r(1-\xi)]T_i^j + r(1-\xi)T_{i-1}^{j}. \tag{1.29}$$

The three terms of the left hand side of equation (1.29) are unknown, whereas the three terms on the right hand side are usually known. Dividing the $\bar{y}$ interval $0 \le \bar{y} \le 1$ of the slab into n equal interval, $n-1$ internal grid points are obtained per row. It follows that for $j = 0$ and $i = 1, \dots, n-1$, then equation (1.29) gives a system of linear $n-1$ equations for $n-1$ unknown values. The unknown values in the system are $T_2^{j+1}, T_3^{j+1}, T_4^{j+1}, \dots, T_{i-1}^{j+1}$ and they are interior grid points at $t = (j+1)\Delta t$ as described by Kreyzig [41].

The symbolic form of the semi-implicit formula is illustrated by the following figure, which shows only the coefficients of T terms.

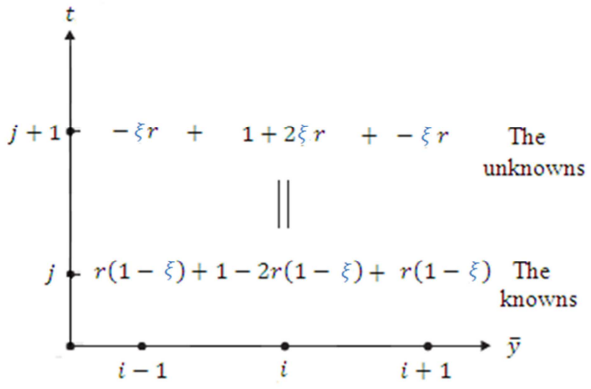

Figure 1.10: Symbolic form of semi-implicit scheme

The system of linear equations resulting from equation (1.29) forms a tridiagonal system. It is necessary therefore to solve the system of equation using the following matrices set up.

$$\begin{pmatrix} b_1 & c_1 & 0 & 0 & \cdots & 0 \\ a_1 & b_2 & c_2 & 0 & \cdots & 0 \\ 0 & a_2 & b_3 & c_3 & 0 & \cdots \\ 0 & 0 & a_3 & b_4 & c_4 & \cdots \\ \vdots & & & & & \\ 0 & \cdots & & & \times 0 & b_m \end{pmatrix} \begin{pmatrix} T_1 \\ T_2 \\ T_3 \\ \vdots \\ T_m \end{pmatrix} = \begin{pmatrix} p_1 \\ p_2 \\ p_3 \\ \vdots \\ p_m \end{pmatrix}$$

The tridiagonal matrix on the left is transformed into an equivalent one as follows

$$\begin{pmatrix} 1 & \delta_1 & 0 & 0 & \cdots & 0 \\ 0 & 1 & \delta_2 & 0 & \cdots & 0 \\ 0 & 0 & 1 & \delta_3 & 0 & \cdots \\ 0 & 0 & 0 & 1 & \delta_4 & \cdots \\ \vdots & & & & & \\ 0 & \cdots & & & \times 0 & 1 \end{pmatrix} \begin{pmatrix} T_1 \\ T_2 \\ T_3 \\ \vdots \\ T_m \end{pmatrix} = \begin{pmatrix} p_1 \\ p_2 \\ p_3 \\ \vdots \\ p_m \end{pmatrix},$$

where

$$\delta_1 = \frac{c_1}{b_1};\ \ \delta_{i+1} = \frac{c_{i+1}}{b_{i+1} - a_i\delta_i} \qquad i = 1,2,\dots,m-2$$

and

$$p_1 = \frac{d_1}{b_1};\ \ p_{i+1} = \frac{d_{i+1} - a_i p_i}{b_{i+1} - a_i\delta_i} \qquad i = 1,2,\dots,m-1.$$

Solving from bottom to top the following can be obtained.

$$T_m = p_m;\ \ T_i = p_m - \delta_i T_{i+1} \qquad i = m-1, m-2, \dots, 2, 1.$$

The simplest way of solving the system above is by following the way of using the formula $Ab = x$, where A is the first matrix on the left of the equation, b represents the unknown 1×1 matrix and x is the known matrix on the right hand side. The system is solved by evaluating the inverse of A and multiplying it by x, that is, $b = A^{-1}x$. This method is applied in chapter 3 to evaluate b and any software can be used to do so.

1.7.2 Runge-Kutta-Fehlberg Method

The Runge-Kutta-Fehlberg method, coupled with the Shooting method discussed under section 1.7.3, will be applied in chapters 4 and 5.

This method is denoted by RKF45 because first, an approximation to the solution of the initial value problem (IVP) is made using a Runge-Kutta method of order 4, and second, a better value for the solution is determined using a Runge-Kutta method of order 5 [11]. In order to arrive at a reasonable accuracy in the solution of an IVP, the problem is solved twice using step sizes h and $h/2$. The answers are then compared at the mesh points corresponding to the larger step size and this task requires much work of computation for the smaller step size. Once it is found that there is no agreement on the answers obtained, the computation must be repeated. The RKF45 is very useful because it covers a procedure that guarantees that a proper step size h is applied [54]. The technique followed is such that at each step, two different approximations for the solution are obtained and also compared, and in case the two answers obtained are closely related then the approximation is peacefully accepted. It follows that if the answers obtained from approximations disagree to a specified accuracy, the step size is reduced and if the answers agree to more significant digits than required, the step size is increased for convenience.

Following Mathews [54], the algorithm of the RKF45 include these steps:

$$k_1 = hf(t_i, y_i)$$

$$k_2 = hf(t_i + \tfrac{1}{4}h, y_i + \tfrac{1}{4}k_1)$$

$$k_3 = hf(t_i + \tfrac{3}{8}h, y_i + \tfrac{3}{32}k_1 + \tfrac{9}{32}k_2)$$

$$k_4 = hf\left(t_i + \frac{12}{13}h, y_i + \frac{1932}{2197}k_1 - \frac{7200}{2197}k_2 + \frac{7296}{2197}k_3\right)$$

$$k_5 = hf\left(t_i + h, y_i + \frac{439}{216}k_1 - 8k_2 + \frac{3680}{513}k_3 - \frac{845}{4104}k_4\right)$$

$$k_6 = hf\left(t_i + \frac{1}{2}h, y_i - \frac{8}{27}k_1 + 2k_2 - \frac{3544}{2565}k_3 + \frac{1859}{4104}k_4 - \frac{11}{40}k_5\right) \quad (1.30)$$

The expression for Runge-Kutta method of order 4 used to approximate the solution of IVP is given by

$$y_{i+1} = y_i + \frac{25}{216}k_1 + \frac{1408}{2565}k_3 + \frac{2197}{4104}k_4 - \frac{1}{5}k_5, \quad (1.31)$$

and Runge-Kutta method of order 5 expression that is used to determine a better value for the solution is as follows

$$z_{i+1} = y_i + \frac{16}{135}k_1 + \frac{6656}{12825}k_3 + \frac{28561}{56430}k_4 - \frac{9}{50}k_5 + \frac{2}{55}k_6. \quad (1.32)$$

In order to compute a numerical approximation for an IVP over a specified interval, it is necessary to use a set of discreet points with error control tolerance ϵ [27]. The error control ϵ is included in the following equation

$$s = 0.840896\left(\frac{\epsilon h}{|z_{i+1} - y_{i+1}|}\right)^{\frac{1}{4}},$$

where s is a scalar, h is step size, and the product sh is the optimal step size. The error estimate is the difference of the z_{i+1} and y_{i+1}. In other words the error $\mathbf{E} = z_{i+1} - y_{i+1}$ is expressed as

$$\mathbf{E} = \frac{1}{360}k_1 - \frac{128}{4275}k_3 - \frac{2197}{75240}k_4 + \frac{1}{50}k_5 + \frac{2}{55}k_6. \quad (1.33)$$

All the algorithms for RKF45 outlined are embedded in Maple software and the solutions of the problem are given using the software.

1.7.3 Shooting Method

This is a numerical method commonly used to find the solution of two-point boundary value problems. The technique of this method involves an iterative algorithm that tries to identify

appropriate initial conditions for a related IVP that gives the solution to the original boundary value problem (BVP) [56]. It should be noted that the related IVP initial conditions are used to approximate boundary conditions for the BVP to the desired accuracy. Should it happen that the boundary conditions are not satisfied accordingly the process is repeated with new set of initial conditions so that ultimately the boundary conditions are satisfied to the desired accuracy. The shooting technique is embedded within Maple and the software is used to solve the combined system of IVP's. When solving the system of equations, one step of the Newton-Raphson method is applied until the boundary conditions are satisfied according to the prescribed tolerance [63]. The Newton-Raphson method is an iterative method that determines approximate roots of a given function. The algorithm according to Parker [62] is briefly described as follows:
Let $Y(t)$ be some specified function of t, say, $Y(t) = e^{2t}$. In order to solve the equation

$$Y(t) = 0, \tag{1.34}$$

we let t be a guess for the root. We can get an improved guess t^{new} by defining

$$\Delta t = t^{\text{new}} - t\,. \tag{1.35}$$

We apply Taylor expansion to solve equation (1.36) as follows:

$$Y(t + \Delta t) \cong Y(t) + Y'(t)\Delta t = 0, \tag{1.36}$$

and rearranging (1.36) we obtain the relation

$$t^{\text{new}} = t - \frac{Y(t)}{Y'(t)}, \tag{1.37}$$

which can now be solved iteratively for t.
The shooting technique follows the following algorithm.
We consider a two point boundary value problem:

$$y'' = cy(x), \tag{1.38}$$

with

$$y(a) = a \text{ and } y(b) = a \tag{1.39}$$

We now let

$$y_1 = y, \qquad y_2 = y', \quad y_3 = c.$$

$$\begin{cases} y'_1 = y_2 \\ y'_2 = y_3 y_1 \\ y'_3 = a \end{cases}$$

$$y_1(a) = a, \qquad y_2(b) = a, \quad y_3(a) = y_3(b)$$

Figure 1.11 illustrates how the shooting technique operates [60]. The arrows indicate the launching of trial integrals that are aimed at satisfying boundary conditions at one endpoint. If boundary conditions are not satisfied as desired, the discrepancies from the desired boundary conditions on the other endpoint are used to adjust the starting conditions. This process is done again and again until desired boundary conditions are acquired at both endpoints.

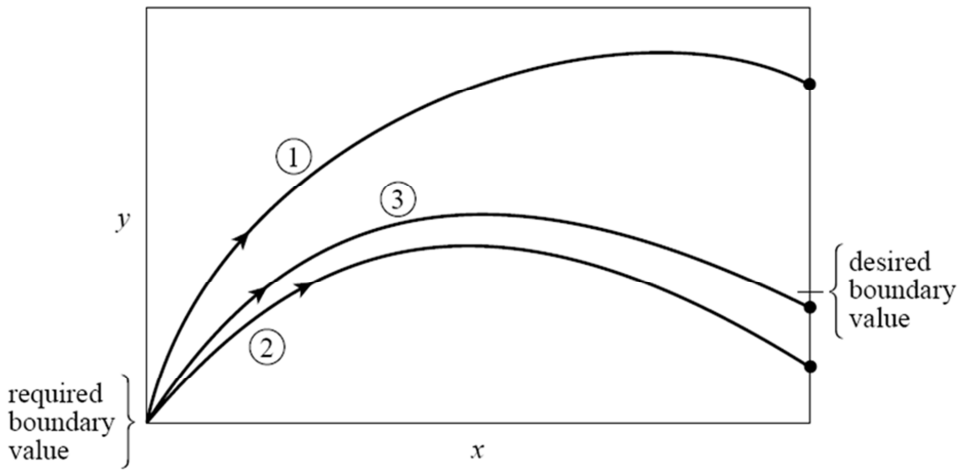

Figure 1.11: Shooting method scheme

The RKF45 coupled with shooting method are embedded in Maple software.

Chapter 2

Derivation of Governing Equations

2.1 Introduction

In this chapter we look at the derivation of governing equations. Three nonlinear partial differential equations describing the temperature, oxygen concentration and carbon dioxide concentration in a reactive slab of combustible material are derived following the derived energy and conservation of species equations.

The investigation of carbon dioxide emission, oxygen depletion and thermal decomposition in a reactive slab of combustible material is based on a stockpile of reactive material as illustrated by figure 1.4 in chapter 1. The exothermic reaction that results with carbon dioxide emission and oxygen consumption is as a result of hydrocarbons spontaneous reaction with oxygen. The chemical reaction involved in the combustion of the stockpile hydrocarbon material is analogous to the conditions involving flow of a viscous fluid in which there is concurrent heat and mass transfer. It should also be noted that combustion involves a system that combines equations of chemical kinetics, heat transfer and diffusion [26]. The objective is to develop differential equations that will predict temperature and species (carbon dioxide and oxygen) concentration fields within the ambient. This is done by applying Newton's second law of motion and conservation of mass, energy and species to a differential control volume as mentioned by Frank-Kamenetskii [26].

Two approaches to the study of fluid flow are the Lagrangian and Eulerian descriptions [35]. The Lagrangian description considers a fluid flow field comprising of a large number of finite sized particles. The particles are considered to have mass, momentum, internal energy and other properties. The Eulerian description of fluid flow considers how properties of fluid flow change at a fluid element confined within a fixed space and time (x, y, z, t), in other words, a control volume is applied. For the derivation of governing equations in this study, the Eulerian description will be used.

The method of the control volume is helpful to demonstrate the origin of each term of the equations. These equations are difficult to solve in their raw form, and as a result most of the solutions that exist are for highly simplified flow situations where certain terms of the equations

have been eliminated by application of some rational process. The concept of control volume is described as follows:

A three dimensional setup for the control volume is illustrated by the figure below.

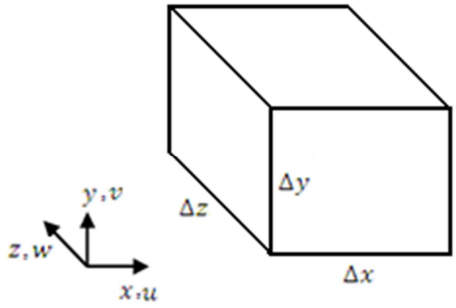

Figure 2.1: Illustration of elemental control volume

For simplicity of the problem, we consider a two dimensional control volume setup as illustrated by figure 2.2, and the setup is briefly discussed below.

A small control volume of lengths Δx and Δy and depth of unity perpendicular to the $x - y$ plane, is considered. Figure 2.2 by Ghirelli & Leckner [29], illustrates the differential control volume $(dx.dy.1)$ for mass conservation in two dimensional reaction mixture flow.

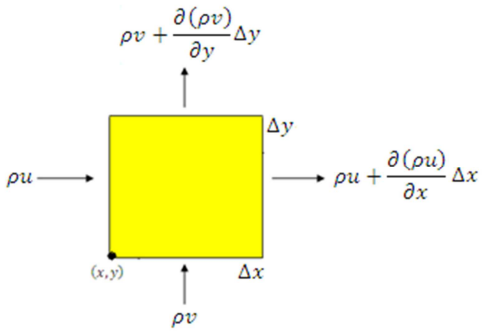

Figure 2.2: Control volume (2-D) for mass conservation

The rate of mass entering a face is the product of the density, fluid velocity and the face area [29]. For example, on the side with the area $A = \Delta y \Delta z$, the density ρ is multiplied by the velocity u in the x direction, so that the rate at which the mass enters the control volume is thus

$$\rho u \Delta y \Delta z.$$

The mass leaving the volume is expressed in the same manner, but in this case the velocity and density may have changed as the fluid passes through the control volume. The small changes in

velocity and density are respectively expressed as $u + \Delta u$ and $\rho + \Delta\rho$. It follows that the mass leaving the control volume, denoted by a negative sign, is expressed as

$$-(\rho + \Delta\rho)(u + \Delta u)\Delta y\Delta z.$$

In this study two types of equations are used to derive governing equations. The first is the energy equation which describes the temperature behavior within a reactive slab, and the second is the set of species conservation equations which describe the depletion of oxygen and emission of carbon dioxide. Both types of equations are discussed in sections 2.2 and 2.3 respectively.

2.2 Energy Equation

The energy equation is based on the first law of thermodynamics. For the fluid element (gas) in a control volume, this law, according to Bakker [4], states thus: *the rate of change of the total energy (internal + kinetic) of a fluid particle is equal to the rate at which total energy enters the control volume, plus the rate of work done on the control volume boundary by the surface forces plus the rate at which heat is added to the control volume at the surfaces by heat conduction.* In other words, the change in energy of the fluid element within the control volume is equal to the net thermal energy transferred into the control volume plus the rate of work done by external forces. Therefore, the energy equation will be derived by setting the total derivative to be equal to the change in energy as a result of the work done by viscous stresses (external forces) and the net heat conduction in the control volume.

The total energy per unit mass of the fluid includes internal energy e and kinetic energy $\frac{V^2}{2}$, where V, the magnitude of the velocity vector in the *x, y* and *z* directions, is expressed by $V^2 \equiv u^2 + v^2 + w^2$ [35]. Therefore

$$\mathcal{E} = e + \frac{1}{2}(u^2 + v^2 + w^2).$$

The rate of change (increase) of total energy in the control volume is described by the expression

$$\frac{\partial(\rho\mathcal{E})}{\partial\bar{t}}\Delta x\Delta y\Delta z.$$

The first law of Thermodynamics can also be expressed in the form

$$\text{internal energy increase rate} = \text{heat tranfer rate} - \text{surface forces work rate.} \tag{2.1}$$

The rate of net transfer of energy through the control volume is analogous to the momentum flux transfer into and out of the control volume, and as a result the use of the following momentum conservation expression is applied

$$\frac{\partial}{\partial \bar{t}}(\rho u) + \frac{\partial}{\partial x}(\rho u)u + \frac{\partial}{\partial y}(\rho v)u + \frac{\partial}{\partial z}(\rho w)u, \tag{2.2}$$

where $(\rho u)u, (\rho v)u$ and $(\rho w)u$ each represents the momentum flux through the $\Delta y \Delta z$ face, $\Delta x \Delta z$ face and $\Delta x \Delta y$ face in the *x* direction. Using (2.2), the net transfer of energy per unit volume through the control volume in the *x* direction is

$$\frac{\partial}{\partial \bar{t}}\rho\left(e + \frac{1}{2}V^2\right) + \frac{\partial}{\partial x}\rho u\left(e + \frac{1}{2}V^2\right) + \frac{\partial}{\partial y}\rho v\left(e + \frac{1}{2}V^2\right) + \frac{\partial}{\partial z}\rho w\left(e + \frac{1}{2}V^2\right). \tag{2.3}$$

Expression (2.3) is obtained by replacing u in (2.2) by the sum of internal and kinetic energies. Expression (2.3) can be shortened as

$$\frac{\partial(\rho \mathcal{E})}{\partial \bar{t}} \Delta y \Delta z. \tag{2.4}$$

The second task is to consider the work done per unit volume by the surface forces in the control volume. The following diagram illustrates the external forces (stresses) working on the volume surfaces in the *x* direction [4].

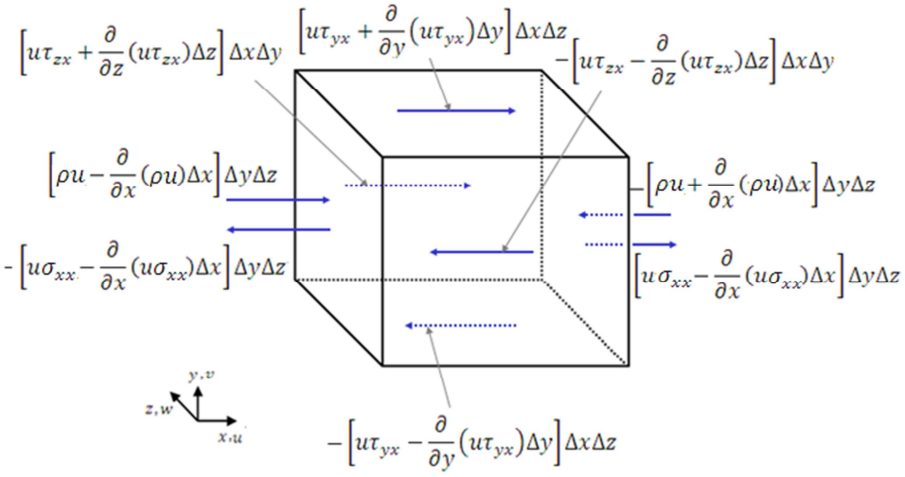

Figure 2.3: Work done by surface stresses (external forces)

In the figure above u is velocity in the *x* direction, σ_{ij} is the normal stress, τ_{ij} is the shear or tangential stress. The subscript *i* represents the plane, either *x*, *y* or *z* and *j* denotes the direction. For example, σ_{xx} describes the normal stress on the *x*-plane in the *x*-direction, whereas τ_{yx} is the shear stress on the *y*-plane in the *x*-direction. Adding all the external forces as shown by figure 2.1 and dividing by $2\Delta x\Delta y\Delta z$, the following is obtained:

$$-\frac{\partial(\rho u)}{\partial x}+\frac{\partial(u\sigma_{xx})}{\partial x}+\frac{\partial(u\tau_{yx})}{\partial y}+\frac{\partial(u\tau_{zx})}{\partial z}. \tag{2.5}$$

Consideration of surface stresses acting in other faces, that is, the $\Delta x\Delta z$ and $\Delta x\Delta y$, in the *y* and *z* directions respectively, the following expressions are obtained:

$$\frac{\partial(\rho v)}{\partial y}+\frac{\partial(v\sigma_{yy})}{\partial y}+\frac{\partial(v\tau_{xy})}{\partial x}+\frac{\partial(v\tau_{zy})}{\partial z}, \tag{2.6}$$

$$-\frac{\partial(\rho w)}{\partial z}+\frac{\partial(w\sigma_{zz})}{\partial z}+\frac{\partial(w\tau_{xz})}{\partial x}+\frac{\partial(w\tau_{yz})}{\partial y}. \tag{2.7}$$

Adding the three expressions above (2.5 – 2.7), the following net expression for the work done by surface stresses is thus:

$$-\frac{\partial(\rho u)}{\partial x}-\frac{\partial(\rho v)}{\partial y}-\frac{\partial(\rho w)}{\partial z}+\frac{\partial(u\sigma_{xx})}{\partial x}+\frac{\partial(u\tau_{yx})}{\partial y}+\frac{\partial(u\tau_{zx})}{\partial z}+\frac{\partial(v\sigma_{yy})}{\partial y}+\frac{\partial(v\tau_{xy})}{\partial x}+\frac{\partial(v\tau_{zy})}{\partial z}+\frac{\partial(w\tau_{xz})}{\partial x}+$$

$$\frac{\partial(w\tau_{yz})}{\partial y}+\frac{\partial(w\sigma_{zz})}{\partial z}. \qquad (2.8)$$

The expression (2.8) can be written thus:

$$-div(\rho \boldsymbol{U})+\frac{\partial(u\sigma_{xx})}{\partial x}+\frac{\partial(u\tau_{yx})}{\partial y}+\frac{\partial(u\tau_{zx})}{\partial z}+\frac{\partial(v\sigma_{yy})}{\partial y}+\frac{\partial(v\tau_{xy})}{\partial x}+\frac{\partial(v\tau_{zy})}{\partial z}+\frac{\partial(w\tau_{xz})}{\partial x}+\frac{\partial(w\tau_{yz})}{\partial y}+$$

$$\frac{\partial(w\sigma_{zz})}{\partial z}, \qquad (2.9)$$

where

$$div(\rho \boldsymbol{U})=\frac{\partial(\rho u)}{\partial x}+\frac{\partial(\rho v)}{\partial y}+\frac{\partial(\rho w)}{\partial z}. \qquad (2.10)$$

The last task on equation (2.1) is to come up with the expression for the total heat per unit volume transferred into the control volume. This is determined by the heat flux q_i. The heat flux will be regarded as positive for heat going out of the control volume to the surrounding *x*, *y* or *z* direction. The following figure illustrates the heat flux as a result of the heat energy transfer through the control volume.

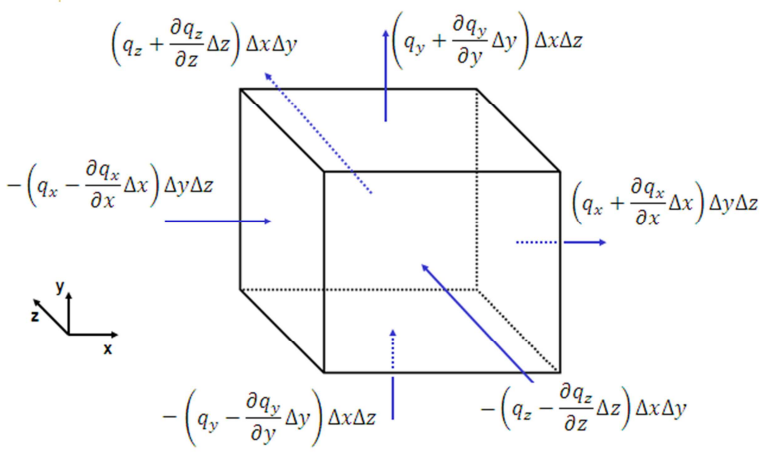

Figure 2.4: Heat flux due to heat energy transfer

Adding all the components shown on figure 2.4, and dividing by $2\Delta x\Delta y\Delta z$, the following result is obtained

$$-\frac{\partial q_x}{\partial x}-\frac{\partial q_y}{\partial y}-\frac{\partial q_z}{\partial z}. \qquad (2.11)$$

Figure 2.4 demonstrates also that the heat conduction effects are associated with the motion of gas molecules which randomly move in and out of the control volume. The motion of the gas

molecules randomly brings also the energy in and out of the control volume, and there is also an exchange of heat energy at the surface boundaries without any exchange in mass, as according to Djavareshnkian *et al* [21]. Fourier's law is applied to relate the heat flow in the *x*, *y* or *z* direction to the rate of change of temperature in the *x*, *y* or *z* direction.

Fourier's law states that: *the rate at which heat flows across the surface of unit area is proportional to the negative of the temperature gradient normal to the surface* [23]. This law is expressed as follows in the *x* direction normal to the $\Delta y \Delta z$ face:

$$q_x = -\omega \frac{\partial T}{\partial x}.$$

It follows that

$$q_y = -\omega \frac{\partial T}{\partial y},$$

and

$$q_z = -\omega \frac{\partial T}{\partial z}.$$

The constant of proportionality ω is called heat conduction coefficient, which is a property of the fluid element (gas), and T represents the temperature of the fluid element (gas) flow. The negative sign indicates that heat flows from hot to cold. Then, expression (2.6) can be written as

$$\frac{\partial}{\partial x}\left(\omega \frac{\partial T}{\partial x}\right) + \frac{\partial}{\partial y}\left(\omega \frac{\partial T}{\partial x}\right) + \frac{\partial}{\partial z}\left(\omega \frac{\partial T}{\partial x}\right), \tag{2.12}$$

which can be written simply as

$$\omega \left(\frac{\partial^2 T}{\partial x^2} + \frac{\partial^2 T}{\partial y^2} + \frac{\partial^2 T}{\partial z^2}\right), \tag{2.13}$$

Adding expressions (2.4), (2.9) and (2.13), the following equation is obtained

$$\frac{\partial(\rho \mathcal{E})}{\partial \bar{t}} = -div(\rho \boldsymbol{U}) + \frac{\partial(\rho u)}{\partial x} + \frac{\partial(u\sigma_{xx})}{\partial x} + \frac{\partial(u\tau_{yx})}{\partial y} + \frac{\partial(u\tau_{zx})}{\partial z} + \frac{\partial(v\sigma_{yy})}{\partial y} + \frac{\partial(v\tau_{xy})}{\partial x} + \frac{\partial(v\tau_{zy})}{\partial z} + \frac{\partial(w\tau_{xz})}{\partial x} + \frac{\partial(w\tau_{yz})}{\partial y} + \frac{\partial(w\sigma_{zz})}{\partial z} + \omega \left(\frac{\partial^2 T}{\partial x^2} + \frac{\partial^2 T}{\partial y^2} + \frac{\partial^2 T}{\partial z^2}\right) + Q_E. \tag{2.14}$$

The Q_E represents the energy or heat source term that may include, potential energy or heat production from nuclear or chemical reactions. The work done due to gravity is also included. Again, using body forces in the *x*, *y* and *z* directions respectively represented by $g_x\rho\Delta x\Delta y\Delta z$, $g_y\rho\Delta x\Delta y\Delta z$ and $g_z\rho\Delta x\Delta y\Delta z$, the work done by gravity forces in the respective directions are $\rho u g_x$, $\rho v g_y$ and $\rho w g_z$ adding the work done to equation (2.14) we have the following:

$$\frac{\partial(\rho E)}{\partial \bar{t}} = \omega\left(\frac{\partial^2 T}{\partial x^2}+\frac{\partial^2 T}{\partial y^2}+\frac{\partial^2 T}{\partial z^2}\right)+\left[-div(\rho \boldsymbol{U})+\frac{\partial(\rho u)}{\partial x}+\frac{\partial(u\sigma_{xx})}{\partial x}+\frac{\partial(u\tau_{yx})}{\partial y}+\frac{\partial(u\tau_{zx})}{\partial z}+\frac{\partial(v\sigma_{yy})}{\partial y}+\right.$$
$$\left.\frac{\partial(v\tau_{xy})}{\partial x}+\frac{\partial(v\tau_{zy})}{\partial z}+\frac{\partial(w\tau_{xz})}{\partial x}+\frac{\partial(w\tau_{yz})}{\partial y}+\frac{\partial(w\sigma_{zz})}{\partial z}\right]+\rho u g_x+\rho v g_y+\rho w g_z+Q_E. \quad (2.15)$$

Equation (2.15) is called the energy conservation equation and it is a symbolic expression for equation (2.1). If the system is incompressible and viscous stresses are neglected, the following equation is obtained

$$\frac{\partial(\rho \mathcal{E})}{\partial \bar{t}} = \omega\left(\frac{\partial^2 T}{\partial x^2}+\frac{\partial^2 T}{\partial y^2}+\frac{\partial^2 T}{\partial z^2}\right)+Q_E. \quad (2.16)$$

2.3 Conservation of Species Equations

There is a transport of species if the fluid element (gas) consists of a binary mixture, or as in the combustion within a slab, there is diffusion of a particular species. It is necessary to come up with an equation that describes the diffusion and conservation of a species. As it has been done in the previous case, the control volume is considered. The following figure illustrates the transportation of species *A* by diffusion, in each of the *x*, *y* and *z* directions.

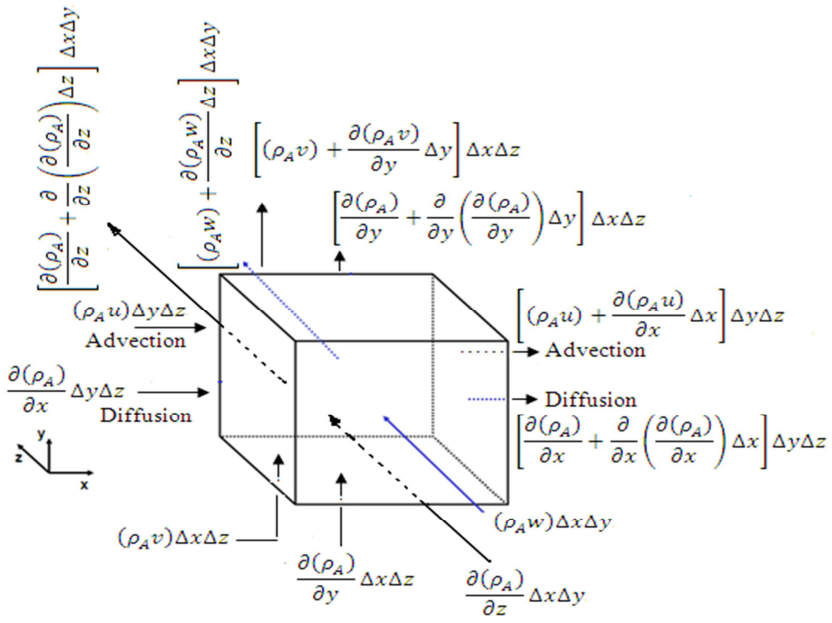

Figure 2.5 Control volume for species conservation

The net transfer of species *A* by diffusion in the *x* direction is given by

$$-\frac{\partial}{\partial x}\left(\frac{\partial(\rho_A)}{\partial x}\right)\Delta x\Delta y\Delta z=\left\{\frac{\partial(\rho_A)}{\partial x}-\left[\frac{\partial(\rho_A)}{\partial x}+\frac{\partial}{\partial x}\left(\frac{\partial(\rho_A)}{\partial x}\right)\Delta x\right]\right\}\Delta y\Delta z. \tag{2.17}$$

Similarly, in the *y* and *z* directions the species diffusion will be, respectively:

$$-\frac{\partial}{\partial y}\left(\frac{\partial(\rho_A)}{\partial y}\right)\Delta x\Delta y\Delta z=\left\{\frac{\partial(\rho_A)}{\partial y}-\left[\frac{\partial(\rho_A)}{\partial y}+\frac{\partial}{\partial y}\left(\frac{\partial(\rho_A)}{\partial y}\right)\Delta y\right]\right\}\Delta x\Delta z, \tag{2.18}$$

and

$$-\frac{\partial}{\partial z}\left(\frac{\partial(\rho_A)}{\partial z}\right)\Delta x\Delta y\Delta z=\left\{\frac{\partial(\rho_A)}{\partial z}-\left[\frac{\partial(\rho_A)}{\partial z}+\frac{\partial}{\partial z}\left(\frac{\partial(\rho_A)}{\partial z}\right)\Delta z\right]\right\}\Delta x\Delta y. \tag{2.19}$$

The rate of production or immobilization of species *A* within the control volume is represented by

$$Q_A\Delta x\Delta y\Delta z, \tag{2.20}$$

where Q_A may represent the source of reaction rate. The rate of change of the concentration of species *A* within the control volume is given by

$$\frac{\partial C_A}{\partial \bar{t}} \Delta x \Delta y \Delta z. \tag{2.21}$$

The species mass transfer balance is obtained by adding the first four expressions (2.17 - 2.20), equating them to the rate of change of concentration equation (2.21) and dividing by the volume $\Delta x \Delta y \Delta z$, to get the following equation

$$\frac{\partial C_A}{\partial \bar{t}} = -\frac{\partial}{\partial x}\left(\frac{\partial(\rho_A)}{\partial x}\right) - \frac{\partial}{\partial y}\left(\frac{\partial(\rho_A)}{\partial y}\right) - \frac{\partial}{\partial z}\left(\frac{\partial(\rho_A)}{\partial z}\right) + Q_A. \tag{2.22}$$

The negative signs are as a result of subtracting rate of change of masses leaving the control volume from those entering the control volume, for diffusion cases, as illustrated by figure 2.5. For the isotropic (having the same physical properties in the *x*, *y* and *z* directions) medium, and the diffusion obeying the rate equation, following Frank-Kamenetskii [26], it follows that

$$\frac{\partial(\rho_A)}{\partial x} = -\psi \frac{\partial C_A}{\partial x},$$

where ρ_A is the mass flux, and C_A is the mass concentration or mass component of species *A* per unit volume. ψ is the diffusivity coefficient. Equation (2.22) is therefore expressed as follows:

$$\frac{\partial C_A}{\partial \bar{t}} = \frac{\partial}{\partial x}\left(\psi \frac{\partial C_A}{\partial x}\right) + \frac{\partial}{\partial y}\left(\psi \frac{\partial C_A}{\partial y}\right) + \frac{\partial}{\partial z}\left(\psi \frac{\partial C_A}{\partial z}\right) + Q_A. \tag{2.23}$$

Equation (2.23) can also be expressed in vector form as

$$\frac{\partial C_A}{\partial \bar{t}} = div(\psi \; grad \; C_A) + Q_A,$$

and assuming that ψ were independent of *x*, *y*, *z* and C_A, the following would hold

$$\frac{\partial C_A}{\partial \bar{t}} = \psi\left(\frac{\partial^2 C_A}{\partial x^2} + \frac{\partial^2 C_A}{\partial y^2} + \frac{\partial^2 C_A}{\partial z^2}\right) + Q_A \; . \tag{2.24}$$

From the work done above, two equations for describing the transport of a species in a reaction, due to diffusion, were derived. These equations will be used to derive the governing equations as discussed in the next section.

2.4 Governing Equations

For the case of a stockpile of a combustible material in a reactive slab, diffusion of gases is considered in a solid material. To simplify the calculations, a one-dimensional (1-D) set up is considered for the exothermic reaction in a slab. The first equation to consider is the nonlinear partial differential equation describing the temperature field in the reactive slab. If diffusion is considered as the main transport of energy in the system, then the sum of all energies, by conservation, which is equal to the change in internal energy of the system, is related to the temperature change by a specific heat, $d\mathcal{E} = cdT$ [26]. Using equation (2.16) for a 1-D set up, the following equation is obtained:

$$\rho \frac{\partial \mathcal{E}}{\partial \bar{t}} = \rho c \frac{\partial T}{\partial \bar{t}} = \omega \frac{\partial^2 T}{\partial x^2} + Q_E,$$

and it is simplified as

$$\frac{\partial T}{\partial \bar{t}} = k \frac{\partial^2 T}{\partial x^2} + \Theta_E, \tag{2.25}$$

where $k = \frac{\omega}{\rho c}$ is the thermal diffusivity.

It is now necessary to concentrate on the heat source Θ_E, where $\Theta = \frac{1}{\rho} Q$. It should be remembered that the mathematical theory of combustion, especially in the case of combustible stockpile in a reactive slab, deals with combined system of equations of chemical kinetics, of heat transfer and diffusion. The reaction rate, as mentioned in chapter 1, is dependable also on the temperature in a nonlinear fashion given by Arrhenius equation. In this case, the heat source term describes the evolution of heat in a chemical reaction, and the rate at which heat is evolved depends exponentially on the temperature given by Arrhenius equation [26]. The heat source is therefore expressed as

$$\Theta_E = Q\boldsymbol{A}e^{-E/RT}, \tag{2.26}$$

where Q is the heat of reaction, E is the activation energy, R is the gas constant, $\boldsymbol{A}$ is the pre-exponential factor and T is the temperature. Equation (2.25) is now expressed as

$$\frac{\partial T}{\partial \bar{t}} = k\frac{\partial^2 T}{\partial x^2} + Q\boldsymbol{A}e^{-E/RT}. \tag{2.27}$$

It should be noted that equations (2.26) and (2.29) will take appropriate forms in the next chapters for the purpose of this study.

It is also possible to reduce the species transport equation to the form which is similar to heat transfer equation as shown by equation (2.27). For diffusion of gases in this case of exothermic reaction, the components oxygen and carbon dioxide differ in molecular weight, but for convenience, their diffusion coefficients can be regarded as equal to their thermal diffusivity [4]. In the case of reacting species, the pre-exponential factor $\boldsymbol{A}$ of the reaction rate is thought of as depending on the concentration of the reactant species. Using equation (2.24) and considering a 1-D set up as for the heat equation, the following expression is attained

$$\frac{\partial C}{\partial \bar{t}} = \psi\frac{\partial^2 C}{\partial x^2} + Q_A. \tag{2.28}$$

Q_A the source of reaction rate, is also described by the Arrhenius equation as in the case of rate of heat evolution case. Therefore

$$Q_A = Ae^{-E/RT}, \tag{2.29}$$

and it should be noted that the heat of reaction Q is excluded in the case of diffusion of species. Substituting equation (2.29) into equation (2.28) the following equation is obtained

$$\frac{\partial C}{\partial \bar{t}} = \psi\frac{\partial^2 C}{\partial x^2} + Ae^{-E/RT}. \tag{2.30}$$

A 1-D set up for the species transport equation can be written, in general form, as

$$\frac{\partial C}{\partial \bar{t}} = \psi \frac{\partial^2 C}{\partial x^2} \pm Ae^{-E/RT}. \quad (2.31)$$

The plus sign is associated with products of the reaction whereas the minus sign is associated with initial reactants. In this case, the oxygen depletion equation will be associated with the minus sign and the carbon dioxide emission one with the positive sign.

2.5 Boundary and initial conditions

2.5.1 Boundary conditions

According to Newton's Law of Cooling, the rate of change of temperature of an object is proportional to the difference between its own temperature and the ambient temperature [23]. Taking into consideration the left boundary of the slab at $\bar{y} = 0$, Newton's Law can be summarized as follows

$$the\ outward\ flux\ of\ heat = h[T(0, \bar{t}) - T_0], \quad (2.32)$$

where h is heat exchange/transfer coefficient, and it is a measure of how many calories flow across the boundary per unit temperature difference per second per cm. If we assume the slab to be insulated at the surface where $\bar{y} = 0$, then $h = 0$, because there is no heat exchange at the point. The outward flux is the number of calories crossing the end of the slab per second. At the right end of the slab where $\bar{y} = a$, Newton's Law of Cooling is also summarized as

$$the\ outward\ flux\ of\ heat = h[T(a, \bar{t}) - T_a] \quad (2.33)$$

At this point $h \neq 0$, if we assume that the boundary is not insulated. As a result there is heat exchange between the end on the right and the surrounding.

To formulate the boundary conditions, equations (2.32) and (2.33) are used together with Fourier's Law of Cooling which states thus, "the outward flux of heat across a boundary is

proportional to the inward normal derivative across the boundary" [23]. In simpler terms, the law is expressed as follows

$$\left.\begin{array}{l} the\ outward\ flux\ of\ heat\ (at\ \bar{y}=0)\ = k\frac{\partial T}{\partial \bar{y}}(0,t) \\ the\ outward\ flux\ of\ heat\ (at\ \bar{y}=a) = -k\frac{\partial T}{\partial \bar{y}}(a,t) \end{array}\right\} \quad (2.34)$$

where k is the thermal conductivity of the slab. k is also a measure of how well the slab conducts heat. At $\bar{y}=a$ the derivative is negative to indicate that heat flux flows from left to right. In other words, $\frac{\partial T}{\partial x}(a,t) < 0$ and this implies that the temperature decreases.

Combination of equations (2.32) and (2.33) with (2.34) yields the following equations:

$$\left.\begin{array}{c} \frac{\partial T}{\partial \bar{y}}(0,\bar{t})\ = 0 \\ \frac{\partial T}{\partial \bar{y}}(a,\bar{t}) = -\frac{h_1}{k}[T(a,\bar{t})-T_a] \end{array}\right\} \quad (2.35)$$

For convenience sake, $h = h_1$. Equations (2.35) are called boundary conditions of the second and third types respectively.

The temperature distribution equation is of second order and for a moment, consideration of a steady state condition, it can be noticed that integrating $\frac{d^2T}{d\bar{y}^2}$ twice yields $T = b\bar{y} + c$, where b and c are constants of integration. To evaluate these constants, boundary conditions of the first kind specifying T at $\bar{y}=0$ and $\bar{y}=a$ respectively being $T(0)=T_1$ and $T(a)=T_2$, are used. The boundary condition $T(0)$ implies that $c = T_1$, and $T(a)$ implies that $T_2 = b \times a + T_1$, so that $T = \left(\frac{T_2-T_1}{a}\right)\bar{y} + T_1$. Since T_2 is less than T_1, plotting T against $\bar{y}$ will give a linear graph with a negative slope. The following diagram illustrates the plot under discussion.

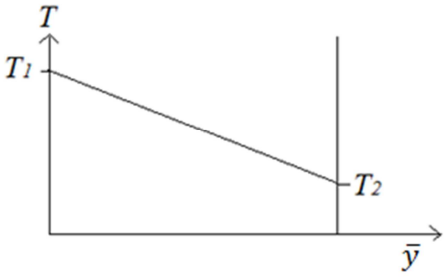

Figure 2.6: Temperature distribution through a slab

The figure above illustrates the temperature gradient in a slab from left to right.
Boundary conditions for diffusion of species are described in a similar manner to the temperature distribution case. The boundary conditions for oxygen depletion in a slab are described as follows,

$$\left.\begin{aligned} \frac{\partial C}{\partial \bar{y}}(0,\bar{t}) &= 0 \\ \frac{\partial C}{\partial \bar{y}}(a,\bar{t}) &= -\frac{h_2}{D}[C(a,\bar{t}) - C_a] \end{aligned}\right\} \tag{2.36}$$

where D is the diffusivity of oxygen, C is its depletion concentration, C_a is its ambient concentration and h_2 is the coefficient of oxygen transfer between the slab and the surrounding air. It follows that boundary conditions for carbon dioxide emission are thus

$$\left.\begin{aligned} \frac{\partial P}{\partial \bar{y}}(0,\bar{t}) &= 0 \\ \frac{\partial P}{\partial \bar{y}}(a,t) &= -\frac{h_3}{\gamma}[P(a,\bar{t}) - P_a] \end{aligned}\right\} \tag{2.37}$$

where γ is the diffusivity of carbon dioxide, P is its emission concentration, P_a is its ambient concentration and h_3 is the coefficient of carbon dioxide transfer between the slab and its surrounding air.

2.5.2 Initial conditions

It should be taken into consideration that all physical processes start at some value of time $\bar{t} = 0$. It is necessary to specify some physical condition at this time. Experiments based on temperature

distribution in a material, show that at some time $\bar{t}$, a constant temperature T_0 may be achieved [23]. The initial condition in a slab can be represented as

$$T(\bar{y}, 0) = T_0, \qquad 0 \leq \bar{y} \leq a.$$

The initial conditions for oxygen depletion and carbon dioxide emission are described similarly. They are respectively stated as

$$C(\bar{y}, 0) = C_0, \qquad 0 \leq \bar{y} \leq a,$$

and

$$P(\bar{y}, 0) = 0, \qquad 0 \leq \bar{y} \leq a.$$

T_0 is the initial temperature of the slab, C_0 is the initial concentration of oxygen in the slab.

2.6 Conclusion

Three governing nonlinear partial differential equations were derived together with boundary and initial conditions. Modified governing equations which are dimensionless will be used in the next chapters for investigations. It should be noted that the heat source and reaction rate source expressions will take appropriate forms also as will be shown by equations expressions.

Chapter 3

Numerical investigation into CO_2 Emission, O_2 Depletion and Thermal Decomposition in a Reacting Slab.

An investigation into carbon dioxide emission, oxygen depletion and thermal decomposition in a slab of reactive material is looked at in this chapter. Studies have shown that the emission of carbon dioxide is always coupled with the depletion of oxygen and the thermal decomposition in a reactive stockpile of combustible material. An example of stockpile of reactive combustible material is fossil fuels which include, among others, coal, oil, and natural gas. It is assumed that the surface of the slab is subjected to a symmetrical convective heat and mass exchange with the surrounding environment. A nonlinear mathematical model for estimating the carbon dioxide emission, oxygen depletion and thermal stability of a reacting slab is presented in this chapter. The model is then tackled using a semi-implicit finite-difference scheme. Numerical and graphical solutions are presented and discussed quantitatively with respect to various parameters embedded in the problem.

3.1 Introduction

The emission of carbon dioxide CO_2 is closely associated with oxygen O_2 depletion and thermal decomposition in a reacting slab. It is also understood that proper assessment of the emission levels provides a crucial reference point for other assessment tools like climate change indicators and mitigation strategies. In this chapter, a nonlinear mathematical model for estimating the CO_2 emission, O_2 depletion, and thermal stability of a reacting slab is presented and tackled numerically using a semi-implicit finite difference scheme. It is assumed that the slab surface is subjected to a symmetrical convective heat and mass exchange with the ambient. Both numerical and graphical results are presented.

Studies relating to transient heating of combustible material due to exothermic oxidation chemical reactions are extremely important and have a wide range of application in industry, engineering, and environmental science [7]. For example, fossil fuel such as coal, oil, and

natural gas, account for 85% of world's primary energy supply, 70% of world's electricity and heat generation and over 94% of energy for transportation [72]. The production and use of these combustible materials contribute up to 80% of CO_2 emission. Given expected increase in global population, economic growth, and energy demand, a continuous rise in emissions is expected unless fundamental technology changes occur in global energy systems which are currently dominated by fossil fuels. The CO_2 pollution is the principal human cause of global warming and climate change [26]. Meanwhile, for proper assessment of the CO_2 emission and O_2 depletion levels together with their impact on both the environment and life on Earth, knowledge of the mathematical models of these complex chemical systems is essential. These provide crucial reference points for other assessment tools like thermal stability of the materials, climate change indicators, and mitigation strategies. It may also help in developing medium to long-term action plans for climate change research and reliable design of the system [19].

An extensive review of detailed chemical kinetic models for the heating-up of combustible material is given by Simmie [70] and it was discussed in chapter one. Simmie's review considered post-1994 work and focuses on the modeling of hydrocarbon fuel oxidation in the gas phase by detailed chemical kinetics and those experiments which validate them. Moreover, thermal combustion analysis has received much attention in the literature [5, 47, 72]. Several studies have been directed towards obtaining critical condition for thermal ignition to occur in the form of a critical value for the Frank-Kamentskii parameter [26]. As discussed in chapter one, usually, chemical processes include many, up to a several hundred, intermediate elementary reactions [9]. For example, in combustion science, it is very common to use complex multistep reaction mechanism to predict the oxidation on hydrocarbons [75]. However, the use of one-step decomposition kinetics clearly simplifies the complicated chemistry involved in the problem but is both practical and necessary without additional information about the individual decomposition reaction steps [68, 77]. Meanwhile, analytical solutions of the partial differential equations governing transient heating of the combustible material undergoing oxidation reactions are usually impossible or extremely difficult to obtain. The exothermic nature of such reactions leads to complex nonlinear transient interaction of heat conduction, mass diffusion, and chemical reactions, as indicated in chapter two, resulting in steep concentration and temperature gradients [68]. In such circumstances, a better understanding of the system behavior can only be

accomplished by conducting numerical simulations to capture the frontal behavior of the processes.

The basic objective in this chapter, as mentioned earlier, is to provide a numerical estimate for the thermal stability together with the rate of CO_2 emission and O_2 depletion in transient heating of a slab of combustible material in the presence of convective heat and mass exchange with the ambient at the slab surface. The mathematical formulation of the problem is established in section 3.2. In section 3.4, the semi-implicit finite difference technique is implemented to tackle the problem. Numerical and graphical solutions are presented and discussed with respect to various parameters embedded in the system. This is done in section 3.5, followed by the conclusion.

3.2 Mathematical Model

A stockpile of combustible material in a rectangular slab is considered in this chapter. It is assumed that the slab is undergoing an n^{th} order oxidation chemical reaction and that the surfaces of the slab are also assumed to be subjected to boundary conditions. The following figure illustrates the set up for the study:

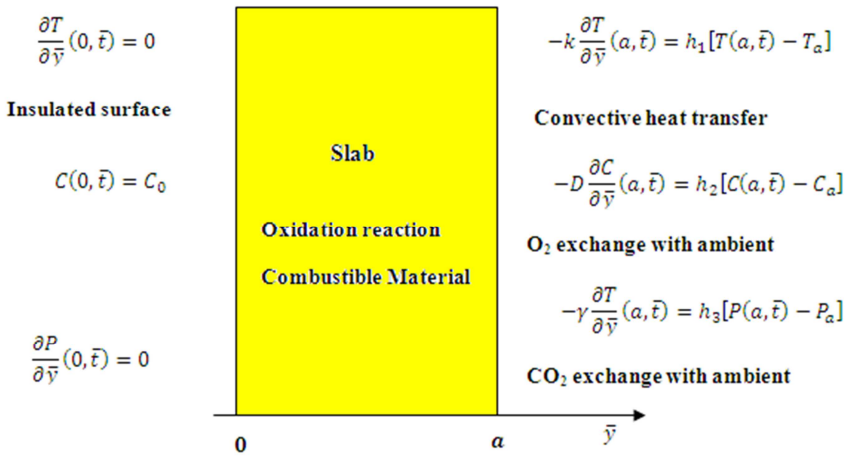

Figure 3.1: Geometry of the problem

Another assumption is that one of the surfaces is insulated while the other one is subjected to convective heat and mass exchange with the ambient. The complicated chemistry involved in this problem is simplified by assuming a one-step finite-rate irreversible reaction between the combustible material and the air oxygen.

Following Bebernes & Eberly [7], Koriko & Omowaye [40], Makinde [47], Simmie [70], Warnatz et al [75], and Williams [77] the nonlinear partial differential equations describing temperature, oxygen and carbon dioxide concentration in the combustible material can be written as

$$\begin{aligned} \rho c_p \frac{\partial T}{\partial \bar{t}} &= k \frac{\partial^2 T}{\partial \bar{y}^2} + QA\left(\frac{KT}{vl}\right)^m (C - C_0)^n exp\left(\frac{-E}{RT}\right), \\ \frac{\partial C}{\partial \bar{t}} &= D \frac{\partial^2 C}{\partial \bar{y}^2} - A\left(\frac{KT}{vl}\right)^m (C - C_0)^n exp\left(\frac{-E}{RT}\right), \\ \frac{\partial P}{\partial \bar{t}} &= \gamma \frac{\partial^2 P}{\partial \bar{y}^2} + A\left(\frac{KT}{vl}\right)^m (C - C_0)^n exp\left(\frac{-E}{RT}\right), \end{aligned} \tag{3.1}$$

with initial and boundary conditions as follows:

$$\begin{aligned} T(\bar{y}, 0) = T_0, \quad C(\bar{y}, 0) = \frac{1}{2} C_a, \quad P(\bar{y}, 0) = 0, \\ \frac{\partial T}{\partial \bar{y}}(0, \bar{t}) = \frac{\partial C}{\partial \bar{y}}(0, \bar{t}) = \frac{\partial P}{\partial \bar{y}}(0, \bar{t}) = 0, \\ -k \frac{\partial T}{\partial \bar{y}}(a, \bar{t}) = h_1[T(a, \bar{t}) - T_a], \\ -D \frac{\partial C}{\partial \bar{y}}(a, \bar{t}) = h_2[C(a, \bar{t}) - C_a], \\ -\gamma \frac{\partial P}{\partial \bar{y}}(a, \bar{t}) = h_3[P(a, \bar{t}) - P_a], \end{aligned} \tag{3.2}$$

where T is the absolute temperature, C is the oxygen concentration, P is the carbon dioxide emission concentration, T_a is the ambient temperature, C_a is the oxygen concentration in the surrounding air, P_a is the carbon dioxide concentration in the surrounding air, $\bar{t}$ is the time, T_0 is the slab initial temperature, C_0 is the initial concentration of oxygen in the slab, ρ is the density, c_p is the specific heat at constant pressure, k is the thermal conductivity of the reacting slab, D is the diffusivity of oxygen in the slab, γ is the diffusivity of carbon dioxide in the slab, Q is the exothermicity, A is the rate constant, E is the activation energy, R is the universal gas constant, l is the Planck number, v is the vibration frequency, K is the Boltzmann constant, a is the slab half

width, $\bar{y}$ is the distance measured transverse direction, h_1 is the coefficient of heat transfer between the slab and its surroundings, h_2 is the coefficient of oxygen transfer between the slab and its surroundings, h_3 is the coefficient of carbon dioxide transfer between the slab and its surroundings, n is the order of exothermic chemical reaction, and m is the numerical exponent such that $m \in \{-2,0,0.5\}$. The three values taken by the parameter m represent the numeric exponent for sensitized, Arrhenius and Bimolecular kinetics, respectively, as indicated by Bebernes & Eberly [7] and Makinde [47].

3.3 Introduction of Dimensionless Parameters

The benefit of introducing dimensionless parameters is that many of the physical parameters can be combined into a smaller number of dimensionless parameters that describe a particular phenomenon of interest [54]. Dimensionless parameters help also to reduce the partial differential equations into a form that can be easily solved using numerical methods. The following dimensionless variables are introduced into equations (3.1 –3.2):

$$\left.\begin{gathered}\theta = \frac{E(T-T_0)}{RT_0^2},\ \ \theta_a = \frac{E(T_a-T_0)}{RT_0^2},\ \ \Phi = \frac{C-C_0}{C_a-C_0},\ \ \Psi = \frac{P}{P_a},\\ \mathrm{Bi}_1 = \frac{ah_1}{k},\ \mathrm{Bi}_2 = \frac{ah_2}{D},\ \ \mathrm{Bi}_3 = \frac{ah_3}{\gamma},\\ \beta_1 = \frac{\rho c_p RT_0^2}{QE(C_a-C_0)}, \beta_2 = \frac{\rho c_p RT_0^2}{QEP_a},\quad \lambda = \left(\frac{KT}{vl}\right)^m \frac{QAEa^2(C_a-C_0)^n}{kRT_0^2} exp\left(\frac{-E}{RT}\right),\\ y = \frac{\bar{y}}{a},\ \ \bar{t} = \frac{kt}{c_p\rho a^2},\ \ \mu = \frac{RT_0^2}{E},\ \ \alpha = \frac{D\rho c_p}{k},\ \ \sigma = \frac{\gamma\rho c_p}{k},\end{gathered}\right\} \tag{3.3}$$

The dimensionless variables on (3.3) are introduced into equations (3.1)-(3.2) by first considering the temperature equation. The equation is made dimensionless for $\theta(y,t)$, by substituting dimensionless parameters into it to get the following

$$\frac{c_p\rho}{E}\frac{\partial(\theta RT_0^2+ET_0)}{\partial\left(\frac{c_p\rho a^2}{k}t\right)} = \frac{k}{E}\frac{\partial^2(\theta RT_0^2+ET_0)}{\partial(ya)^2} + QA\left(\frac{KT}{vl}\right)^m (C-C_0)^n e^{-E/RT} \tag{3.4}$$

Equation (3.4) can be simplified by taking out the constant parameters outside the derivatives, and knowing that the derivative of a constant is zero, means that, $\frac{E\partial T_0}{\partial t} = \frac{E\partial^2 T_0}{\partial y^2} = 0$, the following expression is obtained

$$c_p\rho RT_0^2\frac{k}{c_p\rho Ea^2}\frac{\partial\theta}{\partial t}=\frac{k}{Ea^2}RT_0^2\frac{\partial^2\theta}{\partial y^2}+QA\left(\frac{KT}{\upsilon l}\right)^m(C-C_0)^n e^{-E/RT}.$$

The $c_p\rho$ cancels each other so that the expression is

$$RT_0^2\frac{k}{Ea^2}\frac{\partial\theta}{\partial t}=\frac{k}{Ea^2}RT_0^2\frac{\partial^2\theta}{\partial y^2}+QA\left(\frac{KT}{\upsilon l}\right)^m(C-C_0)^n e^{-E/RT}, \tag{3.5}$$

and dividing through by $RT_0^2\frac{k}{Ea^2}$, equation (3.5) becomes

$$\frac{\partial\theta}{\partial t}=\frac{\partial^2\theta}{\partial y^2}+QA\left(\frac{KT}{\upsilon l}\right)^m\frac{Ea^2(C-C_0)^n}{kRT_0^2}e^{-E/RT}. \tag{3.6}$$

The second part of the right hand side of equation (3.6) contains physical constants that make the whole equation non-dimensionless. It is therefore necessary to introduce λ, Φ, θ and μ described under (3.3) above, to give the following dimensionless partial differential equation:

$$\frac{\partial\theta}{\partial t}=\frac{\partial^2\theta}{\partial y^2}+\lambda(1+\mu\theta)^m\Phi^n\exp\left(\frac{\theta}{1+\mu\theta}\right). \tag{3.7}$$

Similarly, governing partial differential equations for oxygen depletion and carbon dioxide emission are obtained respectively as follows:

$$\frac{\partial\Phi}{\partial t}=\alpha\frac{\partial^2\Phi}{\partial y^2}-\lambda\beta_1(1+\mu\theta)^m\Phi^n\exp\left(\frac{\theta}{1+\mu\theta}\right), \tag{3.8}$$

and

$$\frac{\partial\Psi}{\partial t}=\sigma\frac{\partial^2\Psi}{\partial y^2}+\lambda\beta_2(1+\mu\theta)^m\Phi^n\exp\left(\frac{\theta}{1+\mu\theta}\right). \tag{3.9}$$

In the same pattern, the corresponding initial and boundary conditions then become

$$\left.\begin{aligned}&\theta(y,0)=0,\quad \Phi(y,0)=0.5,\quad \Psi(y,0)=0,\\&\frac{\partial\theta}{\partial y}(0,t)=\frac{\partial\Phi}{\partial y}(0,t)=\frac{\partial\Psi}{\partial y}(0,t)=0,\\&\frac{\partial\theta}{\partial y}(1,t)=-\mathrm{Bi}_1[\theta(1,t)-\theta_a],\\&\frac{\partial\Phi}{\partial y}(1,t)=-\mathrm{Bi}_2[\Phi(1,t)-1],\\&\frac{\partial\Psi}{\partial y}(1,t)=-\mathrm{Bi}_3[\Psi(1,t)-1],\end{aligned}\right\} \tag{3.10}$$

where λ is the Frank-Kamenetskii parameter, μ is the activation energy parameter, β_1 is the oxygen consumption rate parameter, β_2 is the carbon dioxide emission rate parameter, α is the oxygen diffusivity parameter, σ is the carbon dioxide diffusivity parameter, Bi_1, Bi_2 and Bi_3 represent the thermal Biot number, oxygen Biot number and carbon dioxide Biot number respectively. It should be noted that a body of material releasing heat to its surroundings may achieve a safe steady state where the temperature of the body reaches some moderate value and stabilizes. However, when the rate of heat generation in the material exceeds the rate of heat loss to the surroundings, then ignition can occur.

3.4 Numerical Solution

The numerical algorithm is based on the semi-implicit finite difference scheme. The implicit terms are taken at the intermediate time level $(N + \xi)$ where $0 \leq \xi \leq 1$. The algorithm employed in this chapter uses $\xi = 1$ to allow the use of larger steps, and it is therefore possible to work with any value of the time step. The discretization of the governing equations is based on a linear Cartesian mesh and uniform grid on which finite differences are taken.

3.4.1 Semi-Implicit Finite Difference Method

Following the algorithm outlined in section 1.7.1, the semi-implicit finite difference scheme expressions for (3.17) – (3.19) are obtained as follows, by first considering the temperature equation:

$$\frac{\partial \theta}{\partial t} = \frac{\theta_i^{N+1} - \theta_i^N}{\Delta t}. \tag{3.11}$$

It follows that

$$\frac{\partial^2 \theta}{\partial y^2} = \xi \left(\frac{\theta_{i+1}^{N+1} - 2\theta_i^{N+1} + \theta_{i-1}^{N+1}}{(\Delta y)^2} \right) + (1 - \xi) \left(\frac{\theta_{i+1}^{N} - 2\theta_i^{N} + \theta_{i-1}^{N}}{(\Delta y)^2} \right), \tag{3.12}$$

so that equation of (3.7) becomes

$$\frac{\theta_i^{N+1}-\theta_i^N}{\Delta t}=\xi\left(\frac{\theta_{i+1}^{N+1}-2\theta_i^{N+1}+\theta_{i-1}^{N+1}}{(\Delta y)^2}\right)+(1-\xi)\left(\frac{\theta_{i+1}^{N}-2\theta_i^{N}+\theta_{i-1}^{N}}{(\Delta y)^2}\right)+$$

$$+\ \lambda\left[(1+\mu\theta_i)^m{\Phi_{\mathrm{i}}}^n\exp\left(\frac{\theta_i}{1+\mu\theta_i}\right)\right]^N. \qquad (3.13)$$

Boundary conditions have the following finite difference expressions

$$\frac{1}{\Delta y}(\theta_{i+1}^N-\theta_{i-1}^N)=0\Longrightarrow\theta_{i+1}^N=\theta_{i-1}^N,$$

and

$$\frac{1}{\Delta y}(\theta_{i+1}^N-\theta_{i-1}^N)=-\frac{h_1}{k}[\theta_i^N-\theta_{\mathrm{a}}]\Longrightarrow-\theta_i^N\ =\frac{1}{\Delta y}\frac{k}{h_1}(\theta_{i+1}^N-\theta_{i-1}^N)-\theta_a,$$

$$\Rightarrow-\theta_i^N\ =\frac{1}{\Delta y}\frac{k}{h_1}(0)-\theta_a\ \ \therefore\ \theta_i^N=\theta_a.$$

Application of the boundary conditions, together with combining the left hand side and the first two terms on the right hand side of equation (3.13) results with the following equation

$$-\xi r\theta_{i+1}^{N+1}+(1+2\xi r)\theta_i^{N+1}-\xi r\theta_{i-1}^{N+1}=r(1-\xi)\theta_{i+1}^N+[1-2r(1-\xi)]\theta_i^N$$

$$+r(1-\xi)\theta_{i-1}^N$$

$$+\lambda\left[(1+\mu\theta_i)^m{\Phi_{\mathrm{i}}}^n\exp\left(\frac{\theta_i}{1+\mu\theta_i}\right)\right].^N \qquad (3.14)$$

Expressions for the oxygen depletion and carbon dioxide emission are given respectively as follows:

$$-\xi r\alpha\Phi_{i+1}^{N+1}+(1+2\xi r)\alpha\Phi_i^{N+1}-\xi r\alpha\Phi_{i-1}^{N+1}=r(1-\xi)\alpha\Phi_{i+1}^N+[1-2r(1-\xi)]\alpha\Phi_i^N+$$

$$+r(1-\xi)\alpha\Phi_{i-1}^N$$

$$-\lambda\Delta t\beta_1\left[(1+\mu\theta_i)^m{\Phi_{\mathrm{i}}}^n\exp\left(\frac{\theta_i}{1+\mu\theta_i}\right)\right]^N, \qquad (3.15)$$

and

$$-\xi r\sigma\Psi_{i+1}^{N+1} + (1+2\xi r)\sigma\Psi_{i}^{N+1} - \xi r\sigma\Psi_{i-1}^{N+1} = r(1-\xi)\sigma\Psi_{i+1}^{N} + [1-2r(1-\xi)]\sigma\Psi_{i}^{N}$$
$$+r(1-\xi)\sigma\Psi_{i-1}^{N}$$
$$+\lambda\Delta t\beta_2\left[(1+\mu\theta_i)^m\Phi_{\mathrm{i}}{}^n\exp\left(\frac{\theta_i}{1+\mu\theta_i}\right)\right]^N. \quad (3.16)$$

It should be noted that the three terms on the left hand side of each equation (3.14)-(3.16) are unknown and that the first three terms on the right hand side are known. This system of equations uses the weight parameter $\xi = 0.5$ which follows the Crank-Nicolson method. But in this study we consider $\xi = 1$ as mentioned above and we have $r = \frac{\Delta t}{(\Delta y)^2}$. The symbolic form of the semi-implicit formula is illustrated by the figure 1.12 under section 1.6.1.

The system of linear equations resulting from each equation (3.14)-(3.16) forms a tridiagonal system, which is solved using tridiagonal matrices as discussed under section 1.7.1.
The semi-implicit schemes for temperature, oxygen concentration and carbon dioxide concentration are respectively represented by:

$$\left.\begin{aligned}
\frac{\theta^{(N+1)}-\theta^{(N)}}{\Delta t} &= \frac{\partial^2}{\partial y^2}\theta^{(N+\xi)} + \lambda\left[(1+\mu\theta)^m\Phi^{\mathrm{n}}\exp\left(\frac{\theta}{1+\mu\theta}\right)\right]^{(N)},\\
\frac{\Phi^{(N+1)}-\Phi^{(N)}}{\Delta t} &= \alpha\frac{\partial^2}{\partial y^2}\Phi^{(N+\xi)} - \lambda\beta_1\left[(1+\mu\theta)^m\Phi^{\mathrm{n}}\exp\left(\frac{\theta}{1+\mu\theta}\right)\right]^{(N)},\\
\frac{\Psi^{(N+1)}-\Psi^{(N)}}{\Delta t} &= \sigma\frac{\partial^2}{\partial y^2}\Psi^{(N+\xi)} + \lambda\beta_2\left[(1+\mu\theta)^m\Phi^{\mathrm{n}}\exp\left(\frac{\theta}{1+\mu\theta}\right)\right]^{(N)}.
\end{aligned}\right\} \quad (3.17)$$

Equations (3.14) to (3.16) can be represent by $\theta^{(N+1)}$, $\Phi^{(N+1)}$ and $\Psi^{(N+1)}$ respectively, and their graphical solutions are given in the following section.

3.5 Results and Discussion

The following parameter values were employed to give graphical solutions:

$$\begin{aligned}
&m = 0.5, \quad n = 1, \quad \theta_a = 0.1, \quad \alpha = 1, \quad \sigma = 1,\\
&\beta_1 = 1, \quad \beta_2 = 1, \quad \mathrm{Bi}_1 = 1, \quad \mathrm{Bi}_2 = 1, \quad \mathrm{Bi}_3 = 1,\\
&\mu = 0.1, \quad \Delta y = 0.01, \quad \Delta t = 1, \quad t = 200.
\end{aligned} \quad (3.18)$$

These will be the default values for the work in this chapter, therefore in any graph where any of these parameters is not explicitly mentioned, it will be understood that such parameters take on the default values.

3.5.1 Transient and Steady Flow Profiles

In this section we first consider the transient solutions which are given graphically and discussed accordingly.

Figure 3.2 shows a transient increase in temperature until a steady-state is reached. A similar scenario is obtained in figure 3.4 in which a transient increase in carbon dioxide emission is observed until a steady state is reached. An opposite situation is noticed in figure 3.3 where a decrease in oxygen concentration is observed with increasing time until a steady state concentration is attained. These results are consistent with intuition regarding exothermic oxidation reactions.

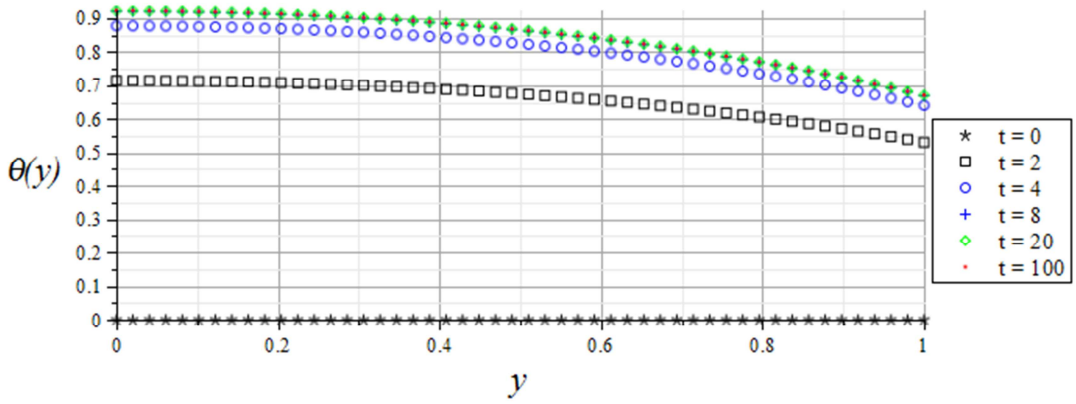

Figure 3.2: Transient and steady state slab temperature profiles

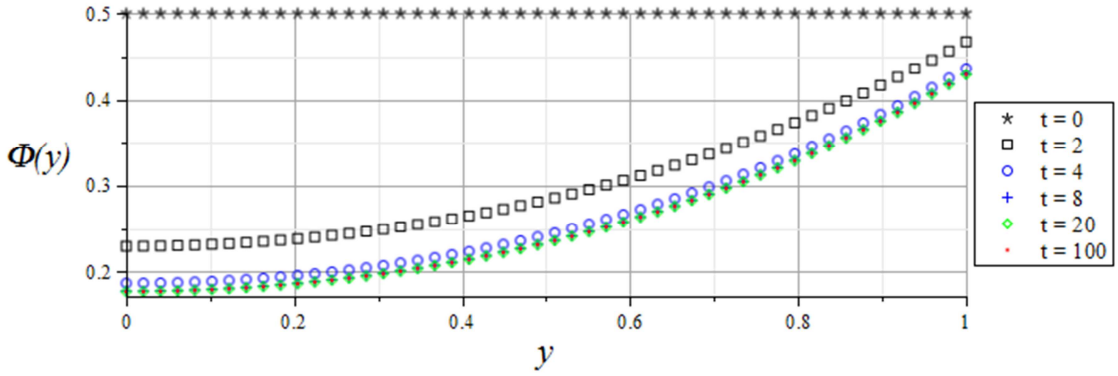

Figure 3.3: Transient and steady state slab oxygen profiles

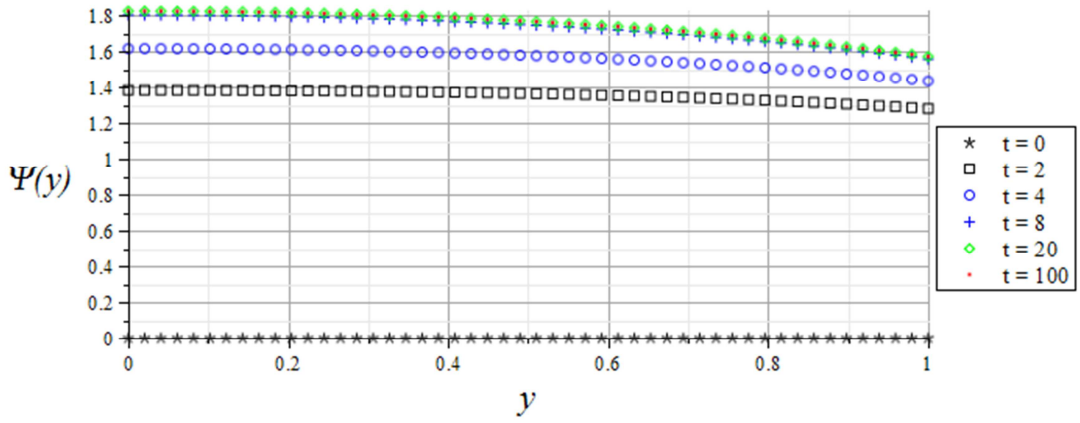

Figure 3.4: Transient and steady state slab carbon dioxide profiles

3.5.2 3-D Transient and Steady Flow Profiles

Figures 3.5 to 3.7 show three dimensional temperature distribution, oxygen depletion and carbon dioxide emission respectively. It is easy to observe from figures 3.5 and 3.7 that both temperature and carbon dioxide profiles increase and that the steady state in both cases is achieved as time *t* increases. From figure 3.6 we can see a decline on the oxygen profiles, and that the steady state is also attained as *t* increases.

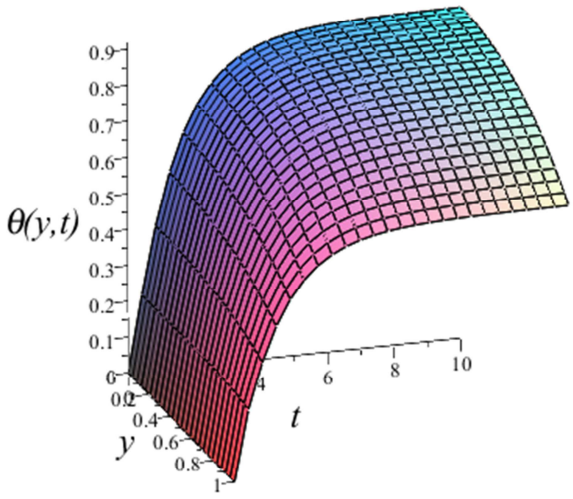

Figure 3.5: 3-D Transient and steady state slab temperature profiles

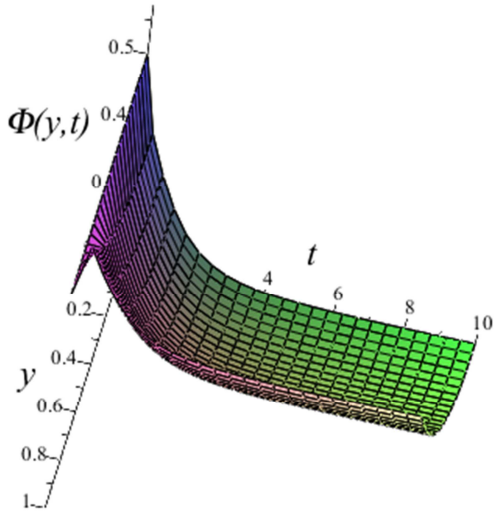

Figure 3.6: 3-D Transient and steady state slab oxygen profiles

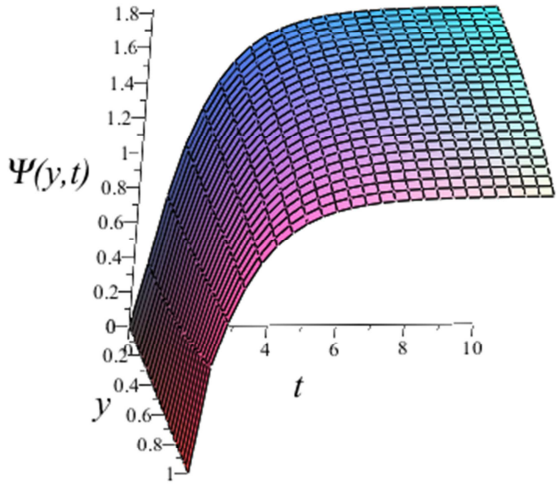

Figure 3.7: 3-D Transient and steady state slab carbon dioxide profiles

3.5.3 Parameter Dependence of Solutions in Steady State

In this subsection, the dependence of solutions in steady state on parameters is looked at. It was seen from results above that the solutions reached steady state at times $t > 4$. The solutions given in this sub-section are given at $t = 200$, and are understood to be steady state solutions.

3.5.3.1 Effects of parameters on temperature

Figures 3.8 to 3.15 show dependence of temperature on parameters. It should be understood that parameters that are not mentioned show no effect on temperature. We observe from figure 3.8 that increasing *n* the order of reaction reduces the temperature profiles. In figure 3.9 an opposite situation is observed which shows how the temperature is affected by the following types of exothermic oxidation reactions, sensitized (m = -2), Arrhenius (m = 0) and biomolecular (m = 0.5). We see that the temperature profiles increase with the numerical exponent m. The temperature is low at m = -2, and highest during bimolecular reactions at m = 0.5. Effect of Bi_1 on temperature is illustrated by figure 3.10 from which we observe that temperature profiles decrease with increasing Bi_1. We see a different scenario from figure 3.11 where the temperature increases as Bi_2 increases. The increased oxygen in the slab increases the oxidation reaction

which results in temperature rise. Figure 3.12 shows the effect of λ on temperature. The observation is that an increase in λ shows a corresponding increase in temperature. In other words the rate of reaction increases the exothermic reaction which results in temperature rise. The oxygen consumption rate β_1 shows that temperature profiles decrease as β_1 is increased as illustrated by figure 3.13 and opposite to this observation we see that figure 3.14 shows that increasing α the oxygen diffusivity parameter, the temperature also increases. More diffusion of oxygen accelerates the exothermic reaction within the slab and thus the rise in temperature. From figure 3.15 we see that increasing the activation energy parameter μ, gives a decline in temperature parameters.

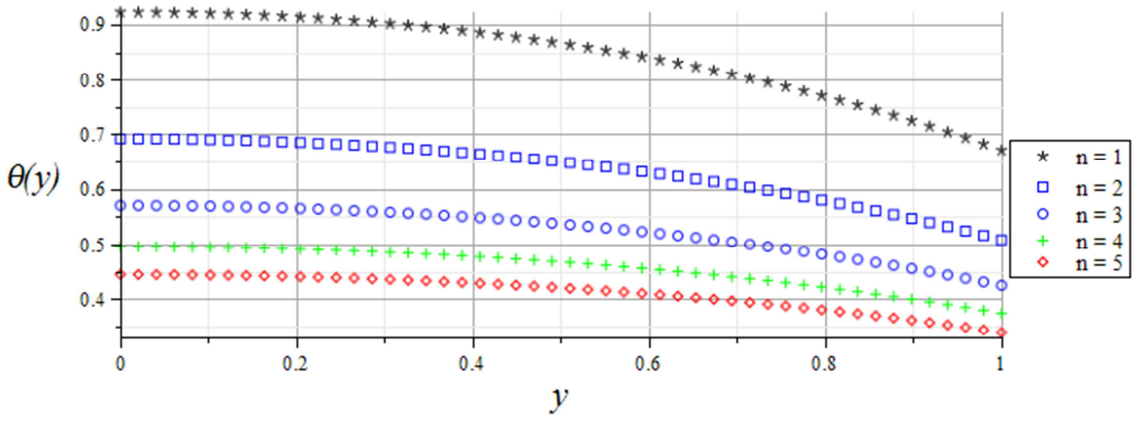

Figure 3.8: Effects of *n* on slab temperature profiles.

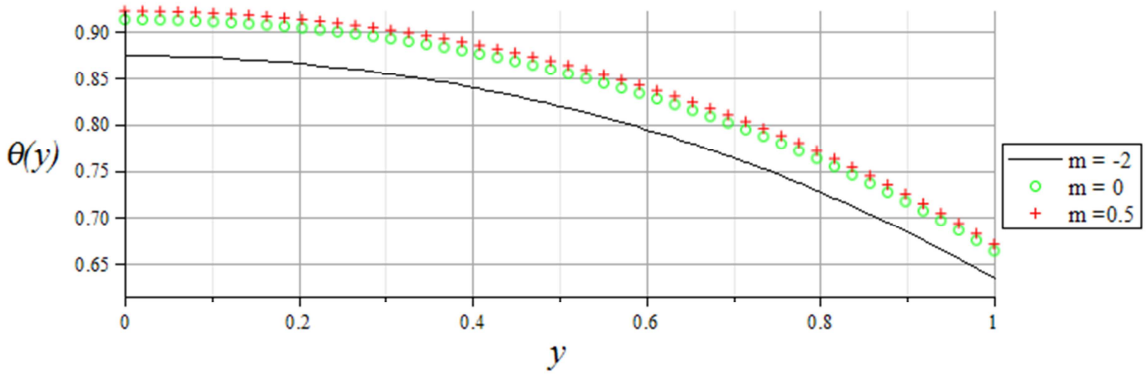

Figure 3.9: Effects of *m* on slab temperature profiles.

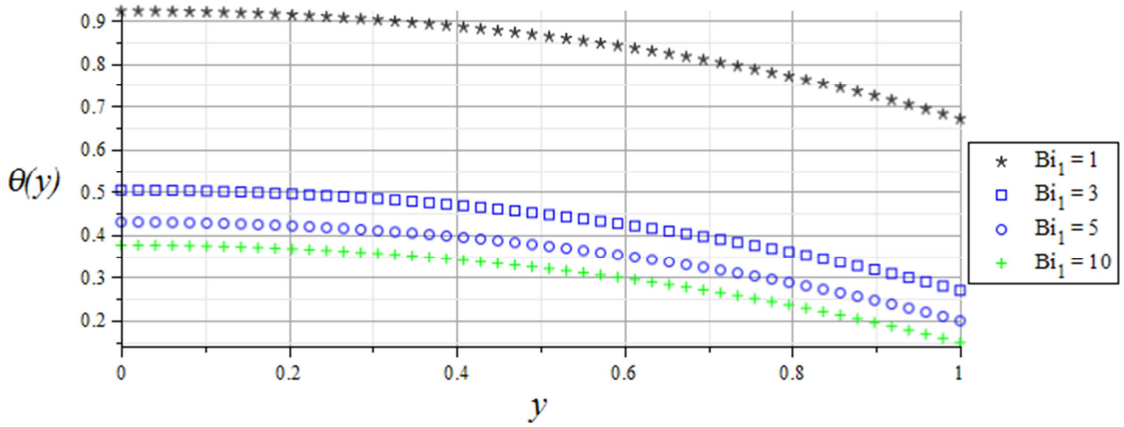

Figure 3.10: Effects of Bi_1 on slab temperature profiles.

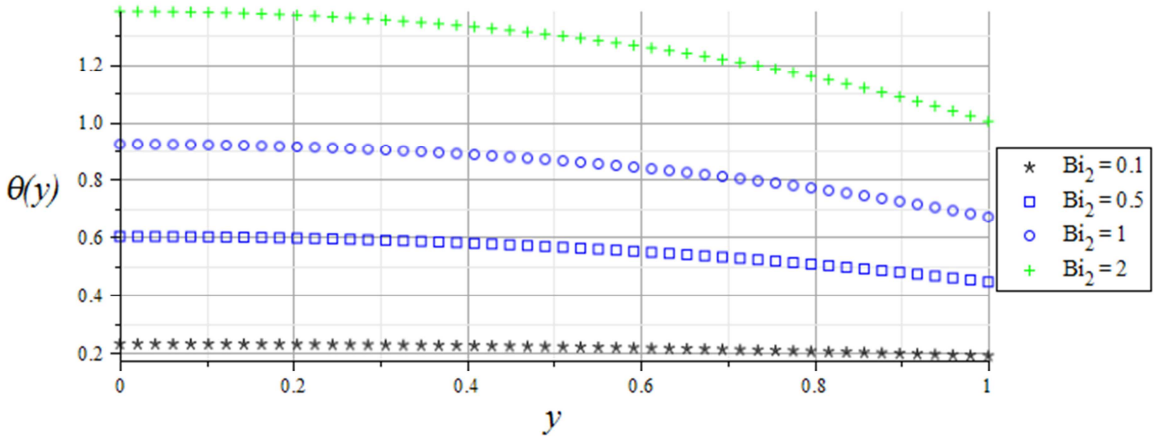

Figure 3.11: Effects of Bi_2 on slab temperature profiles.

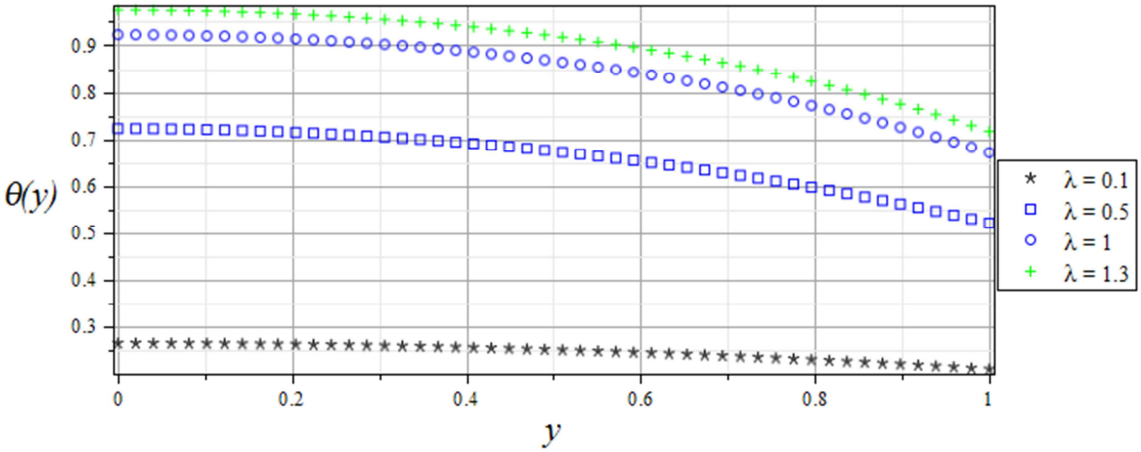

Figure 3.12: Effects of λ on slab temperature profiles.

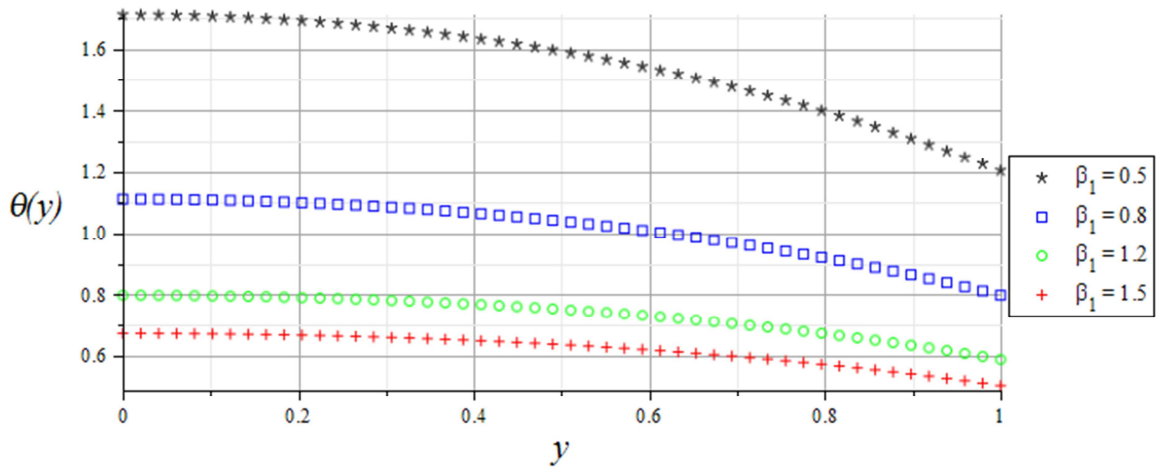

Figure 3.13: Effects of β_1 on slab temperature profiles.

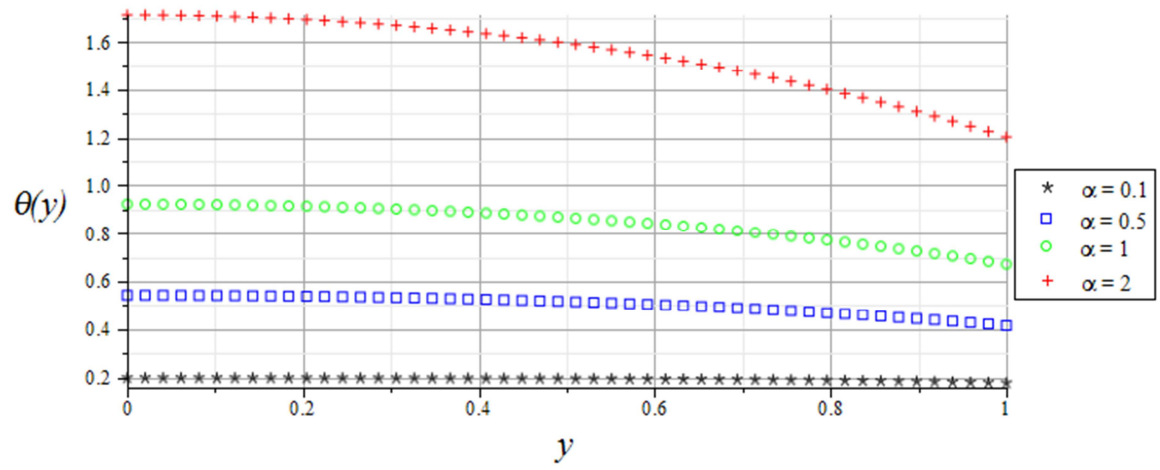

Figure 3.14: Effects of α on slab temperature profiles.

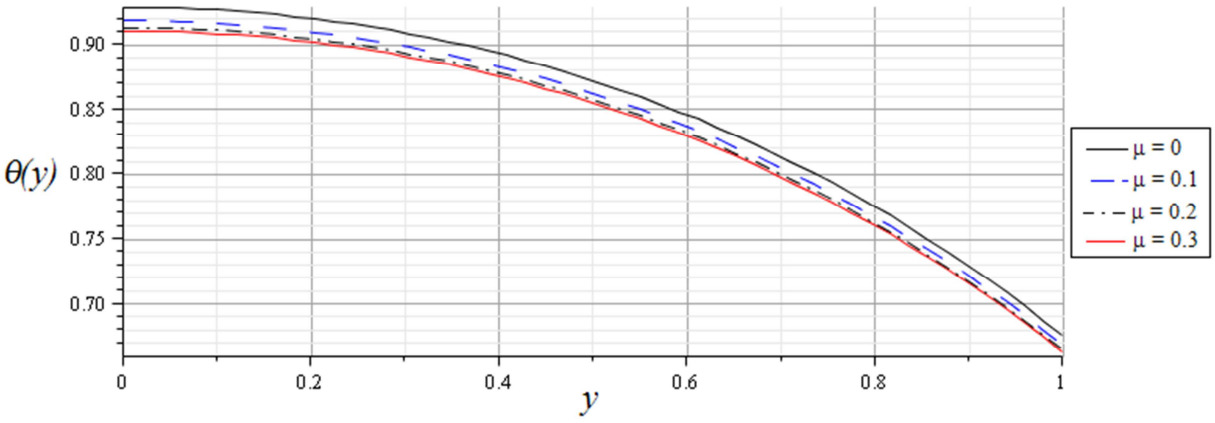

Figure 3.15: Effects of μ on slab temperature profiles.

3.5.3.2 Effects of parameters on oxygen

In this case we look at the effects of parameters on oxygen as illustrated by figures 3.16 to 3.23. It is interesting to investigate how some parameters facilitate the depletion of oxygen, while others help to conserve it during an exothermic reaction. From figure 3.16 we observe that as n increases, there is a corresponding increase in oxygen profiles. This means that the oxidation reaction is reduced and hence less consumption of oxygen corresponds to oxygen concentration increase. But, figure 3.17 shows that oxygen is depleted as m increases and that the depletion is high during bimolecular reactions. An opposite scenario is observed from figure 3.18 where an increase in Bi_1 shows corresponding increase in oxygen profiles, meaning little consumption thereof. This is also shown by figure 3.19 where an increase in Bi_2 increases oxygen concentration within the slab. Figure 3.20 shows the effect of λ on oxygen. We observe that increasing λ decreases the oxygen concentration during exothermic reaction and this means that oxygen is more depleted. We see the same situation in figure 3.21 that an increase in β_1 shows a decrease in oxygen profiles which also causes oxygen depletion. From figure 3.22 we observe that as α is increased a corresponding increase in oxygen profiles is achieved, and the same scenario is illustrated by figure 3.23 where the oxygen profiles increase with increasing μ. These last parameters favor the conservation of oxygen.

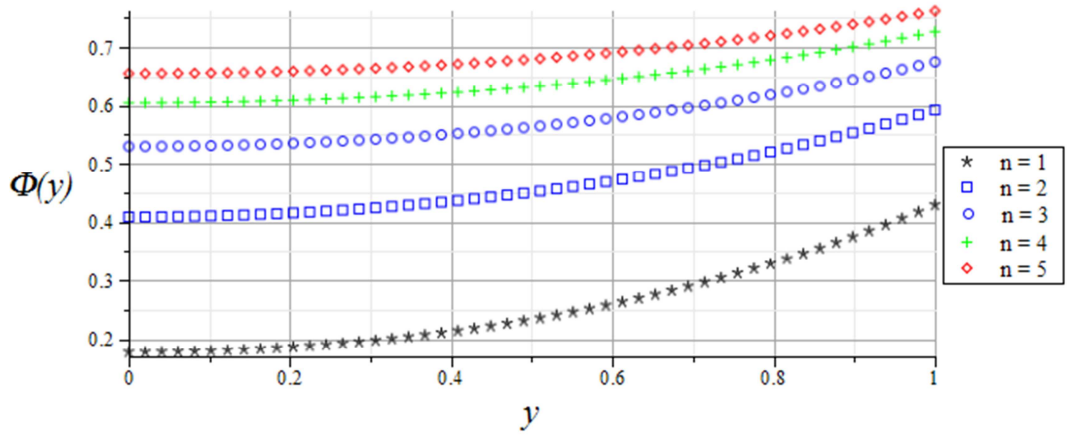

Figure 3.16: Effects of *n* on slab oxygen depletion profiles**.**

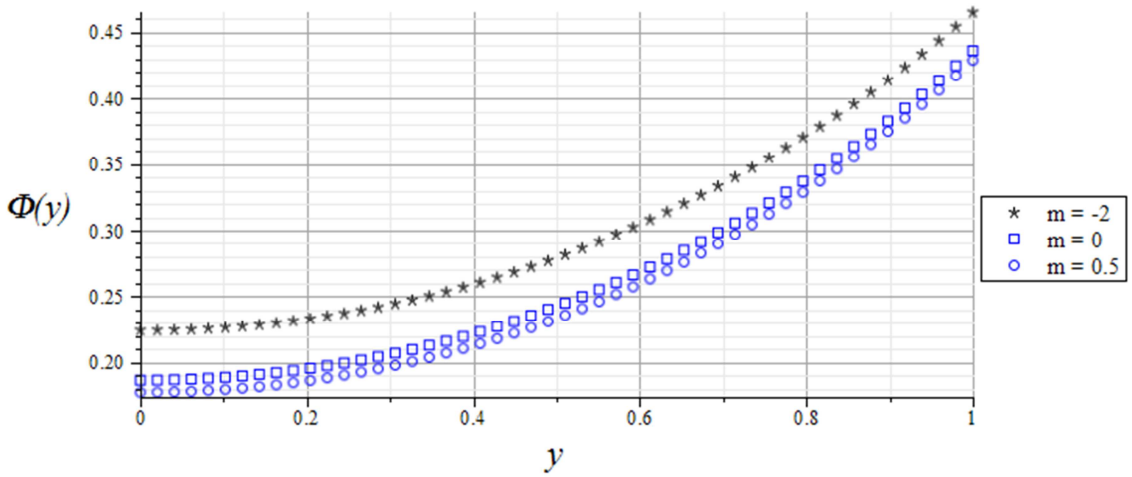

Figure 3.17: Effects of *m* on slab oxygen depletion profiles**.**

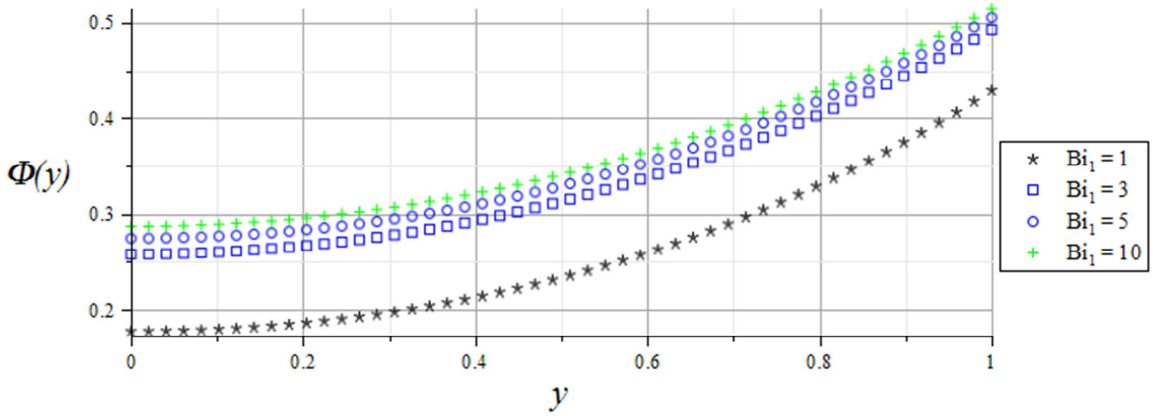

Figure 3.18: effects of Bi_1 on slab oxygen depletion profiles**.**

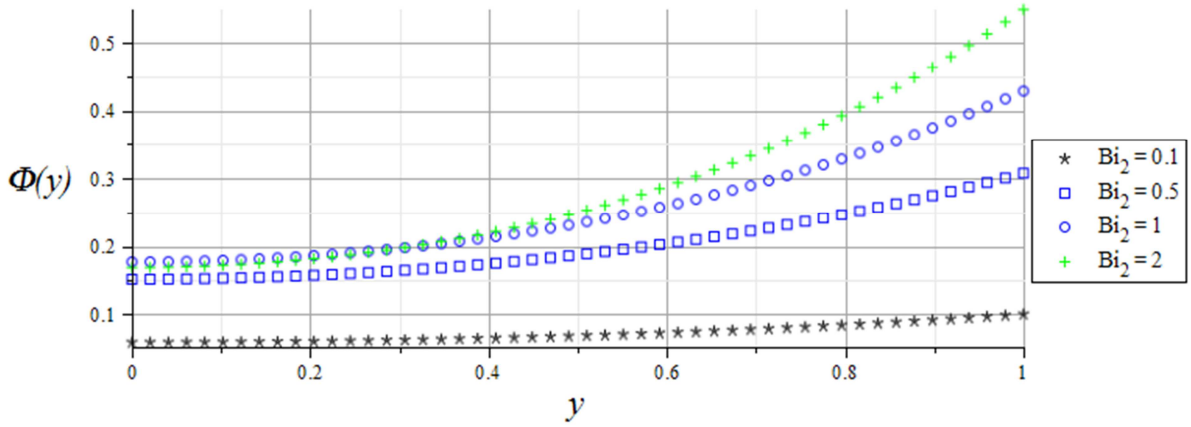

Figure 3.19: Effects of Bi_2 on slab oxygen depletion profiles**.**

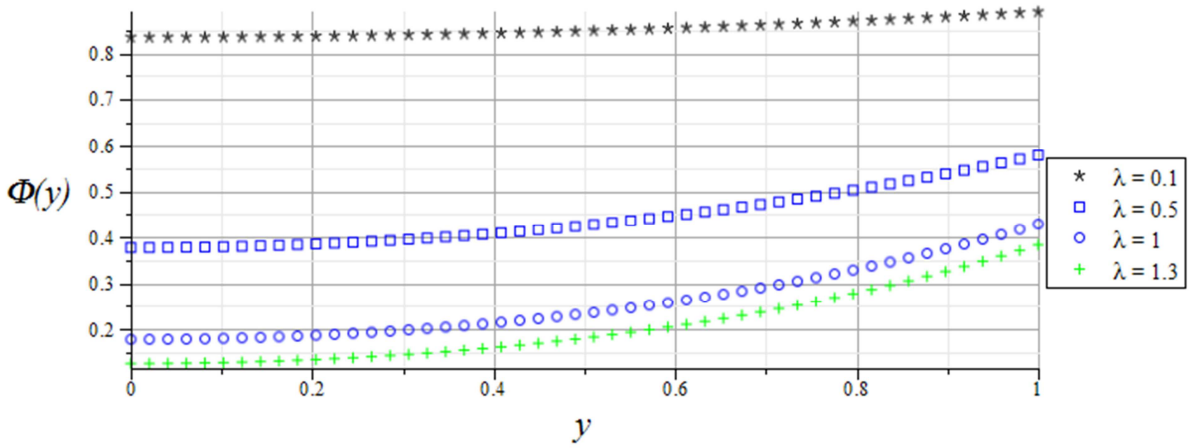

Figure 3.20: Effects of λ on slab oxygen depletion profiles.

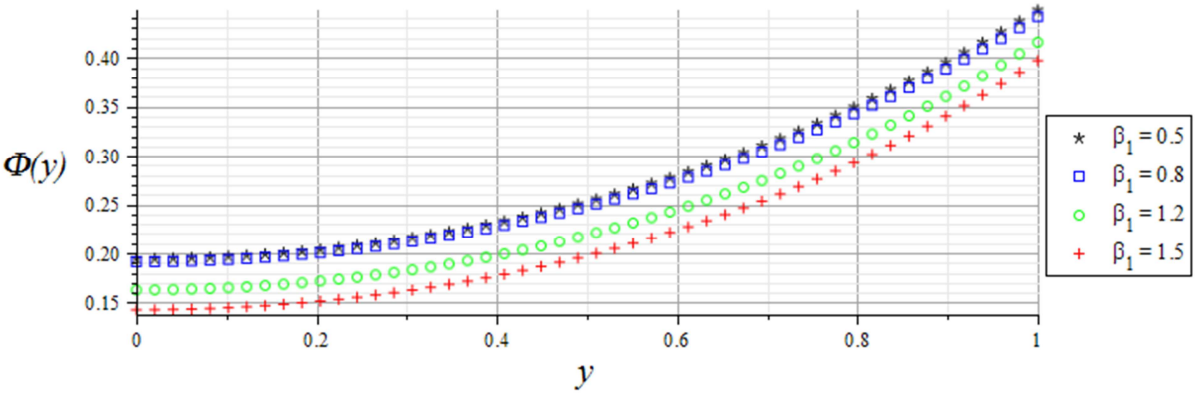

Figure 3.21: Effects of β_1 on slab oxygen depletion profiles.

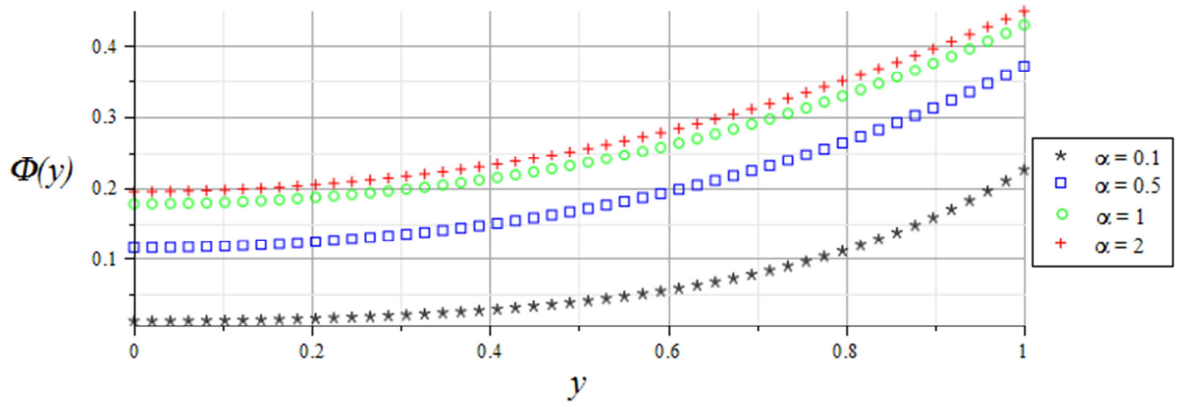

Figure 3.22: Effects of α on slab oxygen depletion profiles.

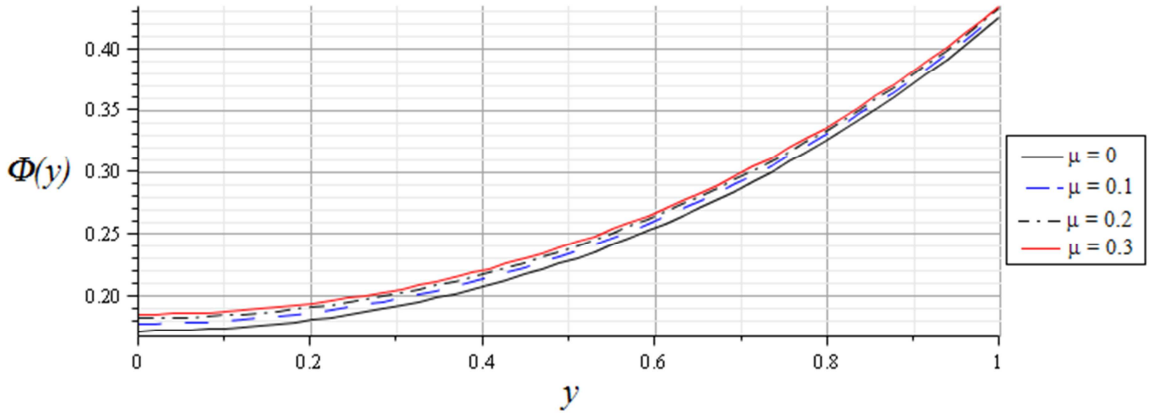

Figure 3.23: Effects of μ on slab oxygen depletion profiles.

3.5.3.3 Effects of parameters on carbon dioxide

We now consider how parameters can facilitate the emission of carbon dioxide in an exothermic reaction within a reactive slab of combustible material. This process is illustrated by figures 3.24 to 3.36. We observe from figure 3.24 that increasing *n* the order of reaction reduces the emission of carbon dioxide because of the decrease in profiles, and when the numerical exponent *m* is increased, we see corresponding increase in carbon dioxide profiles as illustrated by figure 3.25. A different scenario is observed in figure 3.26 where an increase in Bi_1 results with a decrease in carbon dioxide profiles. This is good for reducing carbon dioxide emission which affects the environment in a negative manner. From figure 3.27 we see that carbon dioxide profiles increase as Bi_2 is increased. This parameter increases the emission of the greenhouse gas. But it is interesting to see that the carbon dioxide Biot number Bi_3 reduces the emission of carbon dioxide

as illustrated by figure 3.28, and however, as observed in the temperature case, we see that increasing λ results with increase in carbon dioxide emission as shown by figure 3.29. The effects of β_1 and β_2 on carbon dioxide are illustrated by figures 3.30 and 3.31 respectively. In figure 3.30 an increase in β_1 decreases the concentration of carbon dioxide, whereas the increase in β_2 shows a corresponding increase in the greenhouse gas. We see the same situation in figure 3.32 as in figure 3.31 where an increase in α gives an increase in carbon dioxide emission. We observe the effect of σ, carbon dioxide diffusivity parameter, for the first time on carbon dioxide. It is also interesting to see that this parameter too, does not favor carbon dioxide emission as indicated by figure 3.33 where an increase in σ results with decrease in the greenhouse gas profiles. We see the same result, where carbon dioxide profiles also show a decrease as μ is increased as given by figure 3.34. This observation is experienced for small values of μ, but for higher values of μ, an increase in temperature and carbon dioxide emission profiles is observed. This means that when the activation energy is low, the exothermic chemical reaction is also ineffective and thus oxygen is not depleted which results with less slab's temperature and very little or no carbon dioxide emission.

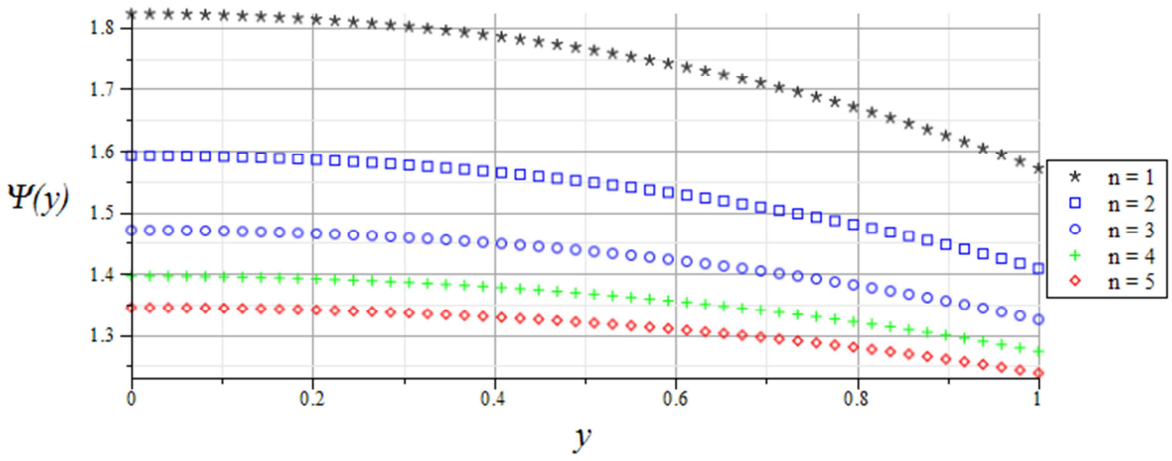

Figure 3.24: Effects of *n* on slab Carbon dioxide emission profiles.

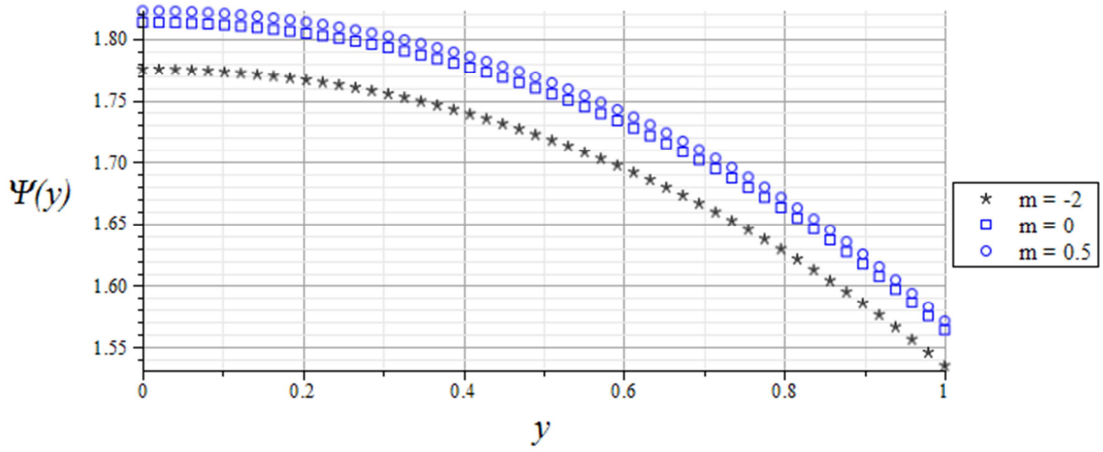

Figure 3.25: Effects of *m* on slab Carbon dioxide emission profiles.

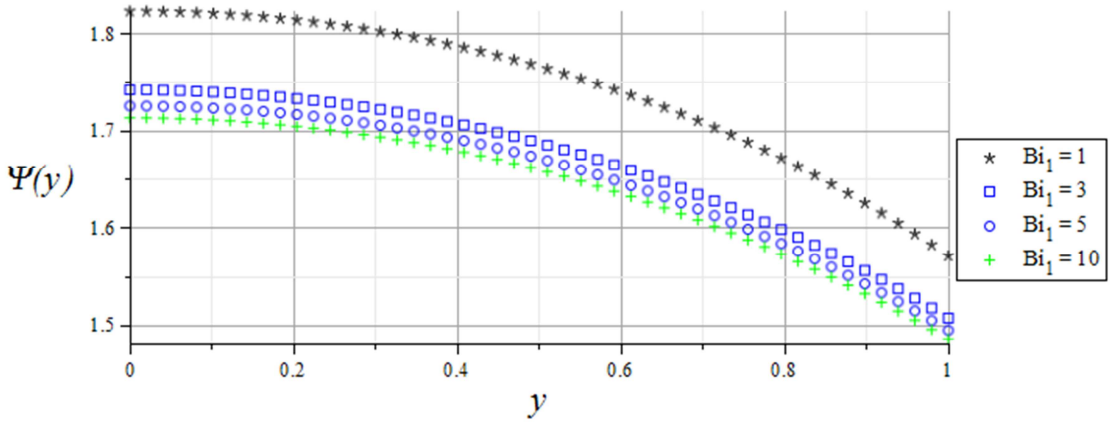

Figure 3.26: Effects of Bi_1 on slab Carbon dioxide emission profiles.

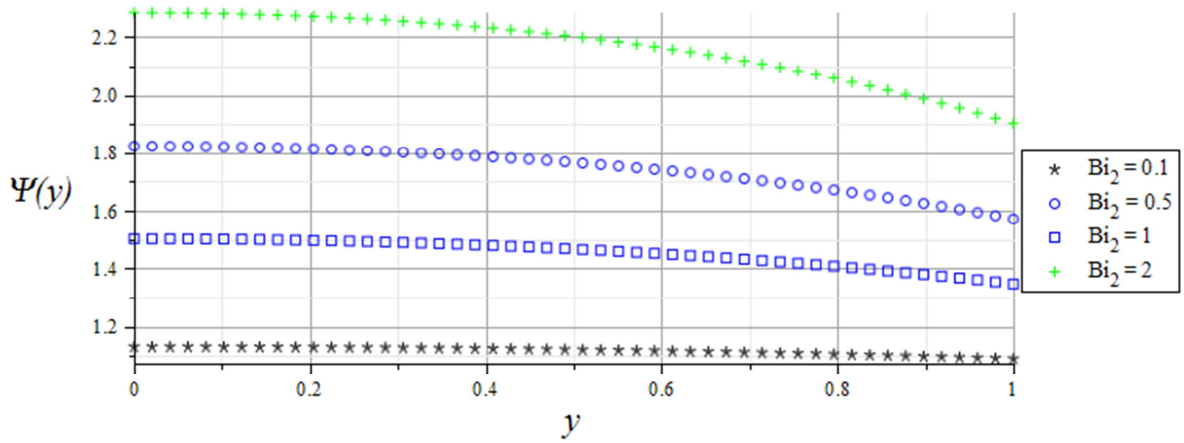

Figure 3.27: Effects of Bi_2 on slab Carbon dioxide emission profiles.

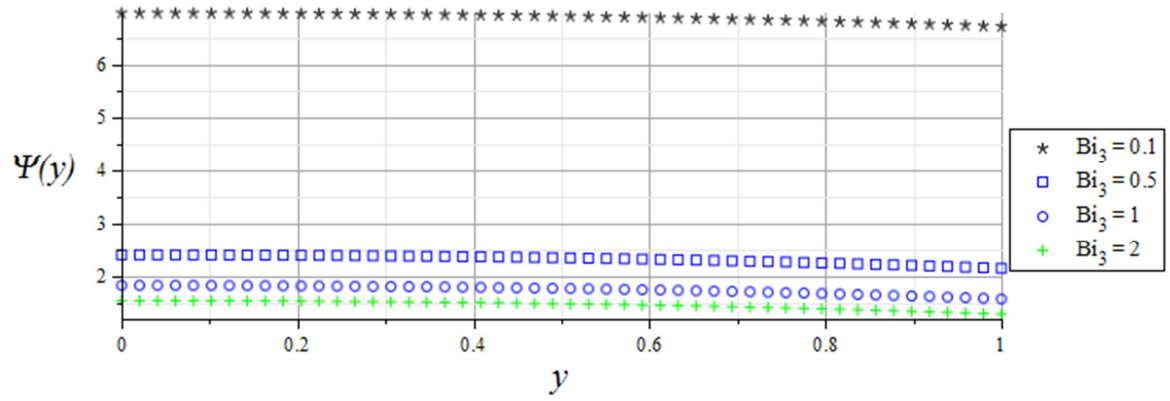

Figure 3.28: Effects of Bi_3 on slab Carbon dioxide emission profiles.

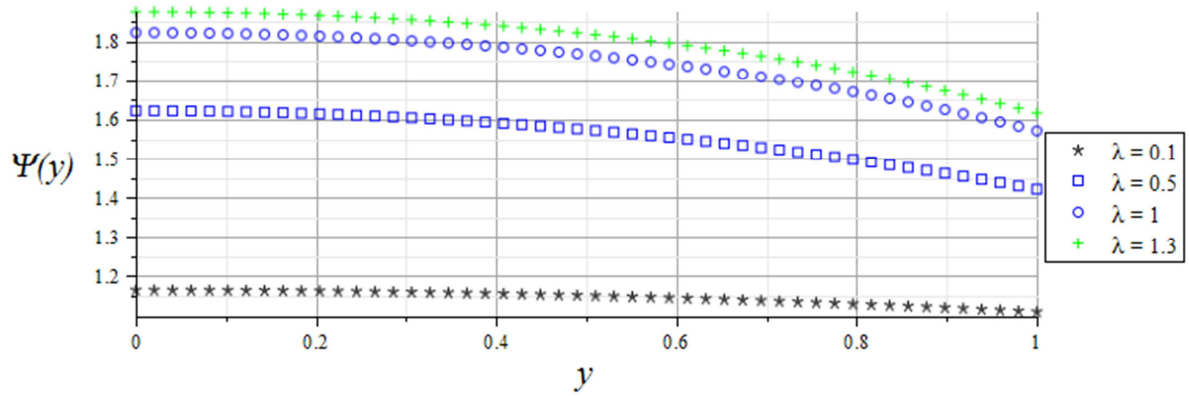

Figure 3.29: Effects of λ on slab Carbon dioxide emission profiles.

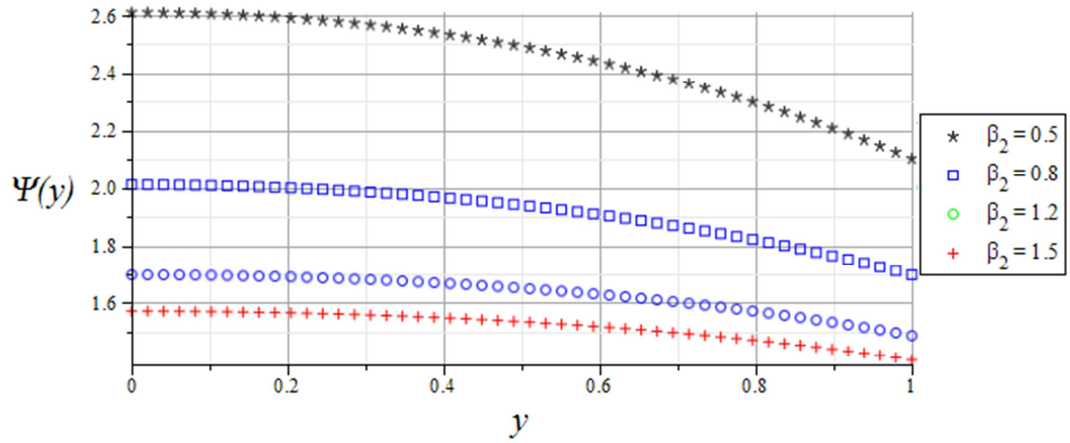

Figure 3.30: Effects of β_1 on slab Carbon dioxide emission profiles.

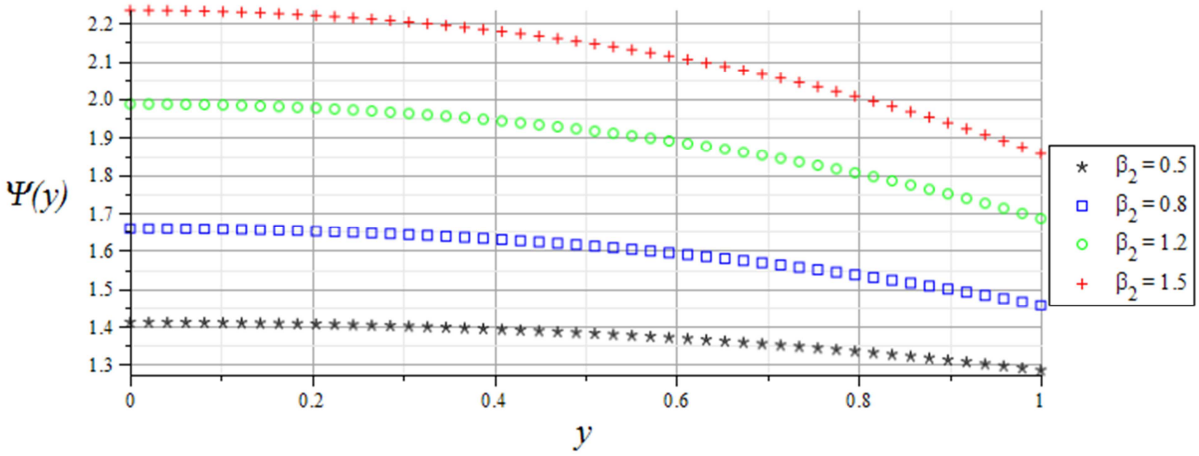

Figure 3.31: Effects of β_2 on slab Carbon dioxide emission profiles.

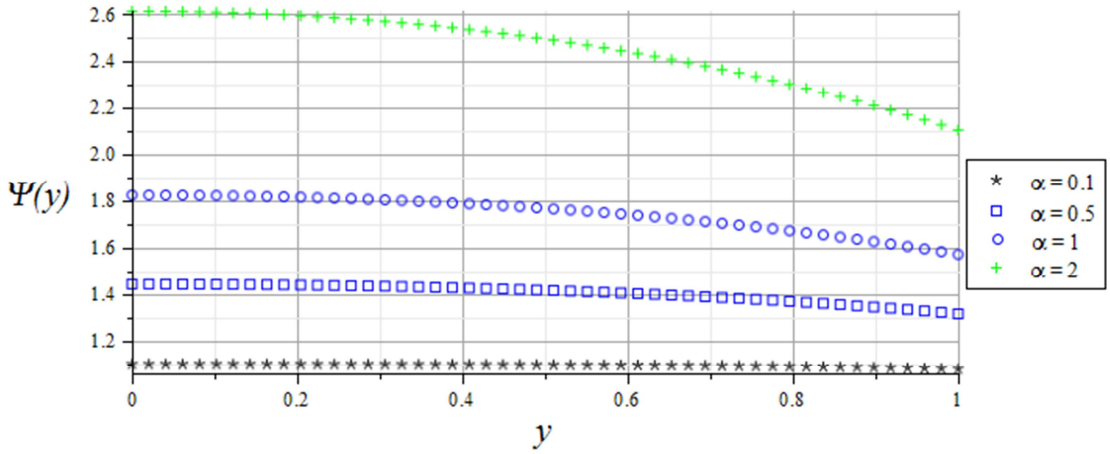

Figure 3.32: Effects of α on slab Carbon dioxide emission profiles.

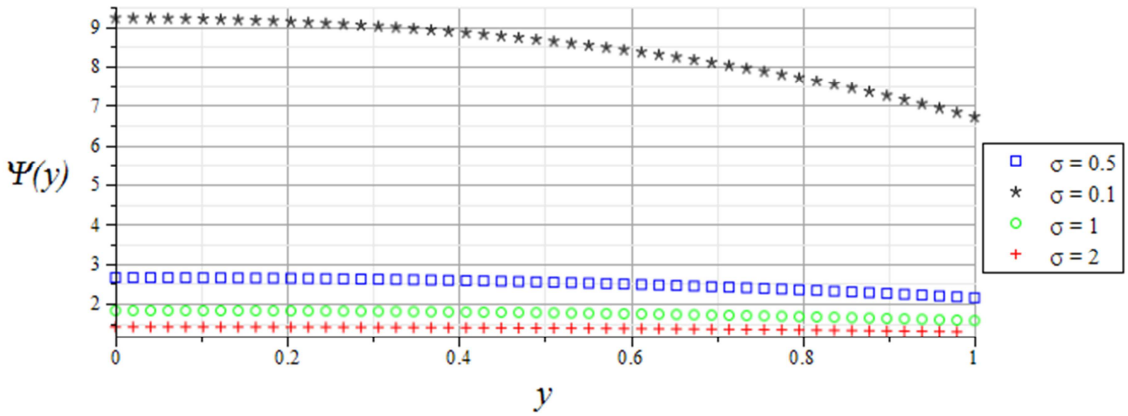

Figure 3.33: Effects of σ on slab Carbon dioxide emission profiles.

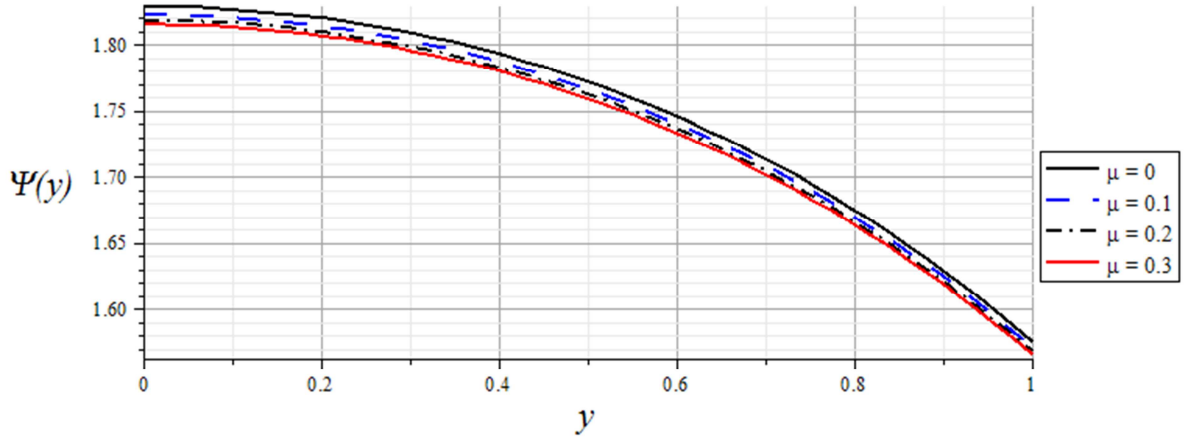

Figure 3.34: Effects of μ on slab Carbon dioxide emission profiles.

3.5.4. Thermal Stability and Blowup

In this subsection, the plots for thermal criticality values $\theta_y(1,t)$, versus the Frank-Kamenetskii parameter λ, or the rate of reaction, are given respectively, for different values of the following parameters, n, m, Bi_1 and Bi_2. Figures 3.35 to 3.38 illustrate the graphical solutions. The solutions are given up to the stage where the values of λ show an onset of blowup in temperature. Figure 3.35 show a decrease in $\theta_y(1,t)$ profiles as n increases. The same scenario is observed as Bi_1 is increased as indicated by figure 3.37. Figures 3.36 and 3.38 show an increase in $\theta_y(1,t)$ profiles as m and Bi_2 are increased respectively. From figures 3.35 and 3.37 we observe that the blow up can be delayed by keeping high values of parameters n and Bi_1 . But figures 3.36 and 3.8 show that the blow up can also be delayed by keeping low values of m and Bi_2.

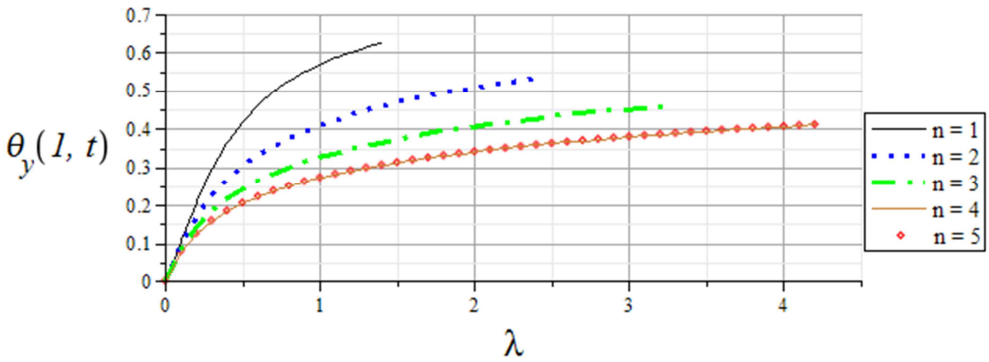

Figure 3.35: Effects of n on $\theta_y(1,t)$

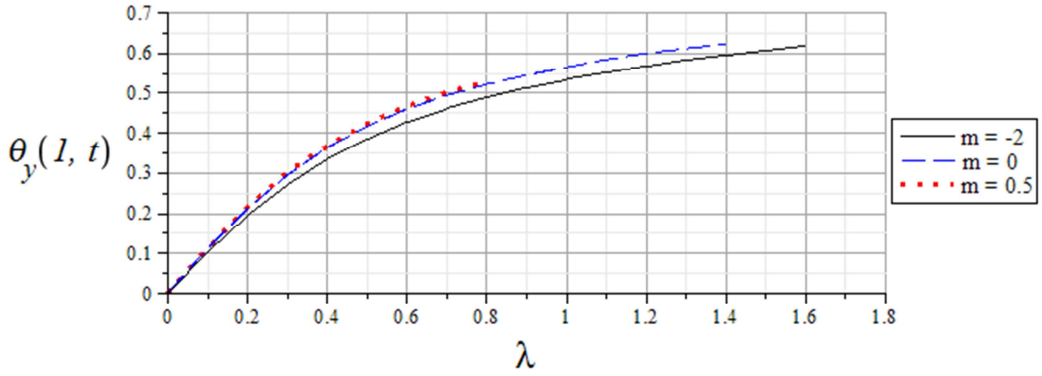

Figure 3.36: Effects m on $\theta_y(1,t)$

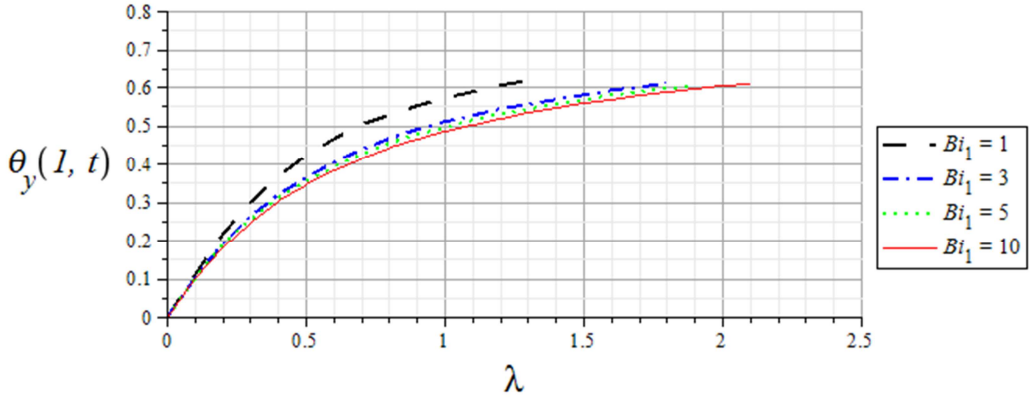

Figure 3.37: Effects of $B\mathrm{i}_1$ on $\theta_y(1,t)$

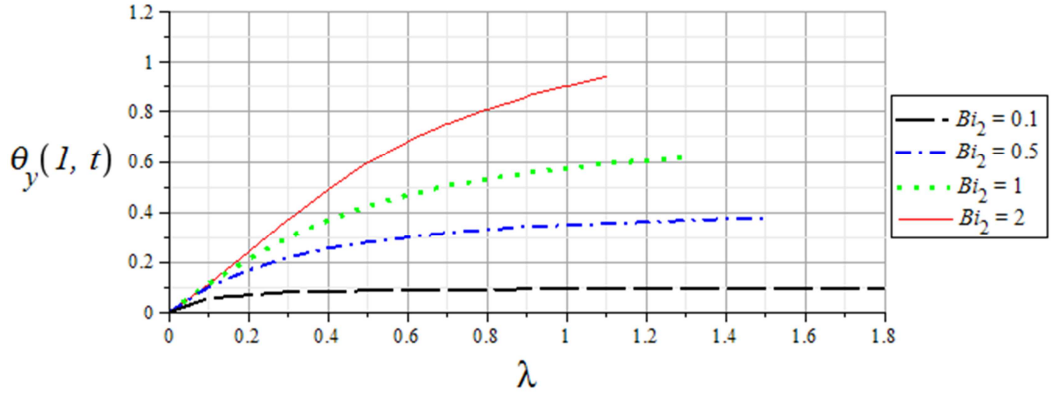

Figure 3.38: Effects of $B\mathrm{i}_2$ on $\theta_y(1,t)$

3.6 Conclusion

The investigation into carbon dioxide emission, oxygen depletion and thermal decomposition in a slab of reactive material was looked at in this chapter. The derived partial derivatives governing the problem were solved using semi-implicit difference method and the results were given graphically and discussed. A common observation is that parameters which increase temperature and carbon dioxide emission increase the depletion of oxygen and vice versa. Blow up results were also presented graphically and discussed accordingly. Knowledge of blow up values for different parameters is very important because if this information is applied appropriately, explosions especially that may be caused by exothermic reactions in stockpiles of reactive materials can be prevented.

Chapter 4

Modelling the effects of Thermal Radiation on CO_2 Emission and O_2 Depletion in a Reactive Slab

In this chapter, we examine the effects of thermal radiation on CO_2 emission and O_2 depletion in an exothermic reactive slab of combustible materials with uniform surface temperature. The governing equations for the nonlinear heat and mass transfer problem are derived and solved numerically using Runge-Kutta-Fehlberg method with shooting technique. Numerical expressions for temperature field, CO_2 emitted and O_2 depleted are derived and utilised to obtain expressions for Nusselt number and Sherwood number at the material surface. The effects of various thermophysical parameters on the temperature field, CO_2 emission and O_2 depletion are depicted graphically and discussed quantitatively.

4.1 Introduction

Internal heat generation in a stockpile of reactive combustible materials and industrial waste such as coal residue, sugarcane baggage, saw dust, etc., may occur due to oxidation chemical reactions [65]. The continuous accumulations of heat in the material do lead to thermal ignition with O_2 depletion and CO_2 emission to the ambient environment [7, 76]. A rise in CO_2 emission to the ambient environment is well known as the major cause of global warming and climate change [64]. Meanwhile, thermal radiation occurs whenever a body's temperature is greater than absolute zero. Thermal radiation is defined as an electromagnetic radiation in the wavelength range of 0.1 to 100 microns, and arises as a result of temperature difference between an object's surface temperature and its surrounding temperature [15, 34, 62]. A reactive slab can be thought of as a gray-body, because it absorbs part of the radiation incident to it, rather than a blackbody which absorbs completely all wavelengths of thermal radiation incident to it [45]. Reactive slab emits thermal radiation due to exothermic reaction of its composing hydrocarbon material with oxygen, which brings about temperature rise in the slab [71]. One of the properties that characterize thermal radiation is that the total amounts of radiation of all frequencies increase

steeply as the temperature rises [69]. Simmie [70], gave an extensive review of chemical kinetic models for the reaction of hydrocarbons with oxygen in combustible materials. It follows therefore that the combustion reaction mechanism, especially of large hydrocarbons, is more complicated and includes many radicals [19]. Moreover, adequate knowledge of the mathematical models of these complex chemical systems is extremely important in assessing the thermal stability property of the materials, climate change indicators, and mitigation strategies [26]. It may also help to develop a long-term action plans for safety of life and properties. Several authors including Makinde [47] and Sadiq & Merkin [68] have examined the thermal stability characteristics of a reacting slab with or without reactant consumption using a one-step decomposition kinetics. Makinde *et al* [50] presented a numerical study of CO_2 emission, O_2 depletion and thermal decomposition in a reacting slab. The thermal stability of reacting masses in a slab with asymmetric convective cooling was studied by Makinde [48]. Recently, the numerical result for thermal decomposition of reactive materials of variable thermal conductivity and heat loss characteristics in a long pipe was presented by Makinde [49]. In all the earlier studies, the effects of radiative heat loss on CO_2 emission, O_2 depletion and thermal stability criteria for stockpile of reactive combustible materials have been ignored. Our objective in this paper is to extend the earlier studies to include the effects radiative heat loss on CO_2 emission, O_2 depletion and thermal stability of rectangular reactive slab of combustible materials. In the following sections, the differential equations governing problem are obtained and solved numerically using Runge-Kutta-Fehlberg method with shooting technique, as highlighted already. Pertinent results are presented graphically and discussed quantitatively with respect to various thermophysical parameters embedded in the system.

4.2 Mathematical Model

We consider a rectangular slab of combustible material with a constant thermal conductivity k, and surface emissivity ε. It is assumed that the slab is undergoing an n^{th} order oxidation chemical reaction. In order to simplify the complicated chemistry involved in this problem, a one-step finite rate irreversible chemical kinetics mechanism is assumed between the material and the oxygen of the air as follows:

$$C_iH_j + \left(i + \frac{j}{4}\right) O_2 \rightarrow iCO_2 + \left(\frac{j}{2}\right) H_2O + \text{heat.} \tag{4.1}$$

Following Stefan-Boltzmann law, the radiative heat loss at the material surface to the surrounding ambient is given by $q = \varepsilon\phi(T^4 - T_0^4)$ and is assumed to solely take place in the $\bar{y}$ direction as illustrated in figure 4.3.1 below,

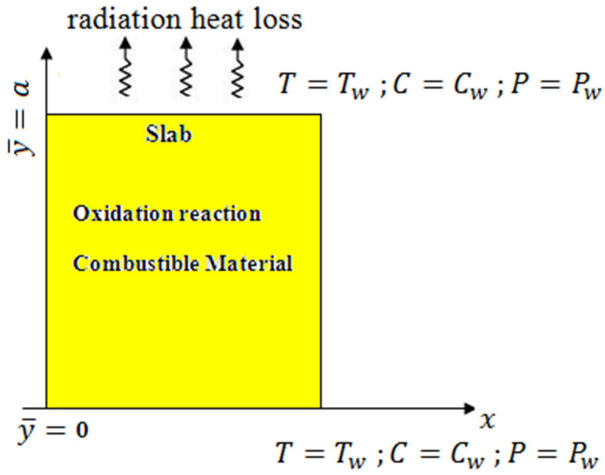

Figure 4.1: Geometry of the Problem

Following Bebernes & Eberly [7], Quadrelli & Peterson [65] and Williams [77] the nonlinear governing differential equations for the heat and mass transfer problem in the presence of thermal radiation, CO_2 emission and O_2 depletion can be written as

$$k\frac{d^2T}{d\bar{y}^2} + QA\left(\frac{KT}{vl}\right)^m C^n exp\left(\frac{-E}{RT}\right) - \varepsilon\phi(T^4 - T_w^4) = 0, \tag{4.2}$$

$$D\frac{d^2C}{d\bar{y}^2} - A\left(\frac{KT}{vl}\right)^m C^n exp\left(-\frac{E}{RT}\right) = 0, \tag{4.3}$$

$$\gamma\frac{d^2P}{d\bar{y}^2} + A\left(\frac{KT}{vl}\right)^m C^n exp\left(-\frac{E}{RT}\right) = 0, \tag{4.4}$$

with boundary conditions:

$$\bar{y} = 0, \quad T = T_w, \quad C = C_w, \quad P = P_w, \tag{4.5}$$

$$\bar{y} = a, \quad T = T_w, \quad C = C_w, \quad P = P_w, \tag{4.6}$$

where T is the slab's absolute temperature, C is the oxygen concentration, P is the carbon dioxide emission concentration, T_w is the slab surface temperature, C_w is the oxygen concentration at the slab surface, P_w is the carbon dioxide concentration at the slab surface, k is the thermal conductivity of the reacting slab, ε is emissivity ($0 < \varepsilon < 1$), ϕ is Stefan-Boltzmann constant ($5.6703\times 10^{-8} W/m^2K^4$), D is the diffusivity of oxygen in the slab, γ is the diffusivity of carbon dioxide in the slab, Q is the heat of reaction, $\boldsymbol{A}$ is the rate constant, E is the activation energy, R is the universal gas constant, l is the Planck number, v is the vibration frequency, K is the Boltzmann constant, n is the order of exothermic chemical reaction, and m is the numerical exponent such that $m \in \{-2,0,0.5\}$. The three values taken by the parameter m represent the numeric exponent for sensitized, Arrhenius and Bimolecular kinetics, respectively [34, 70]. The boundary conditions (4.5) and (4.6) describe the constant temperature conditions at the base and the top of the reactive slab respectively.

4.3 Introduction of dimensionless parameters

Remember that the introduction of dimensionless parameters helps to reduce the partial differential equations into a form that can be easily solved using numerical methods. The same procedure used in chapter 3 section 3.3 is applied to make the ordinary differential equations dimensionless. The following dimensionless parameters are first described, and later introduced to equations (4. 2) – (4. 6)

$$\left.\begin{gathered} \theta = \frac{E(T-T_w)}{RT_w^2},\ \Phi = \frac{C}{C_w},\ \Psi = \frac{P}{P_w}, \\ \beta_1 = \frac{kRT_w^2}{QEDC_w},\ \beta_2 = \frac{kRT_w^2}{QE\gamma P_w}, \\ \lambda = \left(\frac{KT_w}{vl}\right)^m \frac{QAEa^2(C_w)^n}{kRT_w^2} exp\left(-\frac{E}{RT_w}\right), \\ y = \frac{\bar{y}}{a},\quad \mu = \frac{RT_w}{E},\ Ra = \frac{\varepsilon\phi E a^2 T_w^2}{kR}. \end{gathered}\right\} \tag{4.7}$$

Equations (4.2) – (4.6) take the dimensionless form to give the following expressions:

$$\frac{d^2\theta}{dy^2} + \lambda(1+\mu\theta)^m \Phi^n \exp\left(\frac{\theta}{1+\mu\theta}\right) - Ra((\mu\theta+1)^4 - 1) = 0, \tag{4.8}$$

$$\frac{d^2\Phi}{dy^2} - \lambda\beta_1(1+\mu\theta)^m \Phi^n \exp\left(\frac{\theta}{1+\mu\theta}\right) = 0, \tag{4.9}$$

$$\frac{d^2\Psi}{dy^2} + \lambda\beta_2(1+\mu\theta)^m\Phi^n\exp\left(\frac{\theta}{1+\mu\theta}\right) = 0, \tag{4.10}$$

$$y = 0,\ \theta = 0, \quad \Phi = 1, \quad \Psi = 1, \tag{4.11}$$

$$y = 1,\ \theta = 0, \quad \Phi = 1, \quad \Psi = 1, \tag{4.12}$$

where λ is the Frank-Kamenetski parameter, μ is activation energy parameter, is β_1 oxygen consumption rate parameter, β_2 is carbon dioxide emission rate parameter, *Ra* is radiation parameter. It should be noted further that if the rate of heat generation in the slab exceeds the rate of heat loss to its surrounding, ignition can take place. The dimensionless heat and mass transfer rate at the slab surface are expressed in terms of Nusselt number and Sherwood number as

$$Nu = -\frac{d\theta}{dy}(1), \quad Sh_1 = \frac{d\Phi}{dy}(1), \quad Sh_2 = -\frac{d\Psi}{dy}(1). \tag{4.13}$$

4.4 Numerical Solution

The set of equations (4.8) – (4.10) together with the boundary conditions (4.11) – (4.12) including the Nusselt number and the Sherwood numbers in equation (4.13), have been solved numerically using the Runge-Kutta-Fehlberg method with shooting technique [45].

4.4.1 Runge-Kutta-Fehlberg Method

The algorithm outlined under section 1.7.2 is applied together with the shooting method to solve equations (4.8) – (4.10).

4.4.2 Shooting Technique Method

Following Lastman [43], Legodi & Makinde [44] and Makinde [53] the system of equations (4.8) – (4.10) together with boundary conditions (4.11) – (4.12), were solved using shooting method coupled with RKF45 integration algorithm. We let:
$\theta = x_1,\ \theta' = x_2,\ \Phi = x_3,\ \Phi' = x_4,\ \Psi = x_5,\ \Psi' = x_6$. It follows that equations (4.8) – (4.10) are transformed into first order differential equations as follows:

$$
\begin{aligned}
x'_1 &= x_2 \\
x'_2 &= -\lambda(1+\mu x_1)^m (x_3)^n \exp\left(\frac{x_1}{1+\mu x_1}\right) - Ra((\mu x_1+1)^4 - 1) \\
x'_3 &= x_4 \\
x'_4 &= \lambda(1+\mu x_1)^m (x_3)^n \exp\left(\frac{x_1}{1+\mu x_1}\right) - Ra((\mu x_1+1)^4 - 1) \\
x'_5 &= x_6 \\
x'_6 &= -\lambda(1+\mu x_1)^m (x_3)^n \exp\left(\frac{x_1}{1+\mu x_1}\right) - Ra((\mu x_1+1)^4 - 1)
\end{aligned} \tag{4.14}
$$

subject to the initial conditions

$$x_1(0) = 0,\ x_3(0) = 1,\ \ x_5(0) = 1,\ x_1(1) = 0,\ \ x_3(1) = 1,\ x_5(1) = 1 \tag{4.15}$$

The shooting method is coupled with RKF45 to give results to expected accuracy.

4.5 Result and Discussion

In this section, the computational results obtained for the model equations in the above section are presented graphically and discussed quantitatively for various values of thermophysical parameters embedded in the system.

4.5.1 Effects of thermophysical parameter variation on slab temperature profiles

Figures 4.2 – 4.7 illustrate the temperature profiles. Generally, the slab temperature is maximum along the slab centerline region and minimum at the walls satisfying the prescribed boundary conditions. In figure 4.2, we observe that the slab temperature increases with increasing values of λ due to increasing rate of internal heat generation by exothermic chemical reaction. We observe a different case in figure 4.3 where the increase in *Ra* leads to decrease in temperature. This indicates that the more heat is lost due to radiation the temperature of the slab is reduced more. The same scenario is observed with figure 4.4. It can be seen that the slab's temperature decreases with increasing *n* and this indicates that increasing the order of reaction in an exothermic reaction results with minimum temperature drop in a reactive slab. Figure 4.5 illustrates the effects of *m* on temperature. It can be observed that the increase in *m* corresponds to the increase in temperature. The results indicate that exothermic reaction occurs faster during

bimolecular reactions (m = 0.5) which gives highest temperature profile as compared to Arrhenius (m = 0) type of reaction, and that it is slower during sensitized (m = -2) chemical reaction. Effect of increasing μ on slab temperature profiles are illustrated in figure 4.6, which indicates that increasing μ results with decrease in temperature. In other words, increase in the activation energy of the exothermic reaction in a reactive slab lowers the temperature. Figure 4.7 shows the same scenario, where an increase in β_1 results with decrease in temperature. The more oxygen is consumed in the system, the exothermic reaction is reduced and this causes the drop in temperature of the slab.

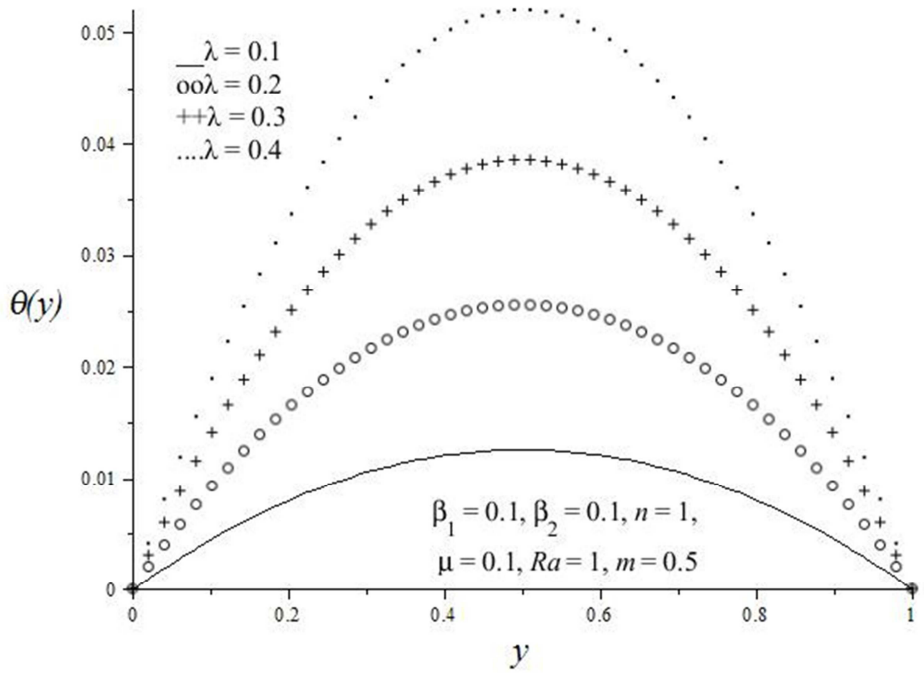

Figure 4.2: Effect of increasing λ on slab temperature profiles.

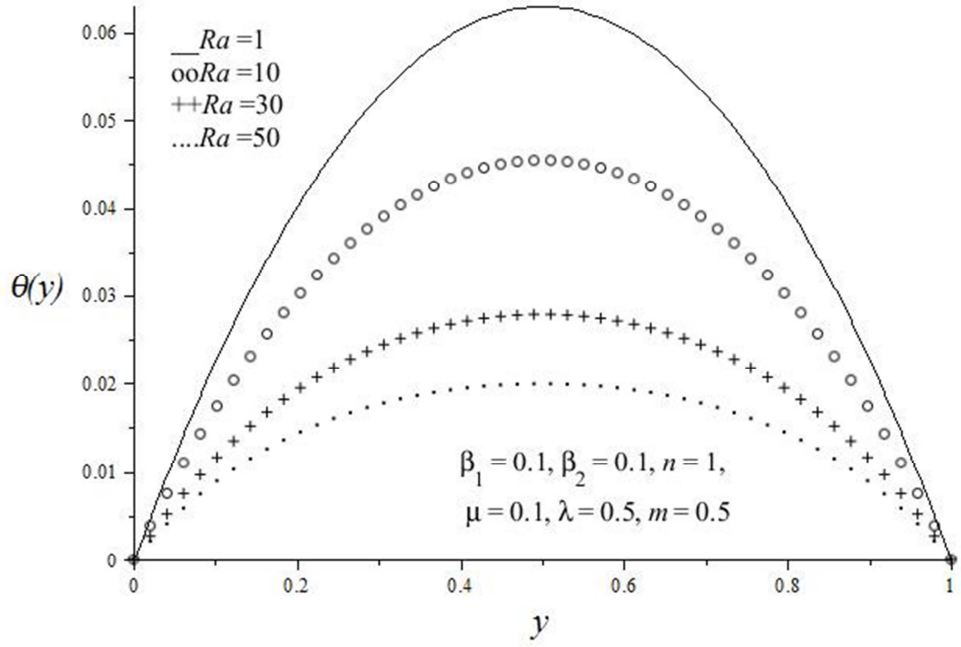

Figure 4.3: Effect of increasing *Ra* on slab temperature profiles

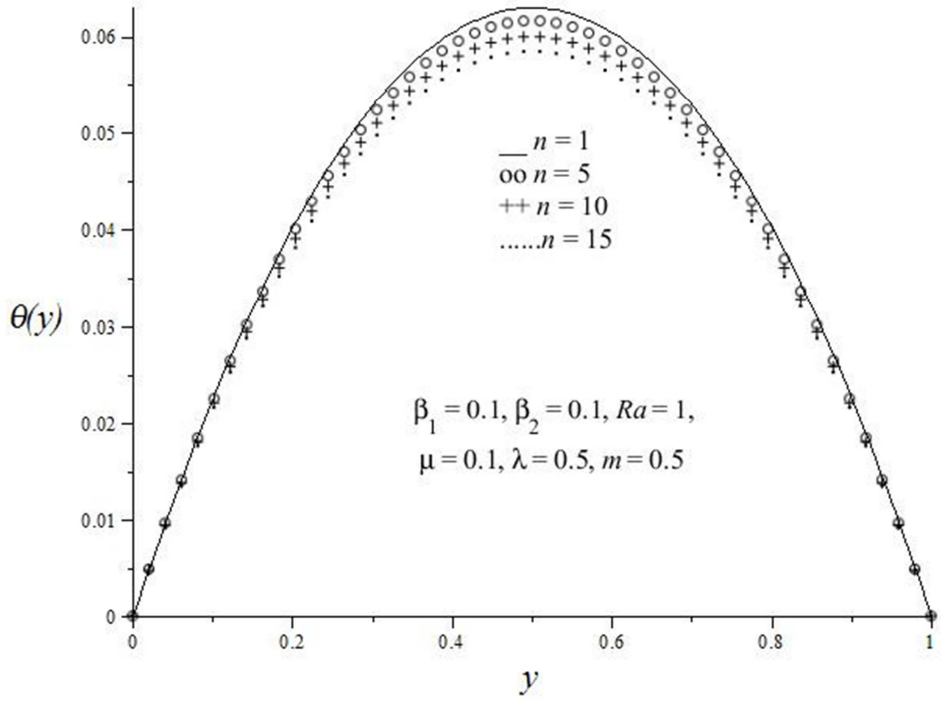

Figure 4.4: Effect of increasing *n* on slab temperature profiles

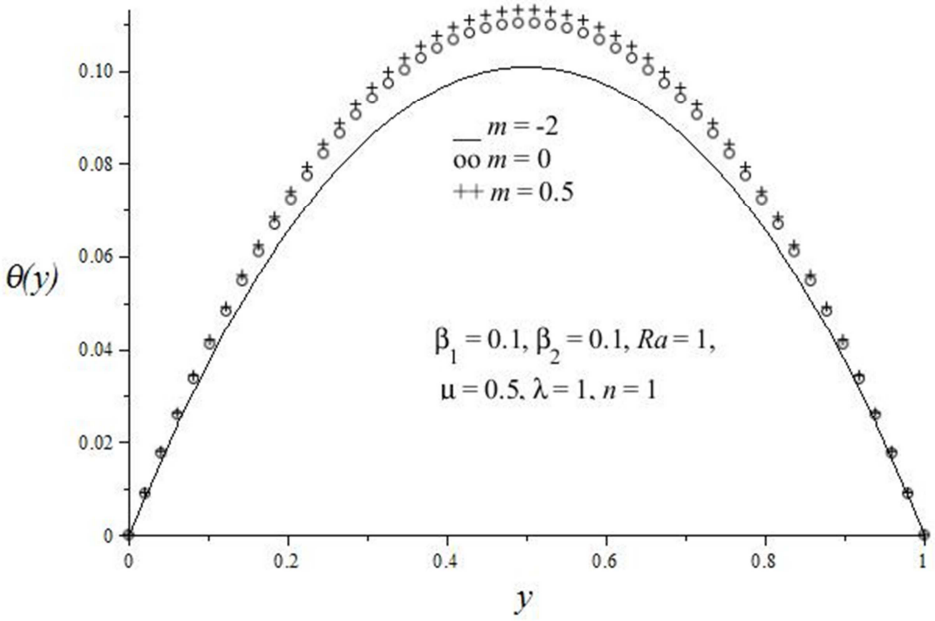

Figure 4.5: Effect of *m* on slab temperature profiles.

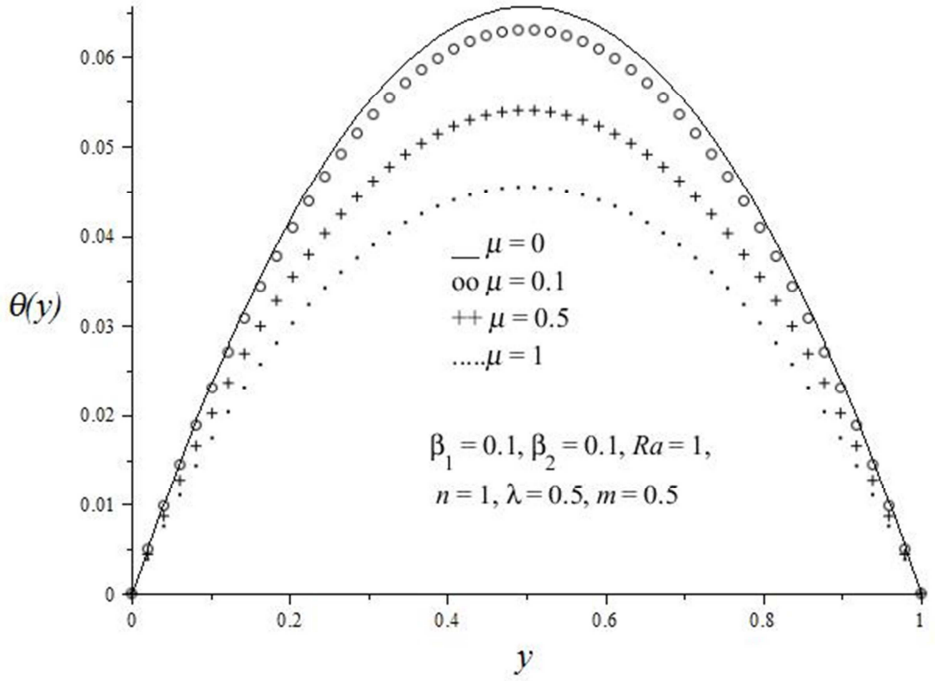

Figure 4.6: Effect of increasing μ on slab temperature profiles

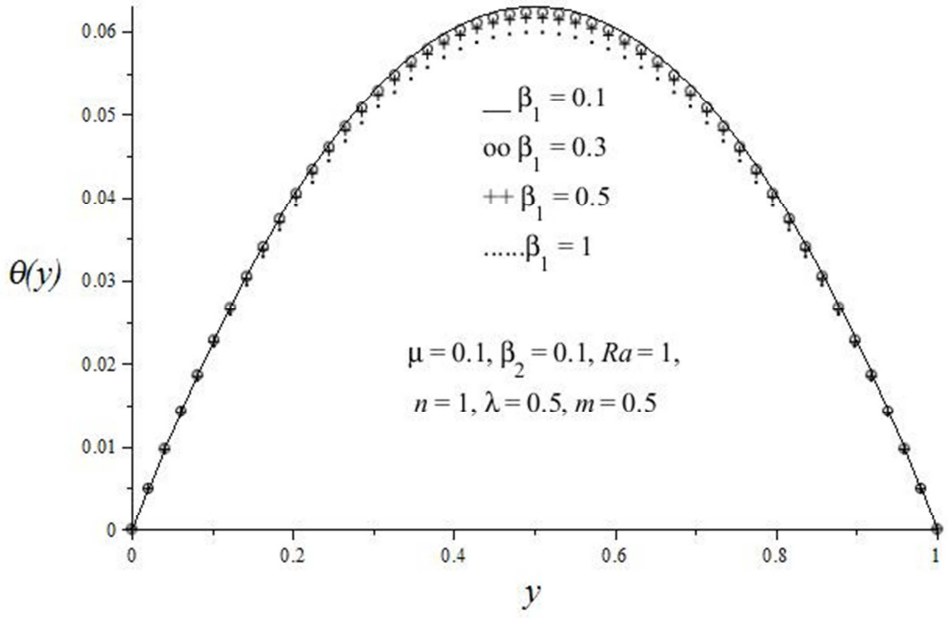

Figure 4.7: Effect of increasing β_1 on slab temperature profiles.

4.5.2 Effects of thermophysical parameter variation on slab O_2 depletion

The effects of parameter variation on slab oxygen depletion are demonstrated in figures 4.8 – 4.12. It is interesting to note that the rate of oxygen depletion within the slab increases with an increase in the exothermic reaction rate as shown in figure 4.8. As λ increases, more oxygen is consumed to generate more heat due to oxidation chemical reaction. From figure 4.9 we observe that as *Ra* is increased, the oxygen concentration is increased. This means that the more the emissivity of slabs surface, the lesser the exothermic reaction and more oxygen preservation. The same scenario is observed with figure 4.10, where an increase in *n* results with increase in oxygen concentration. It is good to note that increasing the order of chemical reaction is favorable to oxygen conservation. Figure 4.11 illustrates that an increase in *m* decreases the temperature concentration. It can be observed that more oxygen is depleted during bimolecular reaction (m = 0.5). Effects of increasing β_1 on slab Oxygen depletion are illustrated by figure 4.12. It can be observed that as β_1 is increased, more oxygen is depleted. The more oxygen is consumed in a reactive slab, the exothermic reaction is reduced and we observed also that the temperature of the slab is decreased.

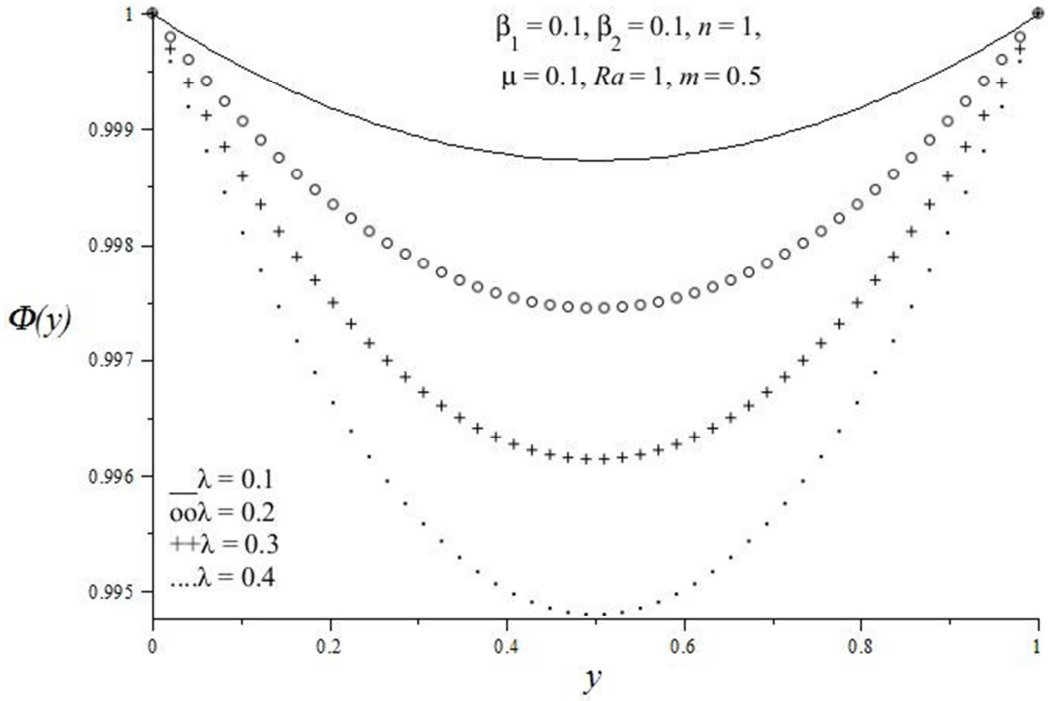

Figure 4.8: Effect of increasing λ on slab Oxygen depletion profiles.

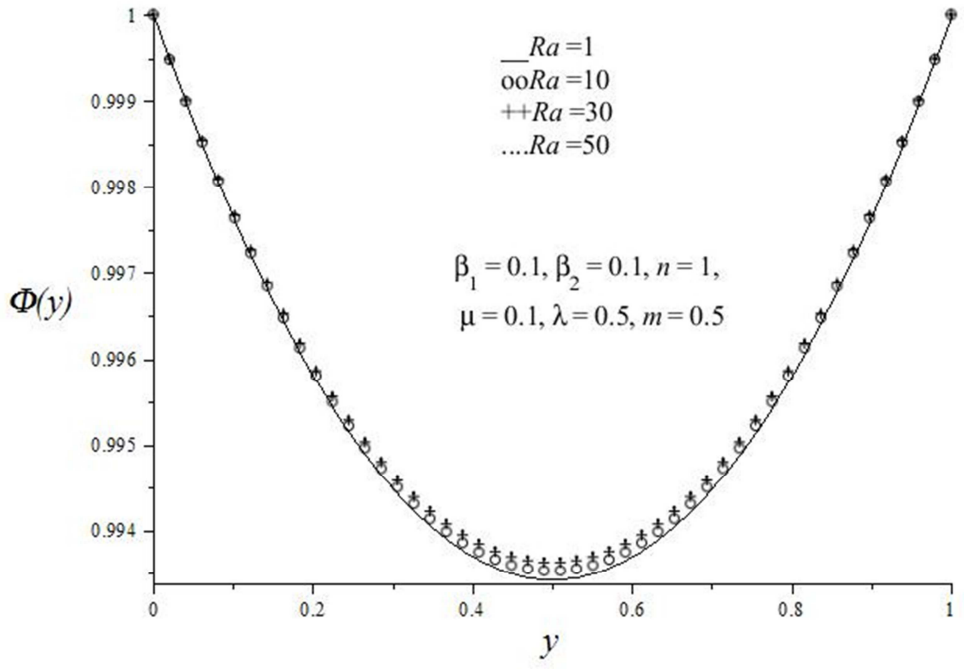

Figure 4.9: Effect of increasing *Ra* on slab Oxygen depletion profiles.

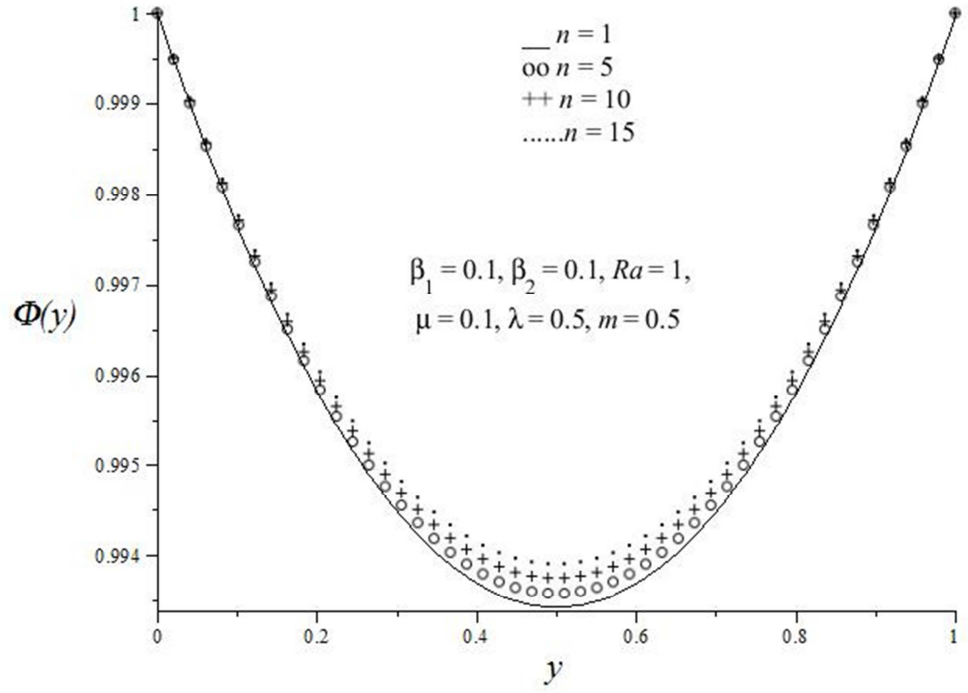

Figure 4.10: Effect of increasing *n* on slab Oxygen depletion profiles

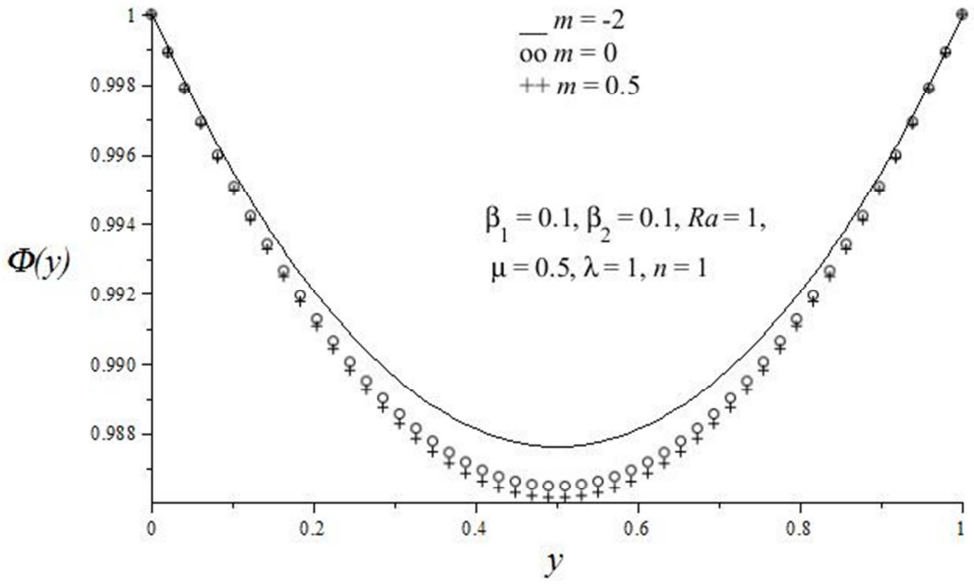

Figure 4.11: Effect of *m* on slab Oxygen depletion profiles

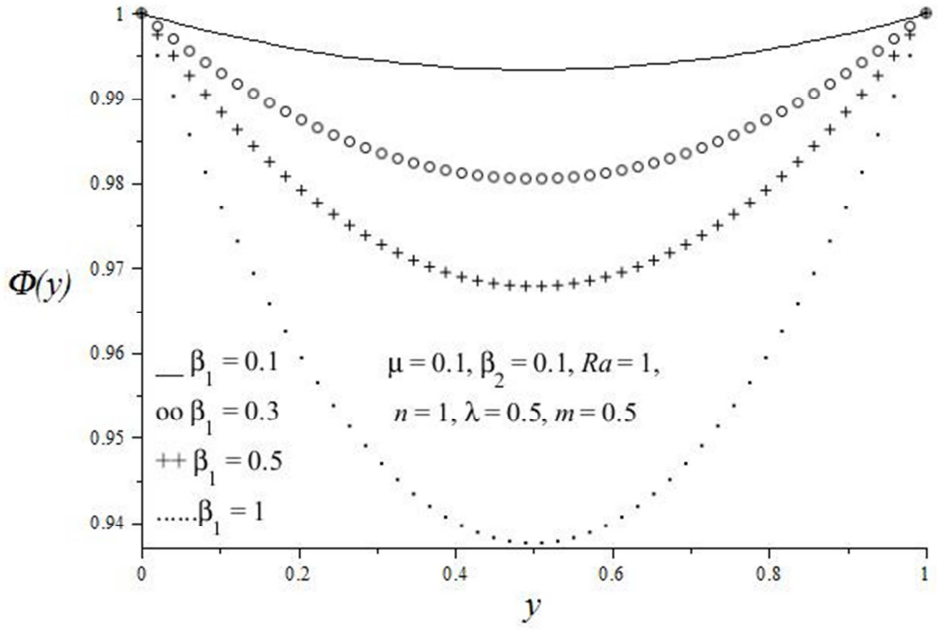

Figure 4.12: Effect of increasing β_1 on slab Oxygen depletion profiles.

4.5.3 Effects of thermophysical parameter variation on slab CO_2 emission

Figures 4.13 – 4.18 depict the slab Carbon dioxide emission profiles. An increase in the exothermic reaction rate represented by increasing values of λ, leads to an increase in the slab Carbon dioxide emission rate as shown in Figure 4.13. The emission is highest within the slab centerline region. In figure 4.14, we observe the effect of increasing *Ra* on slab carbon dioxide emission. It can be seen that increasing the value of *Ra* results with the decrease in carbon dioxide profiles. The same scenario was observed with temperature profiles and this is due to that the more the emissivity of the slab's surface, the lesser oxygen depletion and hence the exothermic reaction is assumed not take place in order to lessen carbon dioxide emission. We observe the same scenario with figure 4.15, where the increase in *n* gives a decrease in carbon dioxide profiles. It is therefore necessary to increase the order of reaction in order to lessen the emission of carbon dioxide. Figure 4.16 illustrates the effect of *m* on carbon dioxide. We observe that an increase in *m* corresponds to an increase in carbon dioxide emission profiles and the highest profile is observed during bimolecular reactions (*m* = 0.5). From figure 4.17 we can see that increasing β_1 decreases the carbon dioxide profiles. This is due to that as more oxygen is consumed, the exothermic reaction is reduced and hence the emission of carbon dioxide is

lessened. Effects of increasing β_2 on slab Carbon dioxide emission profiles are illustrated in figure 4.18. In this case an increase in β_2 corresponds to an increase in carbon dioxide profiles. The presence of more carbon dioxide within a reactive slab reduces the exothermic chemical reaction. During this process oxygen is not used up and the temperature rise cannot be experienced.

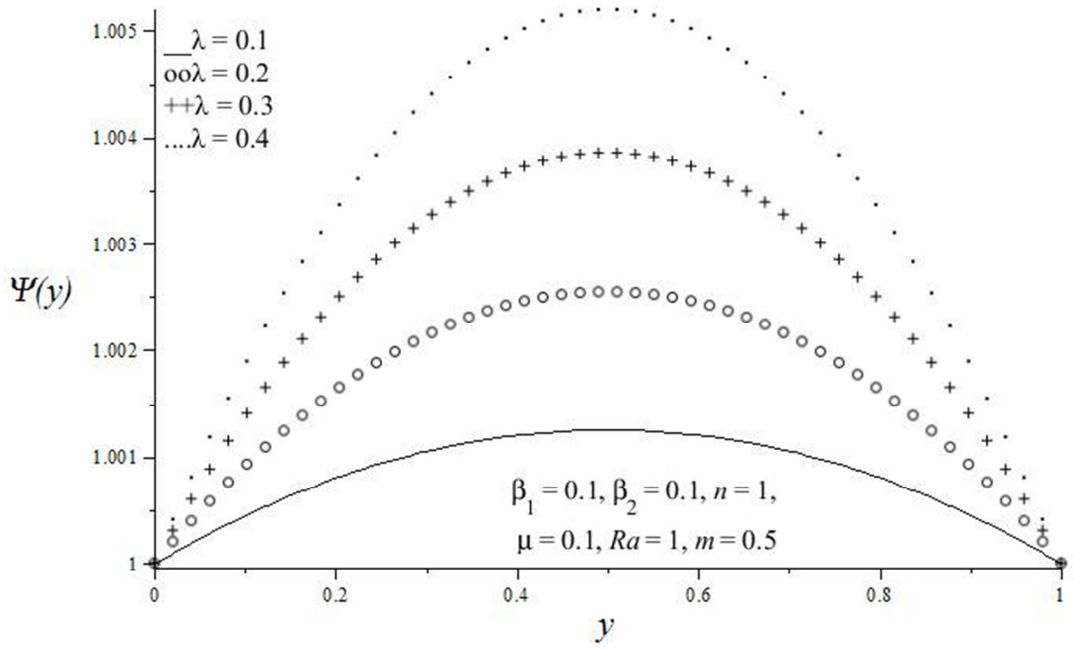

Figure 4.13: Effect of increasing λ on slab Carbon dioxide emission profiles

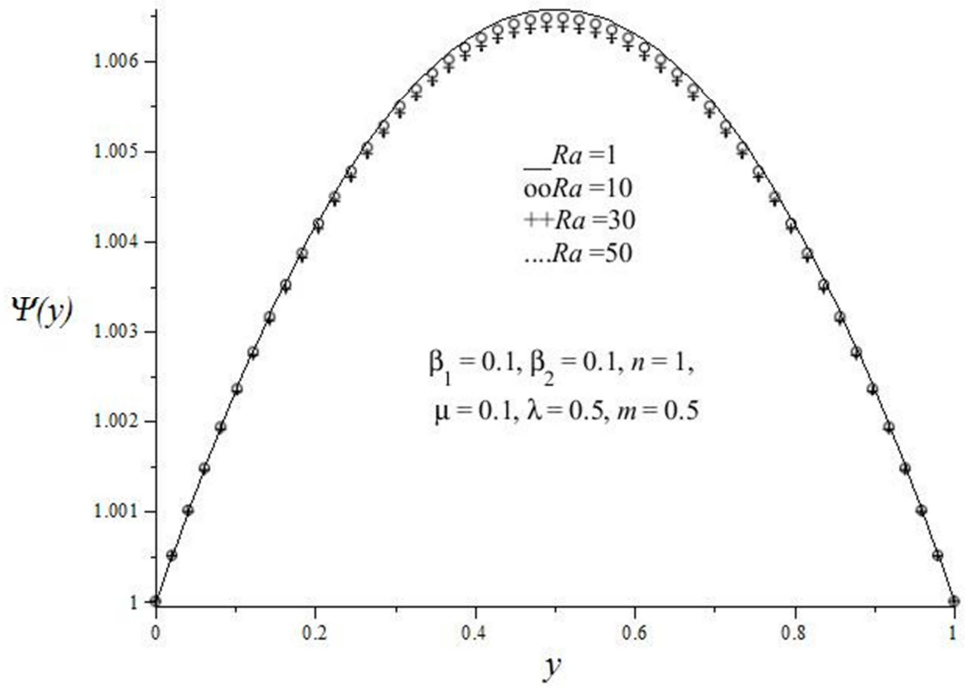

Figure 4.14: Effect of increasing *Ra* on slab Carbon dioxide emission profiles.

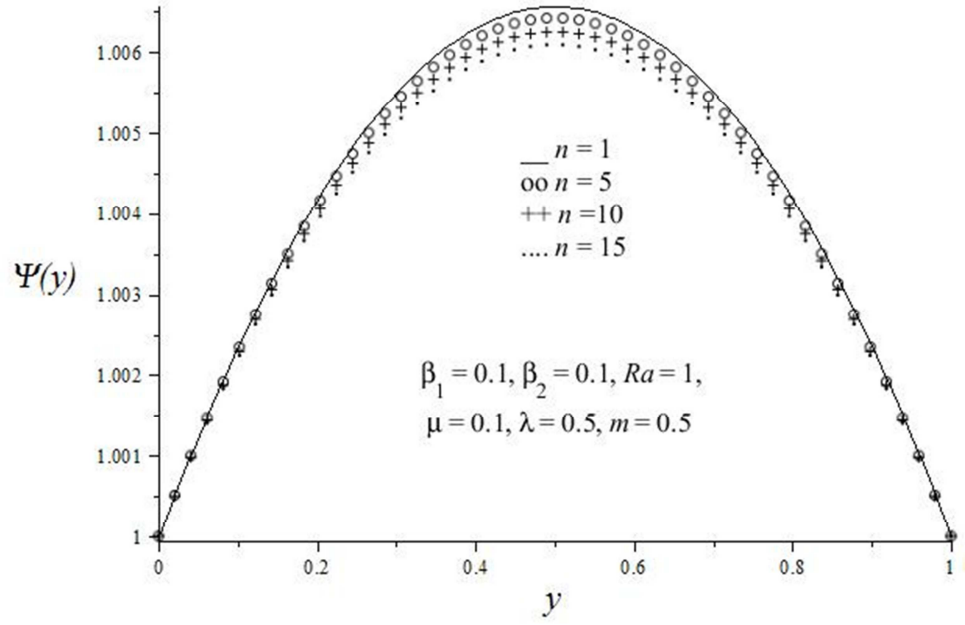

Figure 4.15: Effect of increasing *n* on slab Carbon dioxide emission profiles.

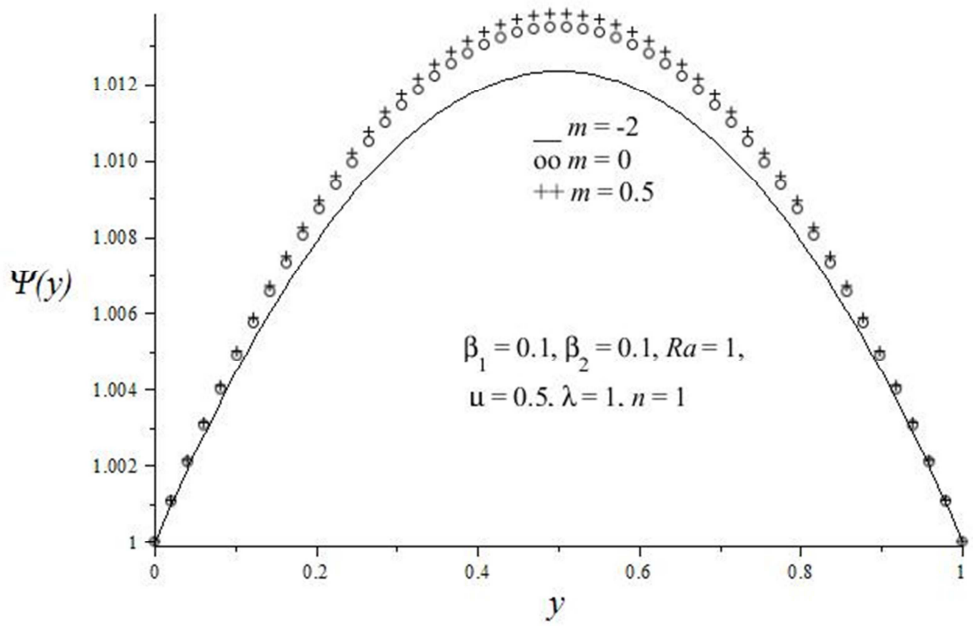

Figure 4.16: Effect of *m* on slab Carbon dioxide emission profiles.

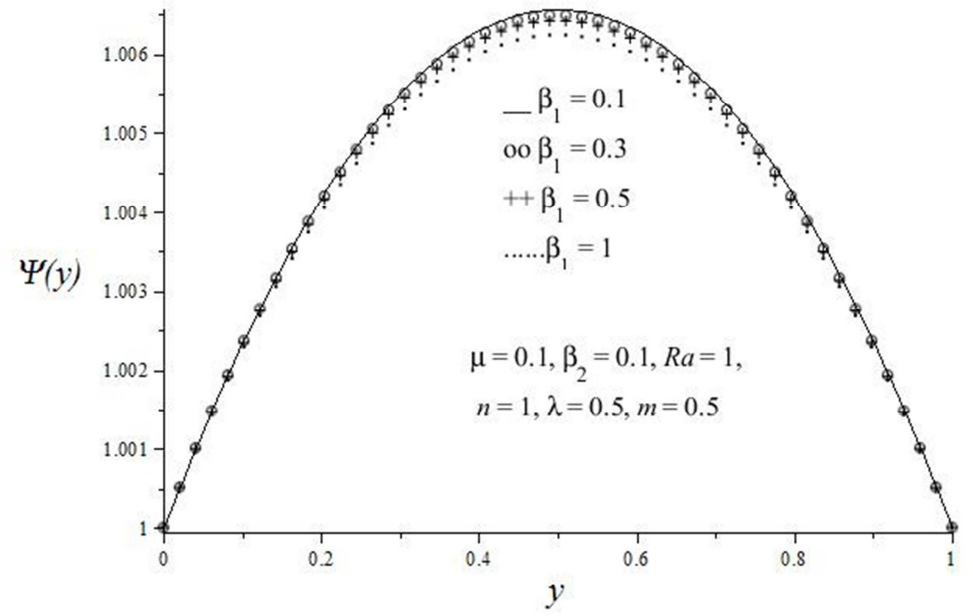

Figure 4.17: Effect of increasing β_1 on slab Carbon dioxide emission profiles.

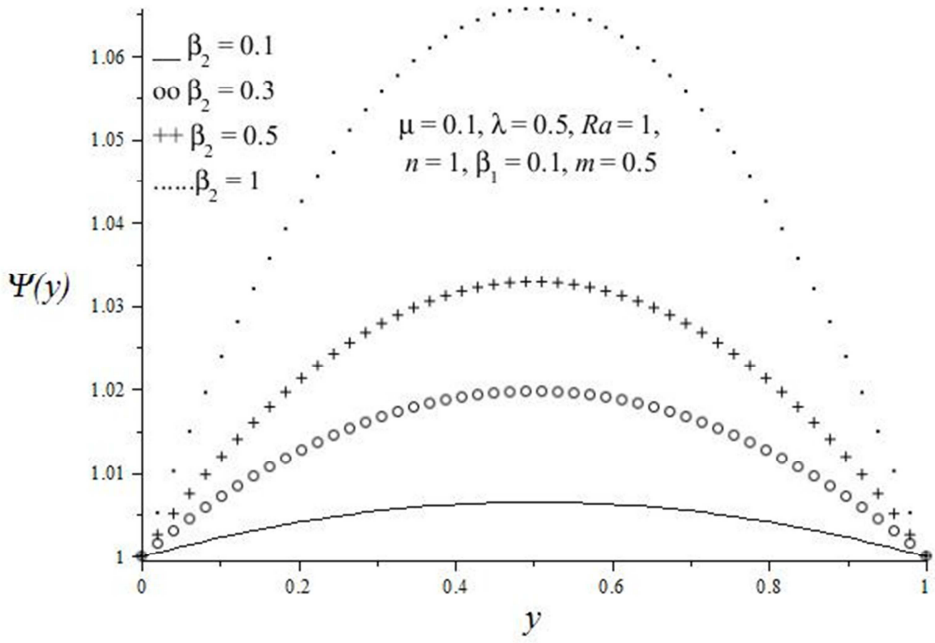

Figure 4.18: Effect of increasing β_2 on slab Carbon dioxide emission profiles

4.5.4 Effects of parameter variation on thermal criticality values or blowups

Here we consider plots for thermal criticality values, Nusselt number *Nu*, versus the rate of reaction, Frank-Kamenetskii parameter λ. We consider manipulating parameters to establish values to help us control the system against any explosion. Results are also represented numerically in a table.

Figure 4.19 shows that at lowest values of *Ra*, the system blow up values are arrived at quicker, as the rate of reaction increases. It can be seen that at high values of *Ra*, the blow up values are high and therefore it is better to allow more radiation to occur in order to avoid explosions. Figure 4.20 shows the same scenario, where an increase in *n* enhances thermal stability as the rate of reaction increases. A different picture is shown by figure 4.21. In this case we observe that as *m* increases, the system becomes thermally unstable because at high values of *m*, blow up values are arrived at quicker. Figure 4.22 illustrates that increasing μ may lead to some thermal stability, because the blow ups occur at high values of rate of reaction as μ increases. Numerical values confirm graphical solutions and they are given in table 4.1.

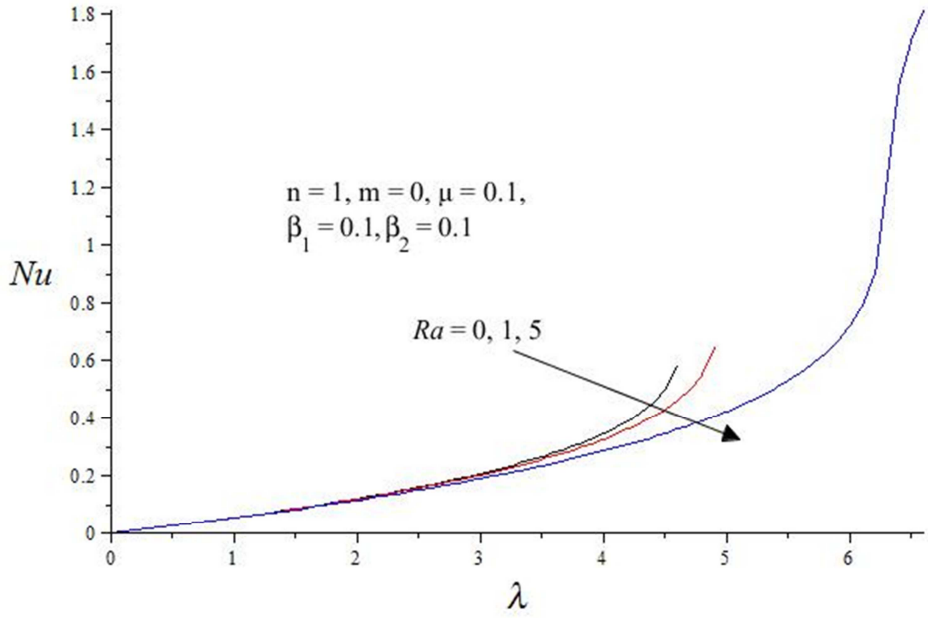

Figure 4.19: Effect of increasing *Ra* on slab thermal criticality values.

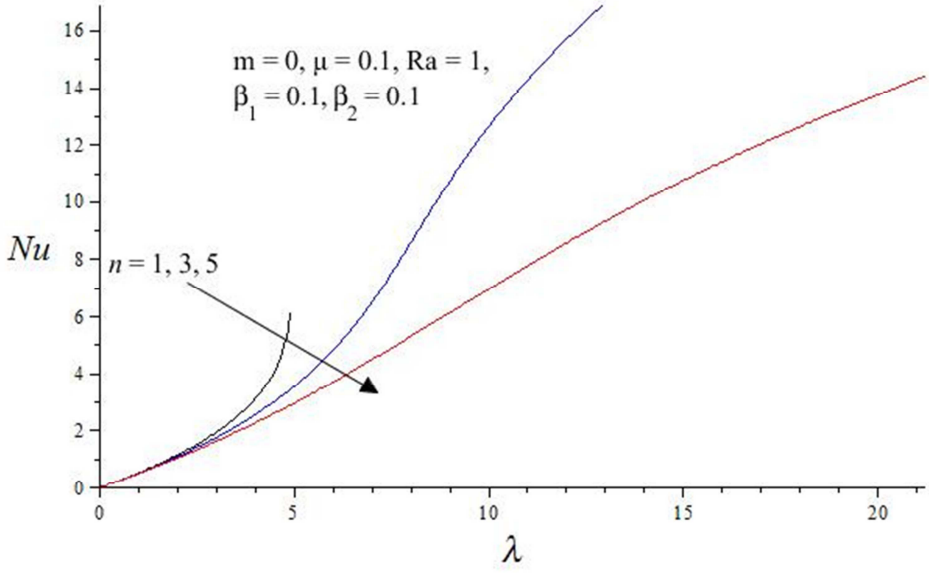

Figure 4.20: Effect of increasing *n* on slab thermal criticality values.

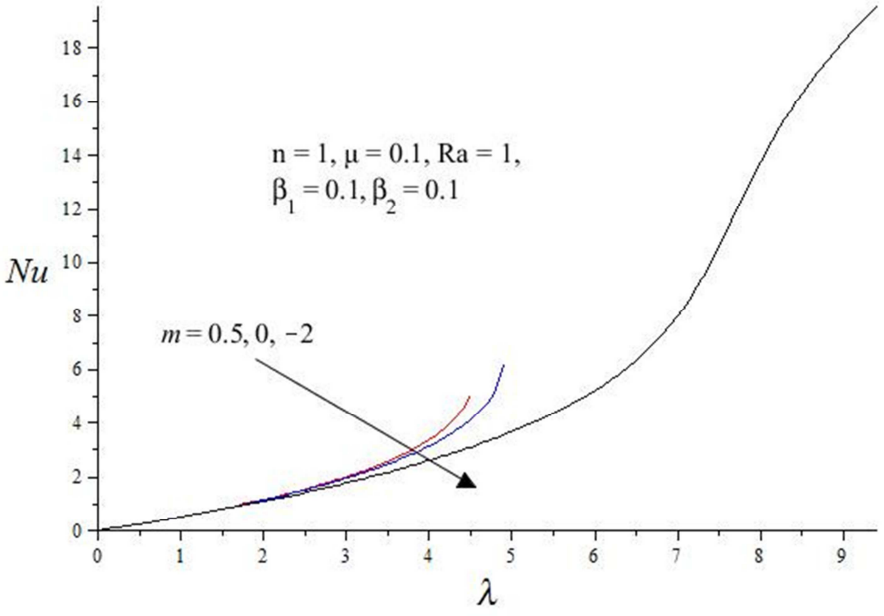

Figure 4.21: Effect of *m* on slab thermal criticality values.

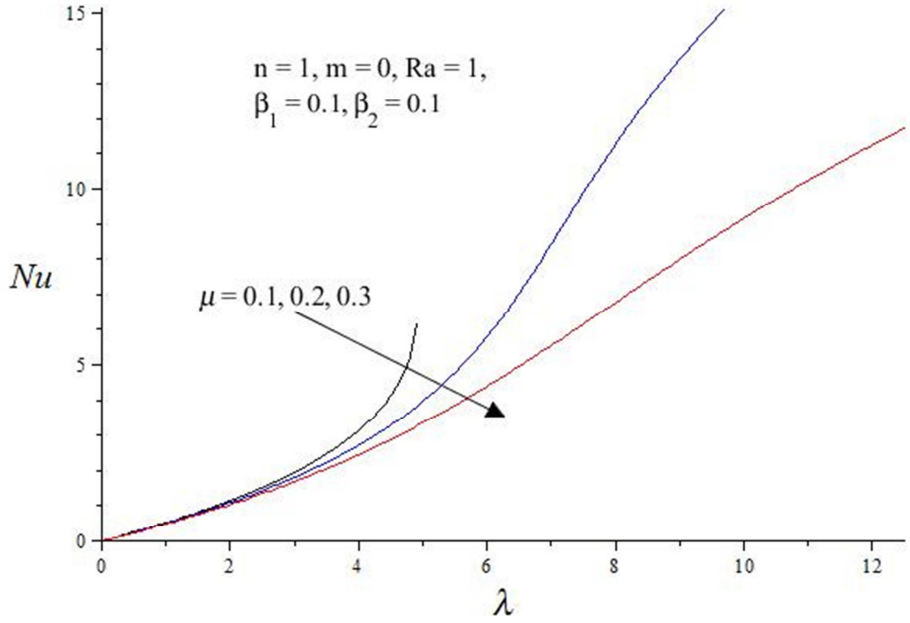

Figure 4.22: Effect of increasing μ on slab thermal criticality values.

Table 4.1: Computations showing the effects of various thermophysical parameters on thermal criticality values $\beta_1 = \beta_2 = 0.1$

m	Ra	n	μ	Nu	λ_c
-2	1	1	0.1	19.7873	9.4878
0	1	1	0.1	6.4966	4.9129
0.5	1	1	0.1	5.8275	4.5581
0	0	1	0.1	6.2069	4.6195
0	5	1	0.1	13.7238	6.6014
0	1	3	0.1	16.9694	12.9801
0	1	5	0.1	14.4564	21.3100
0	1	1	0.2	15.3221	9.8132
0	1	1	0.3	11.8179	12.5963

Table 4.1: Effects of various thermophysical parameters on thermal criticality values

4.6 Conclusion

In this chapter the impact of heat loss due to radiation on CO_2 emission, O_2 depletion and thermal stability in a reactive slab was looked at. Differential equations governing the problem were obtained and solved numerically using Runge-Kutta-Fehlberg method with shooting technique. Results were shown graphically and discussed accordingly. Measures to control the exothermic reaction taking place in a slab from explosion were considered and results were given graphically and numerically.

Chapter 5

Analysis of CO_2 Emission, O_2 Depletion and Thermal Stability in a Convecting and Radiating Reactive Slab

In chapter 4 we considered the effects of radiation on temperature, oxygen depletion and carbon dioxide emission profiles. This chapter investigates coupled convective and radiative heat loss effects on thermal stability, oxygen depletion and carbon dioxide emission in a reactive slab of combustible material. The transient heating in a reactive slab is as a result of exothermic reactions in which oxygen is a reactive species and carbon dioxide and heat are products. We assume the surfaces of the slab to lose heat by convection asymmetrically and by radiation symmetrically with the ambient. The nonlinear differential equations governing the problem are solved numerically using Runge-Kutta-Fehlberg method with shooting technique.

5.1 Introduction

The generation of heat in a reactive slab is due to the exothermic reaction of combustible material within the slab [1, 8, 22, 65]. This process has a wide range of industrial applications in the fields of solids combustion, heavy oil recovery, incineration of waste material, design of internal combustion engines and automobile exhaust system [30, 49], just to mention a few. Studies have shown that exothermic reaction taking place in a reactive slab may result with up to 80% emission of carbon dioxide which contributes to global warming and climate change [50]. It should be noted too that the exothermic reaction, due to reaction of hydrocarbon material with oxygen, within a reactive slab results also with thermal radiation emission, which brings about temperature rise in the slab [72]. On the other hand it is possible that the rate of heat generation due to exothermic reaction within a slab may exceed the rate of heat loss to the cool environment, which may lead to thermal explosion [51]. This phenomenon is known as thermal criticality and it is helpful in combustion theory and provides safe storage criterion for materials that can easily undergo exothermic reaction [2, 6, 26, 42, 46, 49]. Various studies have been carried out on thermal stability characteristics of a reacting slab, and this was done with or

without reactant consumption using one-step decomposition kinetics [44, 47]. It follows also that the complicated chemistry as a result of exothermic chemical reaction taking place in a reactive slab is tackled by considering one-step decomposition kinetics, as according to Williams [77] and this is helpful because the combustion reaction mechanism, especially of large hydrocarbons, is more complicated and includes many radicals [19]. On the other hand the complicated nature of exothermic reactions give rise to nonlinear short-lived interactions involving reacting species and products diffusion, heat conduction and chemical reactions. Furthermore, these interactions lead to steep concentration and temperature gradients [9, 45, 68]. In this regard, Simmie [70] provided a detailed review of chemical kinetic models for the reaction of hydrocarbons with oxygen in combustible materials.

However, to the best of our knowledge nothing or very little studies have been carried out on the effects of convective and radiative heat loss on CO_2 emission, O_2 depletion and thermal stability in a reactive slab of combustible materials. The objective in this chapter is to investigate the effects of heat loss due to convection and radiation on CO_2 emission, O_2 depletion and thermal stability in a stockpile of reactive combustible materials. The nonlinear differential equations governing the problem are presented in section 5.2, and then solved numerically using Runge-Kutta-Fehlberg method with shooting technique. The results are presented graphically and discussed quantitatively for effects of various thermophysical parameters on the temperature field, CO_2 emission and O_2 depletion in section 5.5.

5.2 Mathematical Model

A rectangular slab of combustible material with a constant thermal conductivity k, and surface emissivity ε is considered in this chapter as it was in chapter 4. It is also assumed that the slab is undergoing an n^{th} order oxidation chemical reaction. A one-step finite rate irreversible chemical kinetics mechanism is also assumed, just like in chapters three and four, between the material and the oxygen of the air as follows:

$$C_iH_j + \left(i + \frac{j}{4}\right)O_2 \rightarrow iCO_2 + \left(\frac{j}{2}\right)H_2O + \text{heat.} \tag{5.1}$$

Heat loss as a result of radiation at the material surface to the surrounding ambient is given by $q = \varepsilon\phi(T^4 - T_0^4)$, according to Stefan-Boltzmann law. It is also assumed that radiation solely takes place in the $\bar{y}$ direction, and that convective heat loss takes place at both the lower and the upper surfaces of the slab as illustrated in figure 5.1 that follows:

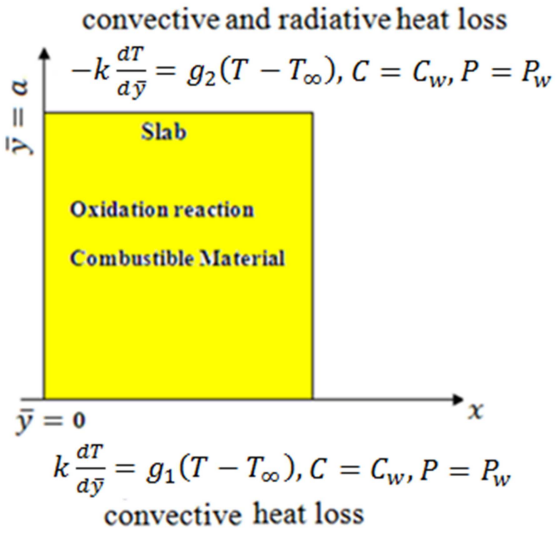

Figure 5.1: Geometry of the Problem

Following Makinde [47], Makinde *et al* [50] and Simmie [70] the nonlinear governing differential equations for the heat and mass transfer problem in the presence of thermal radiation, CO_2 emission and O_2 depletion can be written as

$$k\frac{d^2T}{d\bar{y}^2} + QA\left(\frac{KT}{vl}\right)^m C^n exp\left(\frac{-E}{RT}\right) - \varepsilon\phi(T^4 - T_\infty^4) = 0, \tag{5.2}$$

$$D\frac{d^2C}{d\bar{y}^2} - A\left(\frac{KT}{vl}\right)^m C^n exp\left(-\frac{E}{RT}\right) = 0, \tag{5.3}$$

$$\gamma\frac{d^2P}{d\bar{y}^2} + A\left(\frac{KT}{vl}\right)^m C^n exp\left(-\frac{E}{RT}\right) = 0, \tag{5.4}$$

with boundary conditions at the bottom and the top of the reactive slab respectively as:

$$\bar{y} = 0, \quad k\frac{dT}{d\bar{y}} = g_1(T - T_\infty), \quad C = C_w, \quad P = P_w, \tag{5.5}$$

$$\bar{y} = a, \; -k\frac{dT}{d\bar{y}} = g_2(T - T_\infty), \quad C = C_w, \quad P = P_w, \tag{5.6}$$

where T is the slab's absolute temperature, C is the oxygen concentration, P is the carbon dioxide emission concentration, T_∞ is the ambient temperature, C_w is the oxygen concentration at the slab surface, P_w is the carbon dioxide concentration at the slab surface, k is the thermal conductivity of the reacting slab, ε is emissivity ($0 < \varepsilon < 1$), ϕ is Stefan-Boltzmann constant ($5.6703\times 10^{-8} W/m^2K^4$), D is the diffusivity of oxygen in the slab, γ is the diffusivity of carbon dioxide in the slab, Q is the heat of reaction, $\boldsymbol{A}$ is the rate constant, E is the activation energy, R is the universal gas constant, l is the Planck number, v is the vibration frequency, K is the Boltzmann constant, $\bar{y}$ is the distance measured vertically, g_1 is the heat transfer coefficient at the lower surface of the slab, g_2 is the heat transfer coefficient at the upper surface of the slab, n is the order of exothermic chemical reaction, and m is the numerical exponent such that $m \in \{-2,0,0.5\}$. The three values taken by the parameter m, represent the numeric exponent for sensitized, Arrhenius and Bimolecular kinetics, respectively [8, 49, 66, 71]. The boundary conditions (5.5) and (5.6) describe the temperature conditions due to convective heat loss at the base and the top of the reactive slab respectively.

5.3 Introduction of dimensionless parameters

As mentioned in the previous chapters, the introduction of dimensionless parameters is very useful in reducing the partial differential equations into a form that can be easily solved using numerical methods. The following dimensionless parameters are introduced to equations (5.2) – (5.6)

$$\left.\begin{aligned} \theta = \frac{E(T-T_\infty)}{RT_\infty^2},\ \Phi = \frac{C}{C_w},\ \Psi = \frac{P}{P_w}, \mathbf{Bi_2} = \frac{ah_2}{k} \\ \beta_1 = \frac{kRT_\infty^2}{QEDC_w},\ \beta_2 = \frac{kRT_\infty^2}{QE\gamma P_w}, \mathbf{Bi_1} = \frac{ah_1}{k} \\ \lambda = \left(\frac{KT_\infty}{vl}\right)^m \frac{QAEa^2(C_w)^n}{kRT_\infty^2} exp\left(-\frac{E}{RT_\infty}\right), \\ y = \frac{\bar{y}}{a},\ \ \mu = \frac{RT_\infty}{E},\ Ra = \frac{\varepsilon\phi Ea^2T_\infty^2}{kR}. \end{aligned}\right\} \quad (5.7)$$

Equations (5.2) – (5.6) take the dimensionless form

$$\frac{d^2\theta}{dy^2} + \lambda(1+\mu\theta)^m \Phi^n \exp\left(\frac{\theta}{1+\mu\theta}\right) - Ra((\mu\theta+1)^4 - 1) = 0, \tag{5.8}$$

$$\frac{d^2\Phi}{dy^2} - \lambda\beta_1(1+\mu\theta)^m \Phi^n \exp\left(\frac{\theta}{1+\mu\theta}\right) = 0, \tag{5.9}$$

$$\frac{d^2\Psi}{dy^2} + \lambda\beta_2(1+\mu\theta)^m \Phi^n \exp\left(\frac{\theta}{1+\mu\theta}\right) = 0, \tag{5.10}$$

$$y = 0, \qquad \frac{d\theta}{dy} = \mathbf{Bi_1}\theta, \quad \Phi = 1, \quad \Psi = 1, \tag{5.11}$$

$$y = 1, \qquad \frac{d\theta}{dy} = -\mathbf{Bi_2}\theta, \quad \Phi = 1, \quad \Psi = 1, \tag{5.12}$$

where λ is the Frank-Kamenetski parameter, μ is activation energy parameter, is β_1 oxygen consumption rate parameter, β_2 is carbon dioxide emission rate parameter, $\mathbf{Bi_1}$ is Biot number at slab's lower surface, $\mathbf{Bi_2}$ is Biot number at slab's upper surface, *Ra* is radiation parameter. The dimensionless heat and mass transfer rate at the slab surface are expressed in terms of Nusselt number and Sherwood numbers as

$$Nu = -\frac{d\theta}{dy}(1), \quad Sh_1 = \frac{d\Phi}{dy}(1), \quad Sh_2 = -\frac{d\Psi}{dy}(1). \tag{5.13}$$

Equations (5.8) – (5.10) and the boundary conditions (5.11) – (5.12) are solved numerically using the Runge-Kutta-Fehlberg method with shooting technique [45]. From the process of numerical computation, the Nusselt number and the Sherwood numbers in equation (5.13) are also worked out and their numerical values are presented graphically.

5.4 Numerical Solution

Equations (5.8) – (5.10) including boundary conditions (5.11) – (5.12) and Nusselt number with Sherwood numbers in equation (5.13), have been solved numerically using the Runge-Kutta-Fehlberg method with shooting technique as discussed in the previous chapter. The same procedure used in chapter 4 was applied to solve equations (5.8) – (5.13).

5.5 Result and Discussion

Computational results obtained for the model equations in the above section are presented graphically, and the results are also quantitatively discussed for various values of thermophysical parameters embedded in the system.

5.5.1 Effects of thermophysical parameter variation on slab temperature profiles

The effects of some parameters on temperature profiles are illustrated by figures 5.2 – 5.9. We observe from figure 5.2 that the temperature increases with increasing λ. This means that increasing the rate of reaction in a reactive slab increases exothermic chemical reaction which favors increase in temperature. A different observation is shown by figures 5.3 – 5.8 in which an increase in *Ra*, *n*, μ, $\mathbf{Bi_1}$, $\mathbf{Bi_2}$ and β_1, respectively results with a decrease on temperature profiles. These parameters are helpful to keep the temperature of the slab low and thus the thermal stability of the system is attained. Figure 5.6 shows that as $\mathbf{Bi_1}$ increases, temperature profiles are lower at the bottom of the slab as compared to the top of the slab. An opposite scenario is observed from figure 5.7, where an increase in $\mathbf{Bi_2}$ shows lower temperature profiles at the upper surface of the slab as compared to the lower surface of the slab. Effect of *m* on temperature is illustrated by figure 5.9. In this case we observe that the temperature profiles increase with increasing *m*, and we realize that the temperature is low during sensitized (m = -2) and highest during Bimolecular (m = 0.5) reactions respectively.

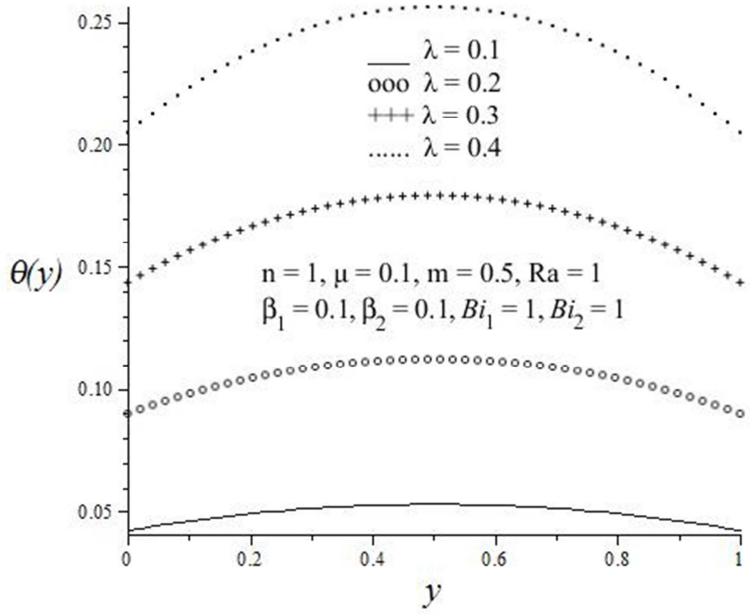

Figure 5.2: Effect of increasing λ on slab temperature profiles.

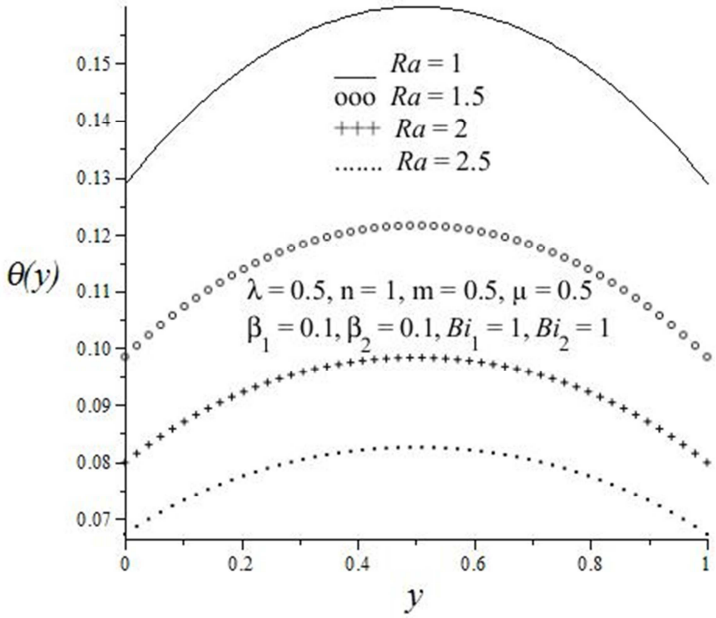

Figure 5.3: Effect of increasing *Ra* on slab temperature profiles

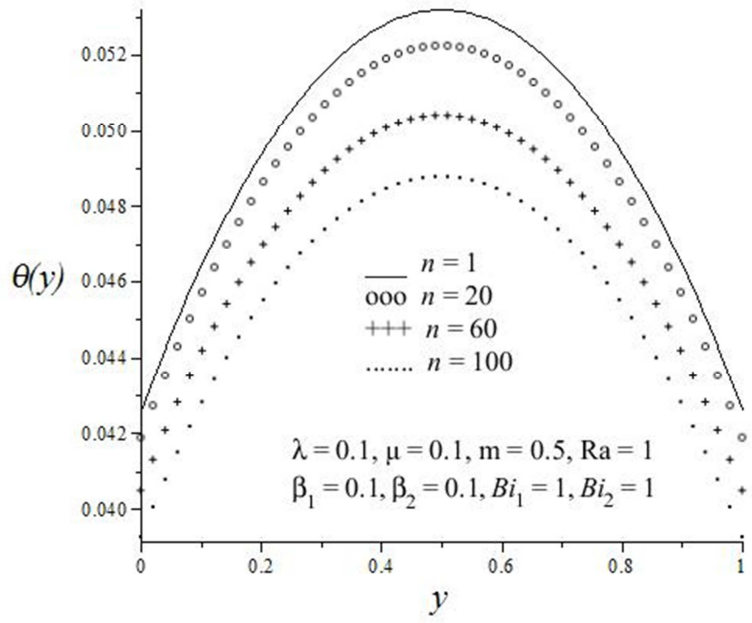

Figure 5.4: Effect of increasing *n* on slab temperature profiles

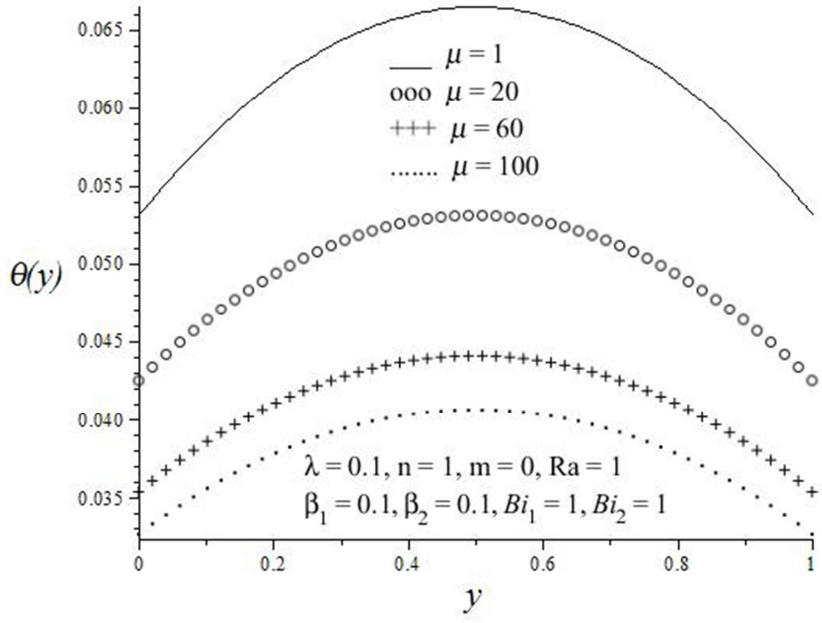

Figure 5.5: Effect of increasing μ on slab temperature profiles

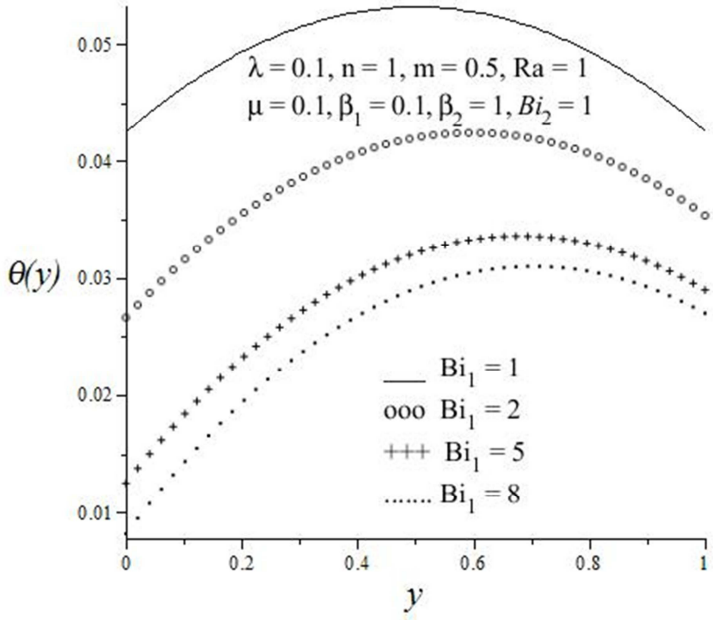

Figure 5.6: Effect of increasing $\mathbf{Bi_1}$ on slab temperature profiles.

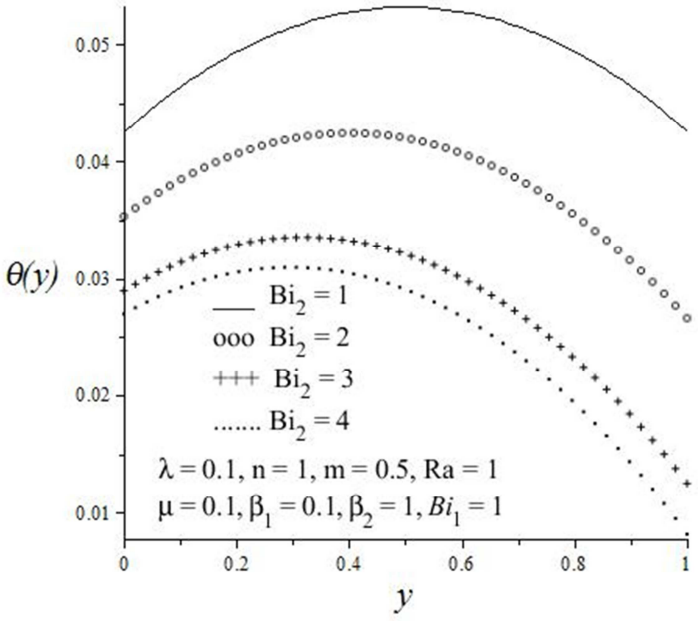

Figure 5.7: Effect of increasing $\mathbf{Bi_2}$ on slab temperature profiles.

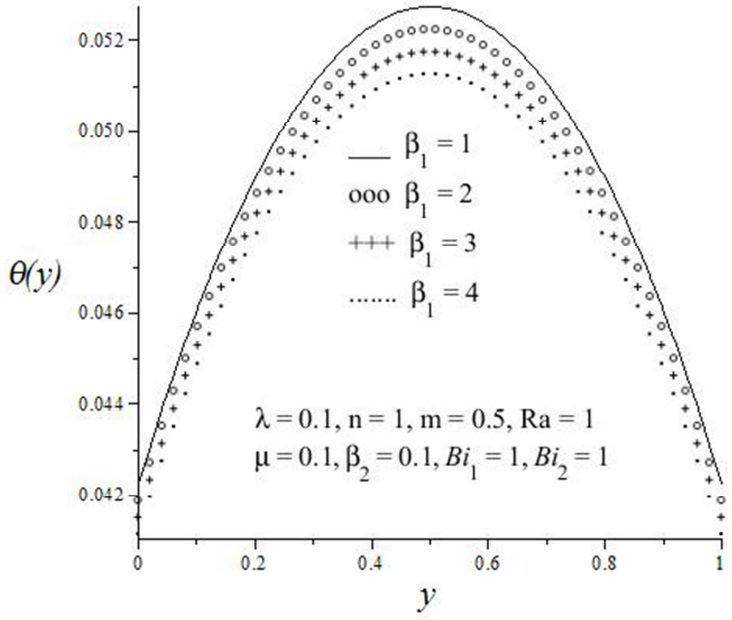

Figure 5.8: Effect of increasing β_1 on slab temperature profiles.

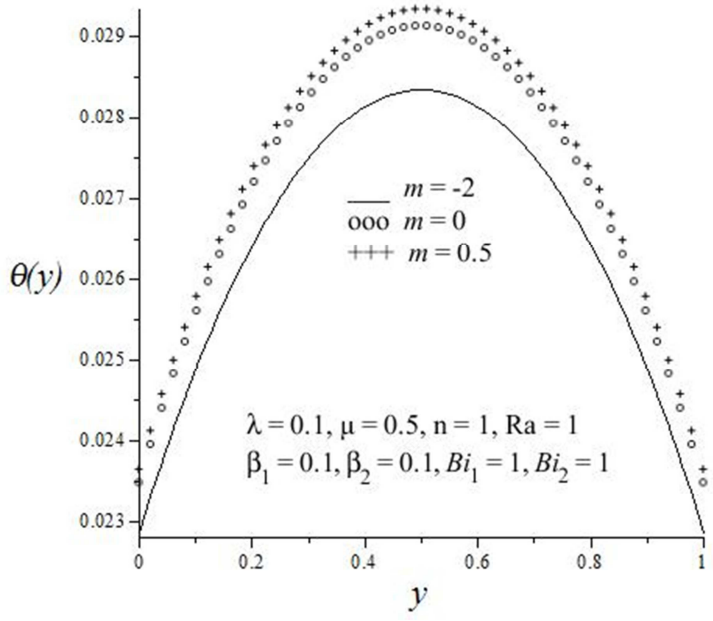

Figure 5.9: Effect of increasing *m* on slab temperature profiles.

5.5.2 Effects of thermophysical parameter variation on slab Oxygen depletion

We now consider effects of parameter variation on slab oxygen depletion in a reactive slab of combustible material. The effects are illustrated by figures 5.10 – 5.17. We observe from figure 5.10 that increasing the rate of reaction λ increases the depletion of oxygen due to accelerated exothermic chemical reaction within a slab. From figure 5.11 we see an opposite scenario that increasing the radiation parameter *Ra*, results with conservation of oxygen concentration as illustrated by increase in oxygen profiles, and the same situation is illustrated by figure 5.12 where an increase in the order of reaction *n* results with corresponding increase in oxygen profiles. An increase on β_1 decreases the oxygen concentration within a reactive slab as shown by figure 5.13. This means that more oxygen is used up during the process which enhances the exothermic reaction. An increase in the activation energy μ shows a corresponding increase in oxygen profiles as illustrated by figure 5.14. This is interesting to note that a chemical reaction with high activation energy will stimulate an exothermic reaction that will not require much of oxygen that is so useful to life. Figure 5.15 illustrates the effect of increasing $\mathbf{Bi_1}$ on slab oxygen depletion profiles. We observe from the figure that as $\mathbf{Bi_1}$ is increased, oxygen profiles also increase, and we observe the same from figure 5.16, where an increase in $\mathbf{Bi_2}$ shows a corresponding increase in oxygen profiles, meaning that the exothermic reaction is decelerated. We also observe a decrease in oxygen profiles as *m* is increased from figure 5.17. Lesser oxygen is used up during sensitized reactions as compared to both Arrhenius and Bimolecular reactions.

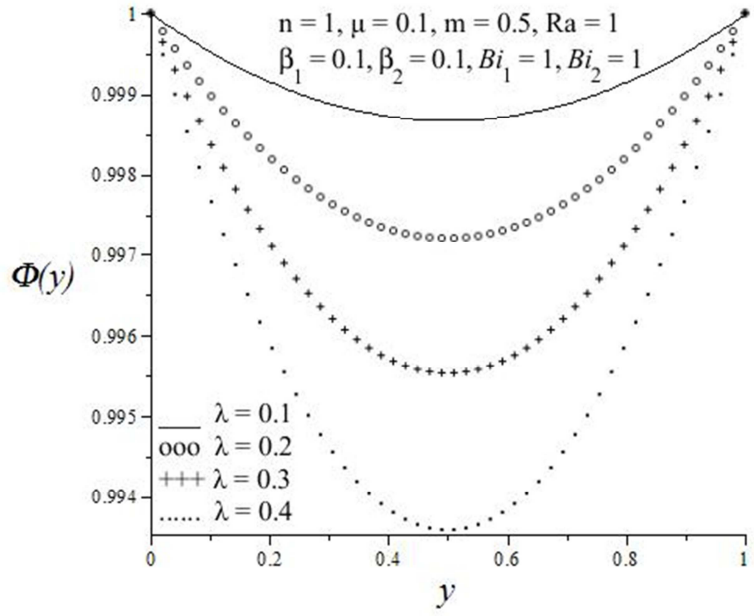

Figure 5.10: Effect of increasing λ on slab Oxygen depletion profiles.

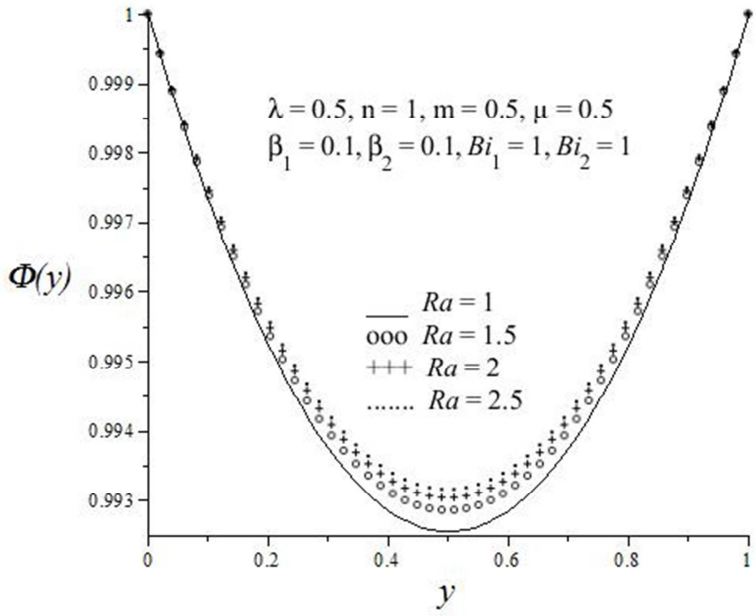

Figure 5.11: Effect of increasing *Ra* on slab Oxygen depletion profiles

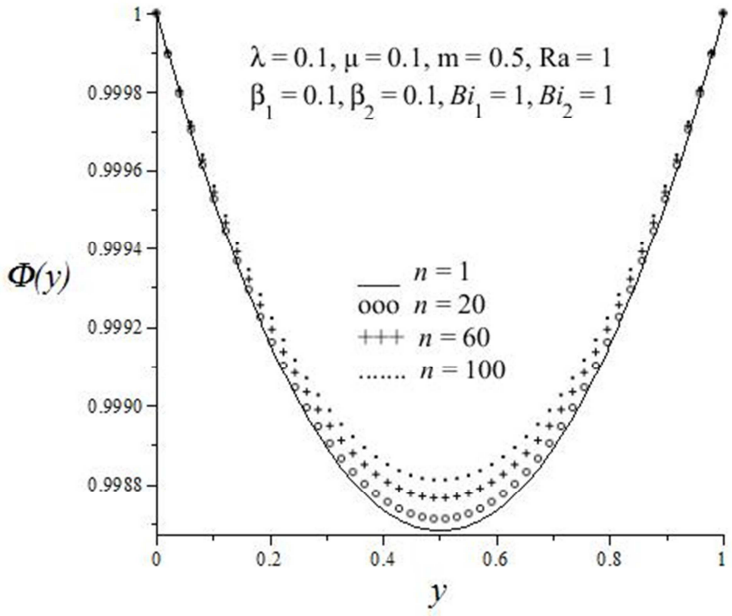

Figure 5.12: Effect of increasing *n* on slab Oxygen depletion profiles

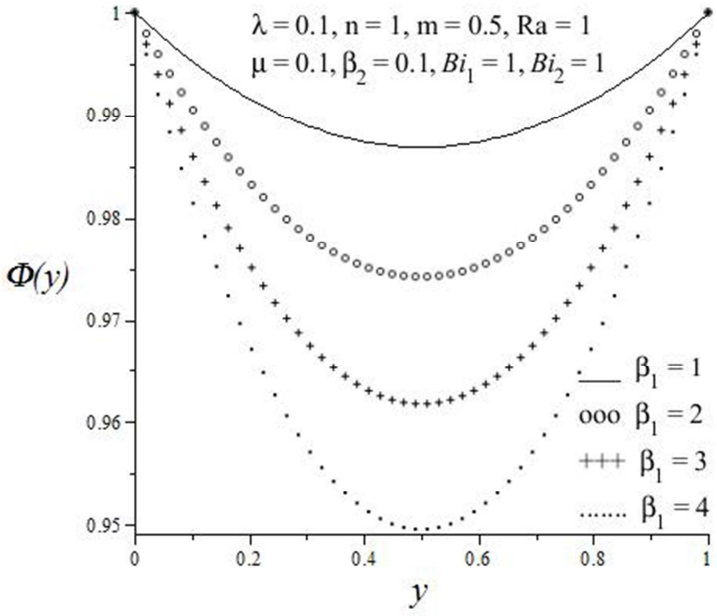

Figure 5.13: Effect of increasing β_1 on slab Oxygen depletion profiles.

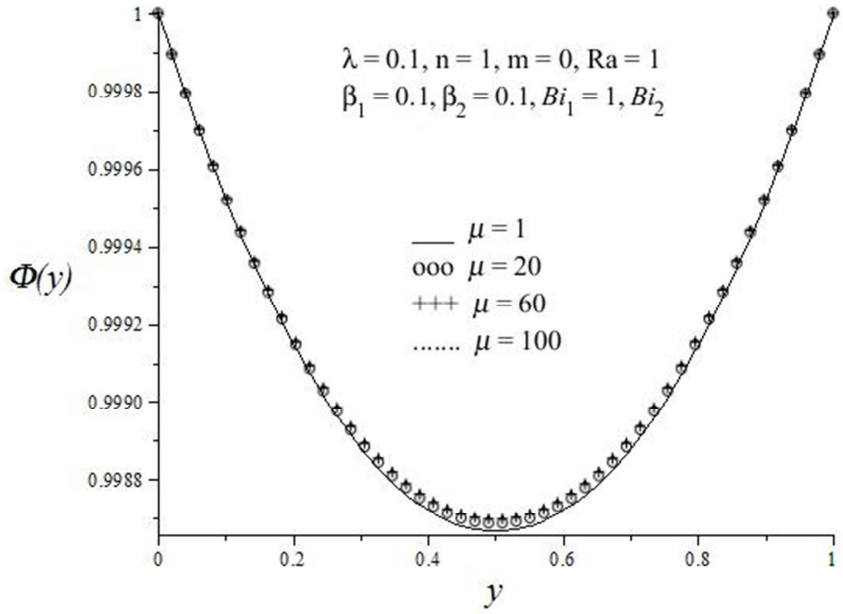

Figure 5.14: Effect of increasing μ on slab Oxygen depletion profiles.

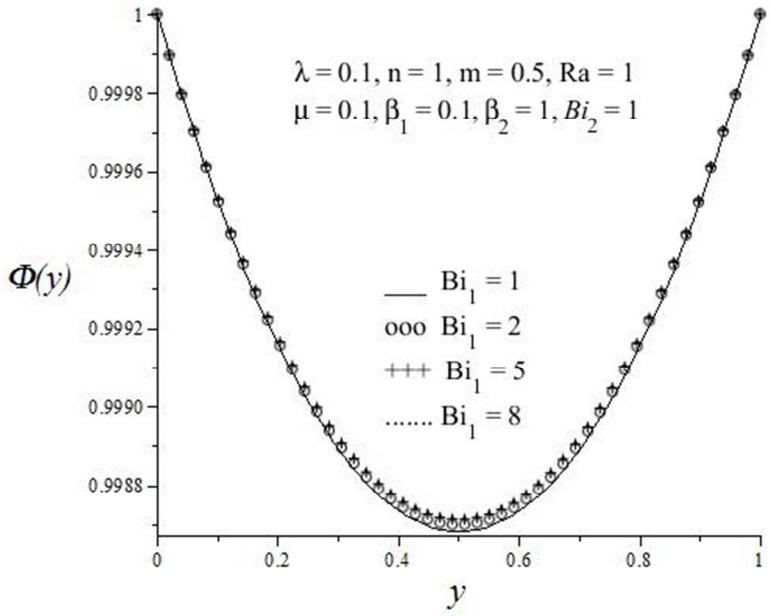

Figure 5.15: Effect of increasing $\mathbf{Bi_1}$ on slab Oxygen depletion profiles.

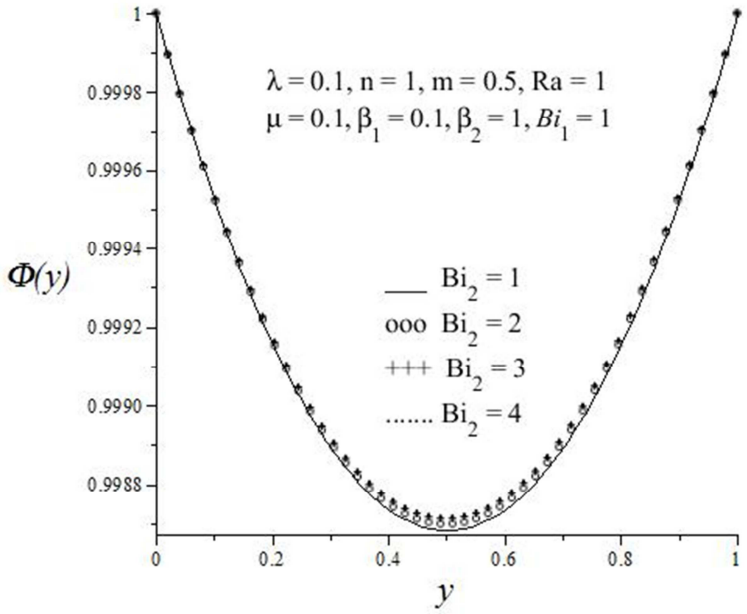

Figure 5.16: Effect of increasing **Bi_2** on slab Oxygen depletion profiles.

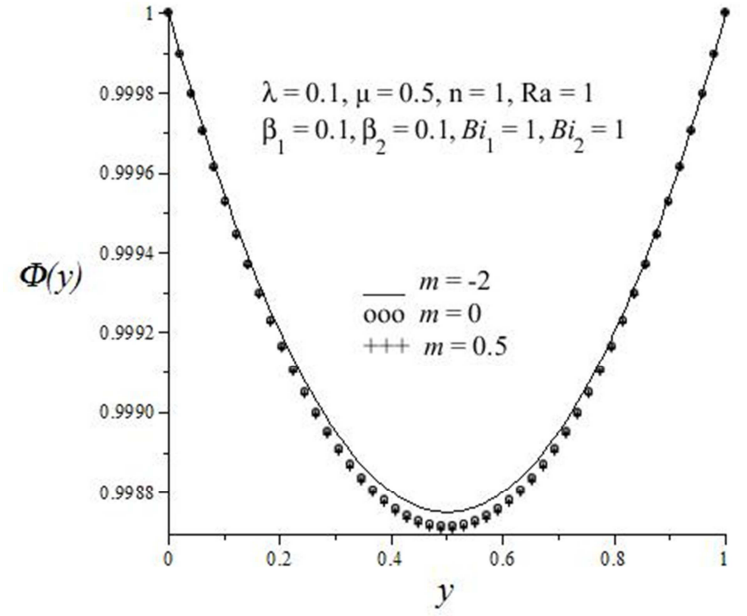

Figure 5.17: Effect of increasing *m* on slab Oxygen depletion profiles.

5.5.3 Effects of thermophysical parameter variation on slab CO_2 emission

In this subsection we look at effects of some thermophysical parameters on carbon dioxide emission. Figures 5.18 – 5.26 illustrate these effects. From figure 5.18 we observe that an increase in the rate of reaction λ results with an increase in carbon dioxide emission. This is due to the accelerated exothermic reaction within the slab which gives out more carbon dioxide as a product. A different scenario is given by figures 5.19 and 5.20, where an increase in both *Ra* and *n*, result with the decrease in carbon dioxide profiles respectively. We have seen from previous discussions that increased order of reaction and radiation parameter saves the depletion of oxygen. The same scenario is observed from figure 5.21 where carbon dioxide profiles decrease with increasing β_1. We observe from figure 5.22 the effect of increasing β_2 on slab Carbon dioxide emission profiles. Increase in β_2, carbon dioxide emission rate parameter, shows a corresponding increase in carbon dioxide emission. Figure 5.23 illustrates that an increase in μ the activation energy of the system does not favor carbon dioxide emission, since we observe a minimal decrease in the profiles. The same situation is observed from figures 5.24 and 5.25, where an increase in both $\mathbf{Bi_1}$, Biot number at the lower surface of the slab, and $\mathbf{Bi_2}$, Biot number at the upper surface of the slab, respectively, show minor decreases in carbon dioxide profiles. We should note that at the upper surface of the slab, both convective and radiative heat loss to the surroundings are experienced. In figure 5.26 we observe effect of *m* on carbon dioxide emission. Increasing *m* results with minor increase in carbon dioxide profiles and the emission of carbon dioxide is highest during Bimolecular reaction.

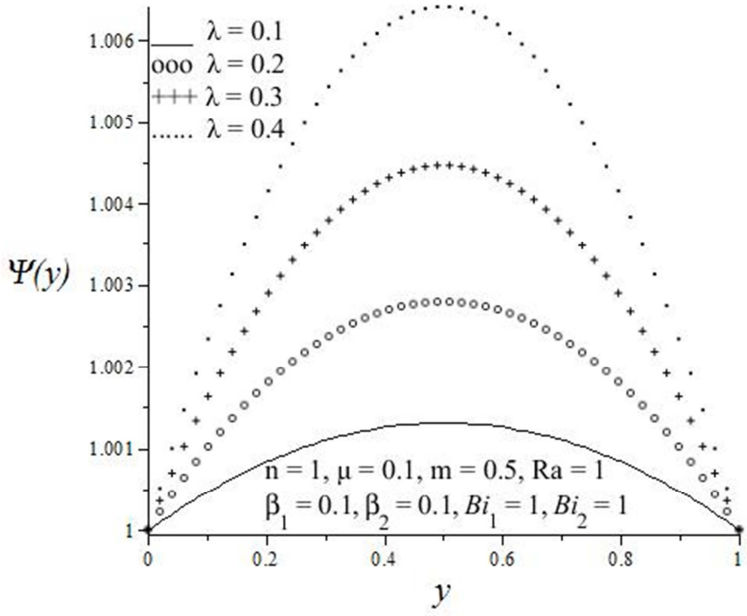

Figure 5.18: Effect of increasing λ on slab Carbon dioxide emission profiles

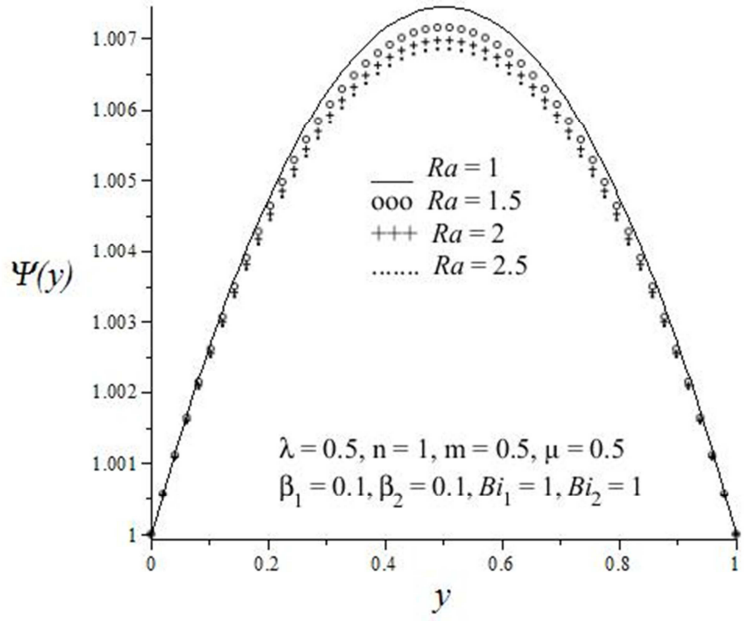

Figure 5.19: Effect of increasing *Ra* on slab Carbon dioxide emission profiles.

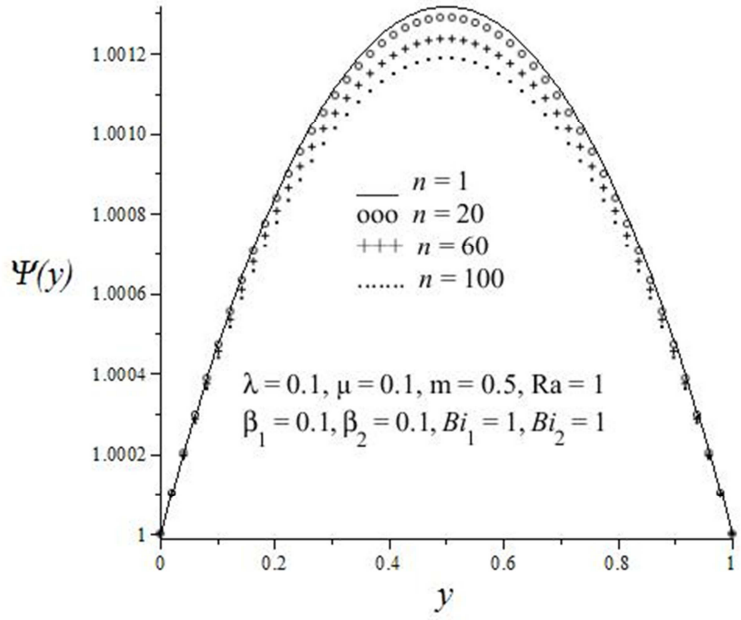

Figure 5.20: Effect of increasing *n* on slab Carbon dioxide emission profiles.

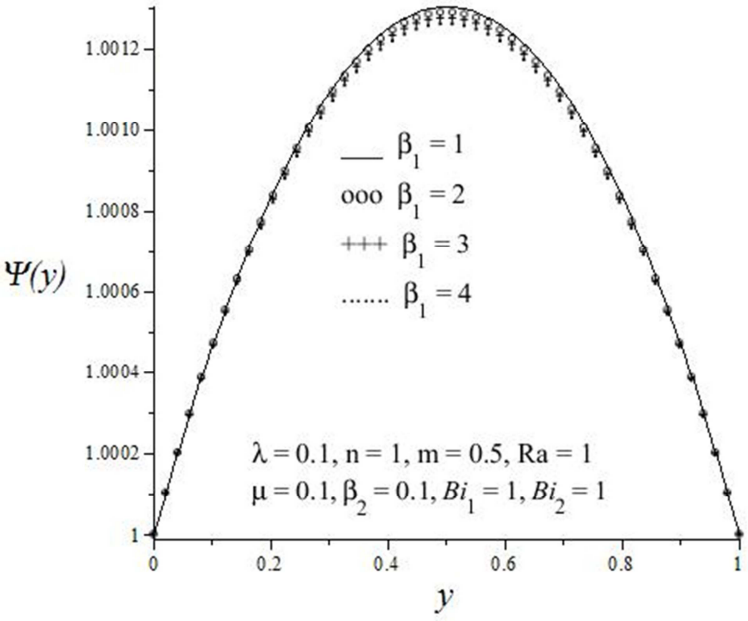

Figure 5.21: Effect of increasing β_1 on slab Carbon dioxide emission profiles

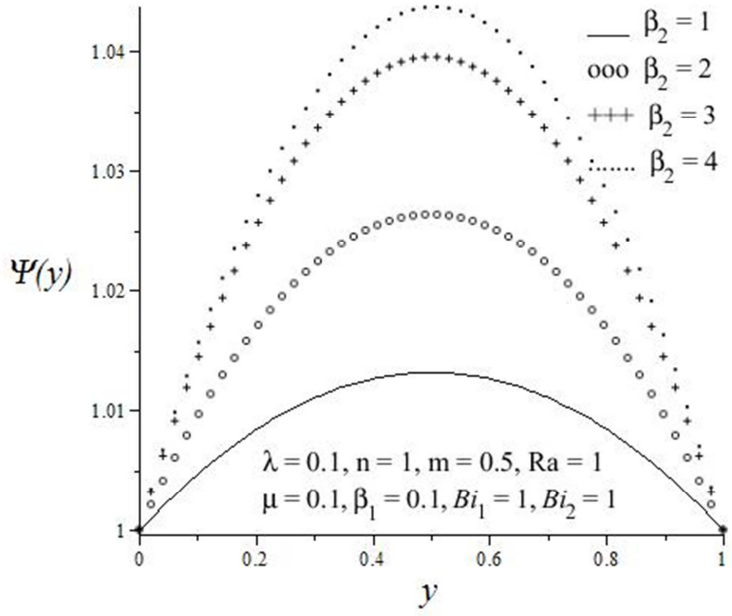

Figure 5.22: Effect of increasing β_2 on slab Carbon dioxide emission profiles

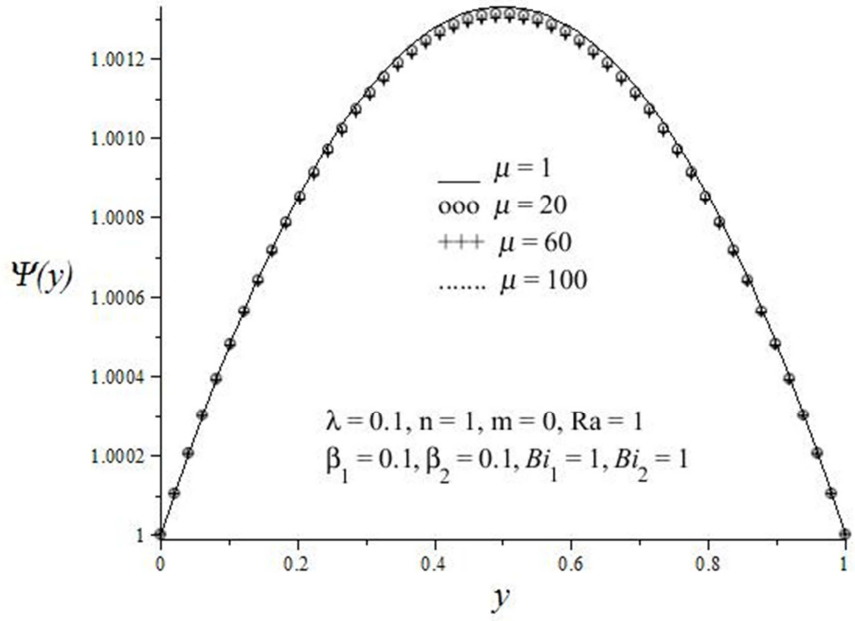

Figure 5.23: Effect of increasing μ on slab Carbon dioxide emission profiles

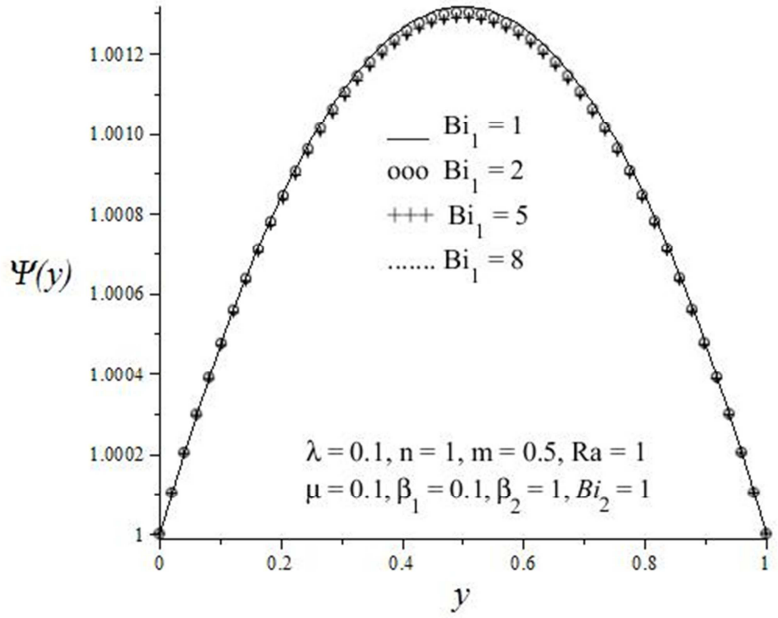

Figure 5.24: Effect of increasing $\mathbf{Bi_1}$ on slab Carbon dioxide emission profiles

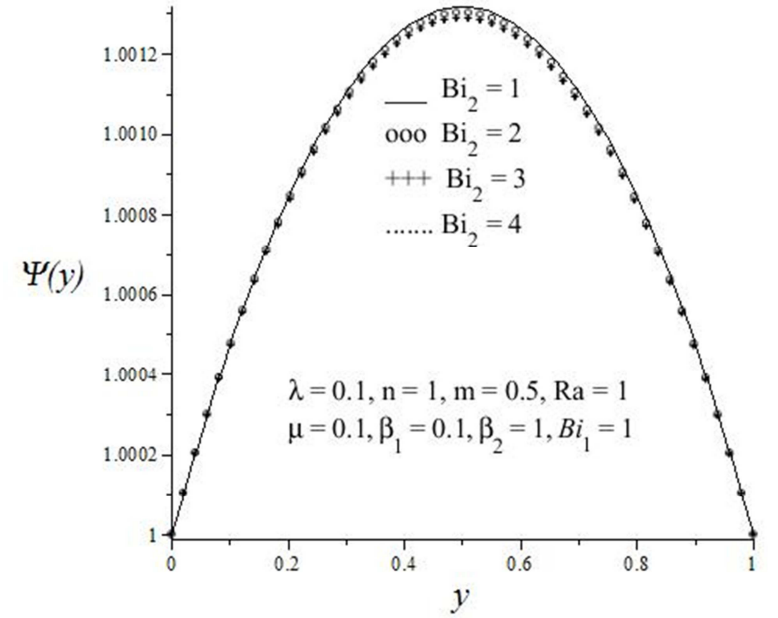

Figure 5.25: Effect of increasing $\mathbf{Bi_2}$ on slab Carbon dioxide emission profiles

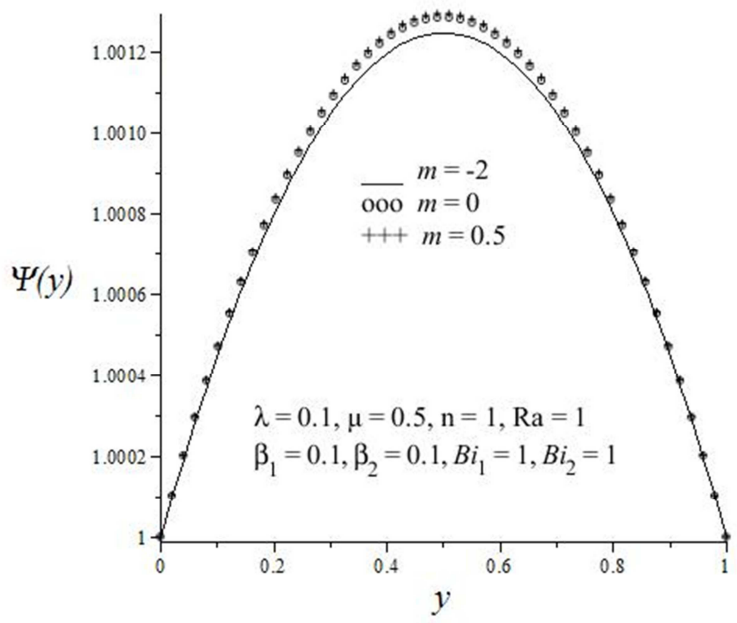

Figure 5.26: Effect of increasing *m* on slab Carbon dioxide emission profiles

5.5.4 Effects of parameter variation on thermal criticality values or blowups

In this case we discuss the variation the rate of reaction, Frank-Kamenetskii parameter λ, with the dimensionless heat transfer rate at the slab surface, Nusselt number *Nu*, for various values of some parameters as shown by the figures plotted. It is important to note that the results obtain for the Nusselt number are exactly the same for Sherwood numbers. Results are also represented in a table.

The effect of increasing *Ra* on slab thermal criticality values is shown by figure 5.27. It can be observed that as *Ra* is increased, *Nu* also increases. It can also be seen that the blow up occurs faster at lower values of *Ra*, as the rate of reaction increases. It is therefore necessary to keep the *Ra* values higher to allow thermal stability of the system. Figure 5.28 illustrates the effect of increasing *n* on slab thermal criticality values. We observe the same scenario as in figure 5.27, that as *n* increases, *Nu* also increases with increasing rate of reaction. The blow ups also occur faster at lower values of both rate of reaction λ and *Nu*. From figure 5.29 we observe the same situation as for figures 5.27 and 5.28. Thermal stability is attained by keeping higher values of both $\mathbf{Bi_1}$ and *Nu*. We also observe the repetition of the process in figures 5.30 and 5.31, where λ

increases with increasing $\mathbf{Bi_2}$ and μ respectively, and that thermal stability can also be attained by taking higher values of $\mathbf{Bi_2}$, μ and λ.The values are indicated in table 5.1 below. We see a different scenario in figure 5.32 where *Nu* decreases with increasing *m* and that thermal stability is attained by keeping low values of *m* and high *Nu* values.

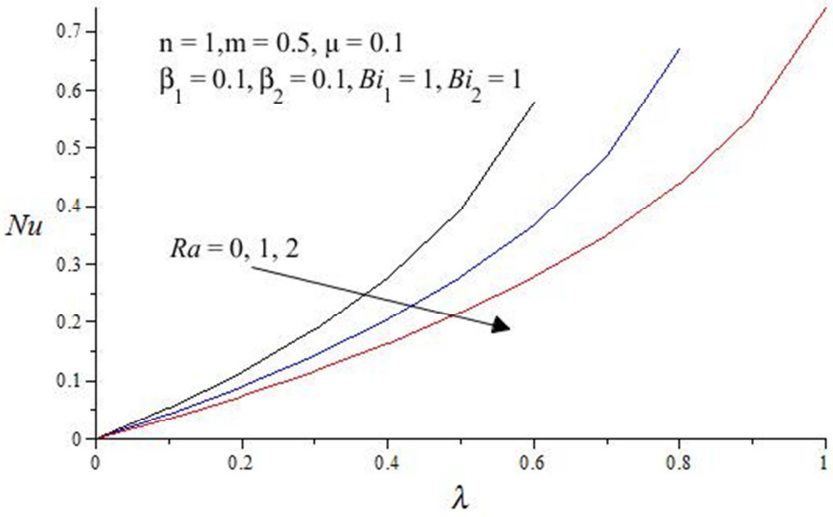

Figure 5.27: Effect of increasing *Ra* on slab thermal criticality values.

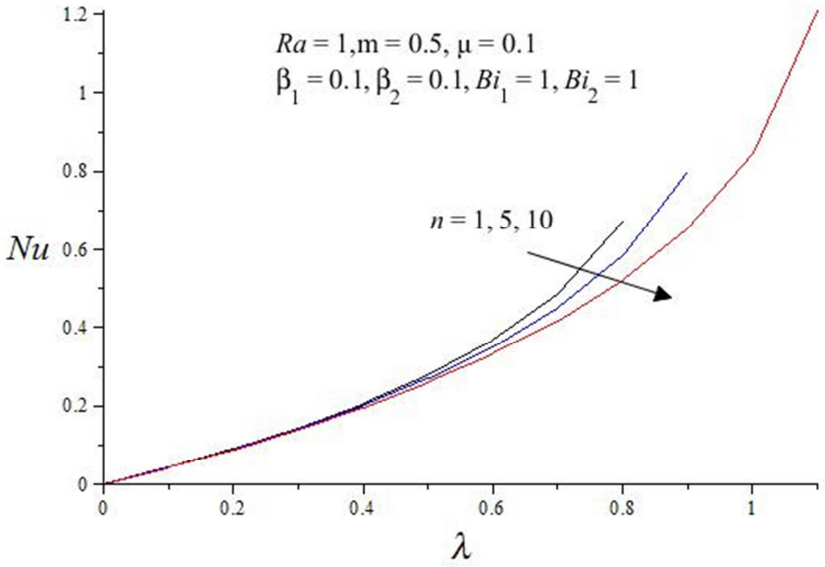

Figure 5.28: Effect of increasing *n* on slab thermal criticality values.

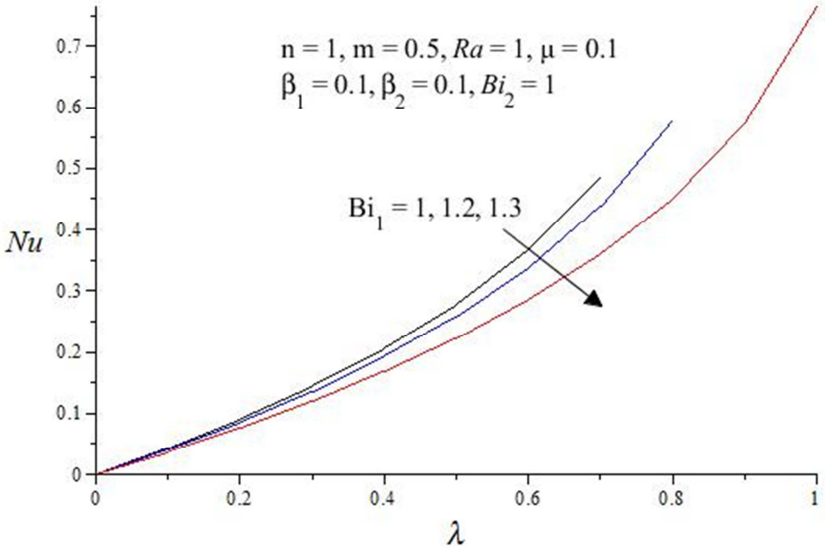

Figure 5.29: Effect of $\mathbf{Bi_1}$ on slab thermal criticality values.

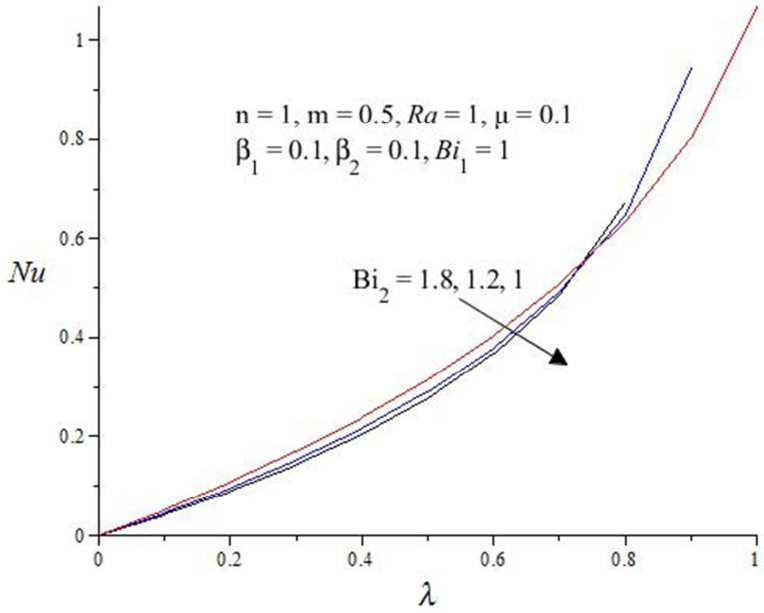

Figure 5.30: Effect of $\mathbf{Bi_2}$ on slab thermal criticality values.

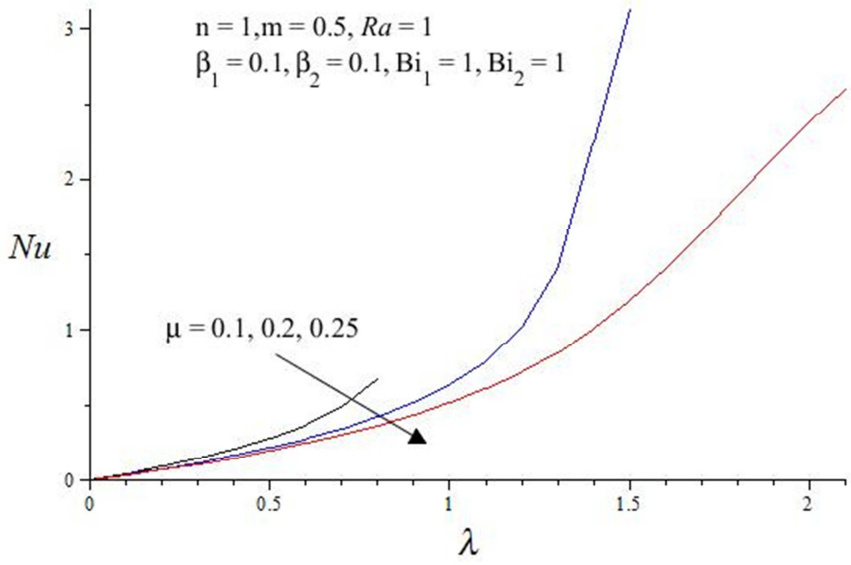

Figure 5.31: Effect of increasing μ on slab thermal criticality values.

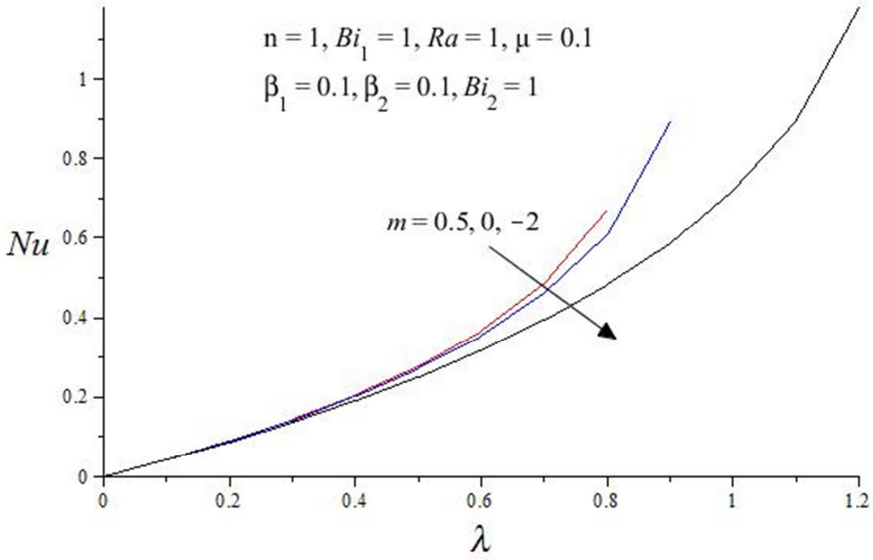

Figure 5.32: Effect of increasing *m* on slab thermal criticality values.

Numerical values for the Nusselt (*Nu*) number against the rate of reaction (λ) are given in the table that follow: